

MAGNETIC GEAR DESIGN FOR HIGH-SPEED APPLICATIONS

A Thesis

by

SHIMA HASANPOUR

Submitted to the Graduate and Professional School of  
Texas A&M University  
in partial fulfillment of the requirements for the degree of

MASTER OF SCIENCE

Chair of Committee,	Hamid Toliyat
Committee Members,	Prasad Enjeti
	Won-Jong Kim
	Jose Silva-Martinez
Head of Department,	Miroslav Begovic

December 2021

Major Subject: Electrical Engineering

Copyright 2021 Shima Hasanpour

## ABSTRACT

Magnetic gears perform the gearing action by employing magnetic fields through a non-contact operation that offers significant potential advantages, such as improved reliability, reduced acoustic noise, and reduced maintenance requirements, over mechanical gears due to eliminating teeth interlock for the power transfer. Utilizing magnetic gears in high-speed applications has electromagnetic and mechanical challenges. This study investigates solutions, introduces new topologies with different magnet arrangements, and compares various magnetic gear designs.

First, the coaxial reluctance magnetic gear (RMG) and the coaxial surface permanent magnet gear (SPMG) topologies are optimized independently. Coaxial SPMGs are found to achieve higher torque densities, better magnet utilization, higher efficiencies, and lower torque ripples than optimal coaxial RMGs.

Second, this study introduces the radial flux reluctance cycloidal magnetic gear (Rel-CyMG) topology and its operating principles. The Rel CyMG replaces the PMs on the inner rotor of a surface permanent magnet (SPM) cycloidal magnetic gear (CyMG) with teeth and slots and requires half of the SPM CyMG's outer rotor pole pair count to achieve the same gear ratio. A genetic algorithm was used to optimize RelCyMGs, SPMCyMGs, and SPM coaxial magnetic gears (CoMGs). This study demonstrates that SPMCyMGs significantly outperform the other two topologies at higher gear ratios in terms of torque density. However, RelCyMGs achieve higher torque densities than SPMCoMGs at higher

gear ratios. RelCyMGs eliminate the required PM retention sleeve and potentially enable smaller air gaps in the optimal designs.

Third, this research compares CyMG topologies with consequent pole (CP) rotors against CyMGs with SPM rotors. CPCyMGs require less PM pieces than SPMCyMGs, which may simplify manufacturing. The simulation results demonstrate that optimal CP-CyMGs achieve lower torque density values than optimal SPMCyMGs. However, if using a CP inner rotor eliminates the need for a PM retention sleeve and enables the use of a smaller effective air gap, CPCyMGs can achieve higher torque densities at high gear ratios than SPMCyMGs.

Last, a CPCyMG prototype is designed, optimized for cost objective, fabricated, and tested to validate the accuracy of the model. Its experimentally measured slip torque achieved a 95% match with the simulated slip torque.

## DEDICATION

To my sister, my soul, my Mina  
For your endless love and support

## ACKNOWLEDGMENTS

I would like to thank my advisor, Dr. Hamid Toliyat, for all of the support and guidance that made this research possible. Additionally, I would like to thank my other committee members, Dr. Prasad Enjeti, Dr. Won-Jong Kim, and Dr. Jose Silva-Martinez, for contributing their time to support my studies and for what I learned from their classes.

I appreciate my lab mates for their advice and aid during my studies. Specifically, I would like to thank Ms. Dorsa Talebi, Mr. Bryton Praslicka, Mr. Shrikesh Sheshaprasad, and Mr. Farid Naghavi. I would like to give special thanks to Dr. Matthew Johnson and Dr. Matthew Gardner, who served as mentors for me. I enjoyed working with them and I am grateful for the time they devoted to training me, help me, and be there as my friend.

I would like to thank Dr. Abas Goodarzi from US Hybrid Corporation for their partial assistance in the design and assembly of this study's prototype. Also, I appreciate NASA Glenn Research Center for their partial technical support on this project.

Also, I would like to thank all of the ECEN department staff who facilitated my study and research at Texas A&M. I would especially like to thank Ms. Anni Brunner and Ms. Katie Bryan, who helped me during these years. Portions of this research were conducted with the advanced computing resources provided by Texas A&M High-Performance Research Computing. I would like to thank ANSYS for their support of the EMPE lab through the provision of FEA software.

## CONTRIBUTORS AND FUNDING SOURCES

### **Contributors**

This work was supervised by a thesis committee consisting of Professor Hamid Toliyat, the advisor, Professor Prasad Enjeti, and Professor Jose Silva-Martinez of the Department of Electrical and Computer Engineering, and Professor Won-Jong Kim of the Department of Mechanical Engineering.

A portion of this work was done in collaboration with Dr. Matthew Gardner and Dr. Matthew Johnson, who assisted in setting up the studies in Sections 4 and 6. The prototype of this study was built using the structural parts of a prototype that was assembled in collaboration with the US Hybrid Corporation and NASA. Mr. Bryton Praslicka also provided additional hands and advice during the assembly and testing of the prototype described in Chapter 7. All other work was completed independently.

### **Funding Sources**

This work was sponsored by the U.S. Army CCDC Army Research Laboratory and was accomplished under Cooperative Agreement Number W911NF-18-2-0289. Its contents are solely the responsibility of the author and do not necessarily represent the official views of the US Army Research Laboratory. Portions of this research were sponsored by NASA SBIR grant No. 28-517790-00001.

## NOMENCLATURE

CP	Consequent Pole
CoMG	Coaxial Magnetic Gear
CyMG	Cycloidal Magnetic Gear
FEA	Finite Element Analysis
GA	Genetic Algorithm
IPM	Interior Permanent Magnet
LCM	Least Common Multiple
MG	Magnetic Gear
MGM	Magnetically Geared Motor
MMF	Magnetomotive Force
PM	Permanent Magnet
PM ST	Permanent Magnet Specific Torque
Rel	Reluctance
RMG	Reluctance Magnetic Gear
SPM	Surface Permanent Magnet
SPMG	Surface Permanent Magnet Gear
ST	Specific Torque
VTD	Volumetric Torque Density

## TABLE OF CONTENTS

	Page
ABSTRACT .....	ii
DEDICATION .....	iv
ACKNOWLEDGMENTS .....	v
CONTRIBUTORS AND FUNDING SOURCES .....	vi
NOMENCLATURE .....	vii
TABLE OF CONTENTS .....	viii
1. INTRODUCTION .....	1
1.1 Mechanical Gears .....	1
1.2 Magnetic Gears .....	2
1.2.1 Coaxial Magnetic Gears .....	2
1.2.2 Cycloidal Magnetic Gears .....	4
1.3 High-speed Application Challenges .....	6
2. MAGNETIC GEAR TOPOLOGIES FOR HIGH-SPEED APPLICATIONS .....	8
2.1 Coaxial Reluctance Magnetic Gear .....	8
2.2 Reluctance Cycloidal Magnetic Gear .....	9
2.3 Consequent Pole Cycloidal Magnetic Gear .....	11
3. OPERATING PRINCIPLES .....	14
3.1 Coaxial Reluctance Magnetic Gear .....	14
3.2 Reluctance Cycloidal Magnetic Gear .....	21
4. COMPARISON OF COAXIAL RELUCTANCE AND SURFACE PERMANENT MAGNET MAGNETIC GEARS .....	27
4.1 Design Study Methodology .....	28
4.2 Results .....	32
4.3 Conclusion .....	49



5. CYCLOIDAL RELUCTANCE MAGNETIC GEARS FOR HIGH GEAR RATIO APPLICATIONS .....	51
5.1 Design Study Methodology.....	53
5.2 Results .....	55
5.3 Conclusion.....	67
6. ANALYSIS AND BENCHMARKING OF RADIAL FLUX CYCLOIDAL MAGNETIC GEARS WITH REDUCED PERMANENT MAGNET PIECE COUNT USING CONSEQUENT POLES .....	69
6.1 Design Study Methodology.....	70
6.2 Results .....	74
6.3 Conclusion.....	91
7. PROTOTYPE CONSEQUENT POLE CYCLOIDAL MAGNETIC GEAR .....	94
8. CONCLUSION.....	103
REFERENCES .....	106

## 1. INTRODUCTION

Electrical machine's size is determined by its torque rating. High-torque machines have lower speed and higher volume and mass than the low-torque machines. The size of high-torque machines is a drawback for applications with volume, mass, and cost objectives optimization. Gearboxes are common solutions to couple a high-speed low-torque electric machine to a low-speed high-torque shaft. Utilizing a geared system potentially reduces the size, mass, and cost.

### 1.1 Mechanical Gears

Mechanical gears transfer the power between high-speed low-torque and low-speed high-torque shafts and they are the most common gearboxes used in the industry. Maintaining mechanical gears is essential as they require lubrication. Also, their acoustic noise during operation is an issue due to their operating principles, where the mechanical contact between interlocking teeth, as shown in Figure 1.1, results in power transfer.

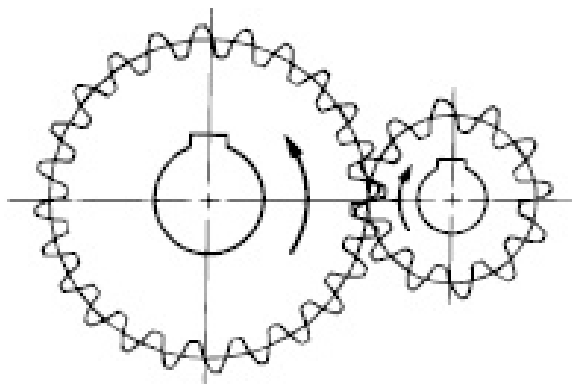


Figure 1.1: A mechanical gearbox.

## 1.2 Magnetic Gears

Magnetic gears have been proposed as an alternative to mechanical gears because of their non-contact operation's benefits for a wide range of applications from wind [1] and wave [2] energy collection, to electric vehicles [3], electric aviation [4], propulsion [5], and space application [6]. Magnetic gears transfer torque between rotors and create the gearing effect using the interaction of magnetic fields instead of mechanical contact which offers a plethora of potential advantages including inherent overload protection, reduced acoustic noise, and reduced maintenance requirements (no lubrication oil).

### 1.2.1 Coaxial Magnetic Gears

The most widely studied magnetic gear topology is the coaxial SPMG shown in Figures 1.2 and 1.3 [1, 3–5, 7–9]. Figure 1.2 is a radial flux coaxial SPMG and Figure 1.3 is an axial flux coaxial SPMG.

The radial flux coaxial SPMG includes three rotors: the inner low pole count, high-speed PM rotor (Rotor 1), the intermediate rotor consisting of ferromagnetic pieces (modulators) separated by nonmagnetic slots (Rotor 2), and the outer high pole count, low-speed PM rotor (Rotor 3). The operating principles of the coaxial SPMGs have been established and presented in detail in [1, 7, 10]. The MMF associated with the PMs on a rotor is modulated by the air gap permeance function, which produces spatial harmonics similar to those associated with the other rotor's PMs. This enables the gearing behavior. Rotor 2 in a coaxial SPMG consists of  $Q_2$  pieces of ferromagnetic modulators that create the permeance function required for the gearing effect.

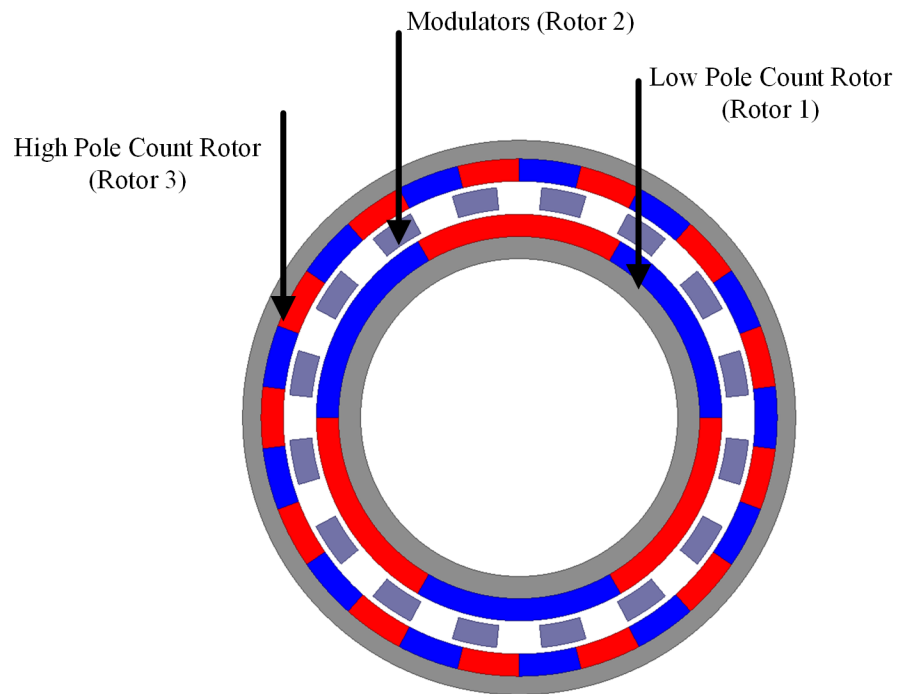


Figure 1.2: Cross section of a radial flux coaxial SPMG.

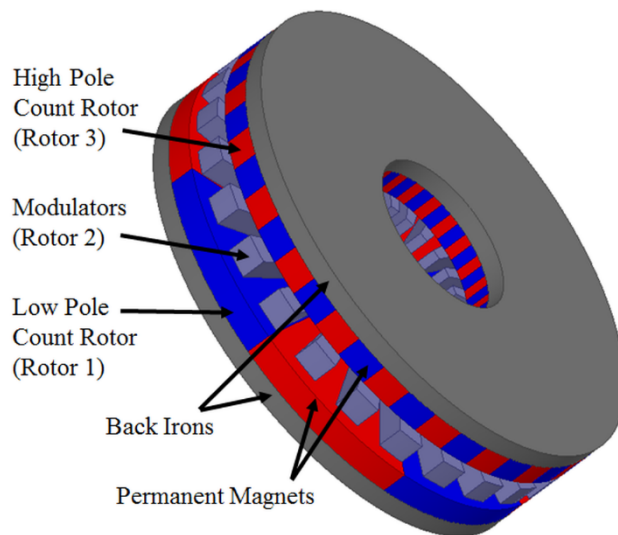


Figure 1.3: Cross section of an axial flux coaxial SPMG.

Optimal operation requires the number of modulators  $Q_2$  to be equal to the sum of the pole pairs on the inner rotor ( $PP_1$ ) and the pole pairs on the outer rotor ( $PP_3$ ), as given by (1.1).  $PP_3$  must be chosen properly to avoid undesired torque ripples [1]. The gear ratio depends on the operating mode, as defined in (1.2) and (1.3). The maximum gear ratio is achieved if Rotor 1 operates as the high-speed rotor and Rotor 2 operates as the low-speed rotor, while Rotor 3 is fixed. In this case, the gear ratio is given by (1.2), where  $\omega_1$  and  $\omega_2$  are the steady-state speeds of Rotor 1 and Rotor 2, respectively.

$$Q_2 = PP_1 + PP_3 \quad (1.1)$$

$$GearRatio_{coaxialSPMG} = \frac{\omega_1}{\omega_2} = \frac{Q_2}{PP_1} \quad (1.2)$$

$$GearRatio_{coaxialSPMG} = \frac{\omega_1}{\omega_3} = \frac{-PP_3}{PP_1} \quad (1.3)$$

### 1.2.2 Cycloidal Magnetic Gears

The coaxial SPMGs are proposed for low-speed, high-torque applications [1, 2, 9, 11, 12]. High gear ratios require more PMs and modulators, which presents magnetic and manufacturing challenges, as discussed in [12]. However, cycloidal SPMGs, such as the one shown in Figure 1.4, have received attention for high gear ratio applications [6, 12–15]. This structure includes two rotors: the inner low pole count, rotating PM rotor (Rotor 1), and the outer high pole count, stationary PM rotor (Rotor 2). A cycloidal SPMG does not use modulators; therefore, it eliminates the highest piece count coaxial SPMG rotor. In a cycloidal SPMG, the movement of Rotor 1 consists of two components, including a

rotation around its own center, and an orbital revolution around the center of Rotor 2 [12–14]. Facilitating this complex motion pattern is the most significant structural challenge in the design of a cycloidal SPMG.

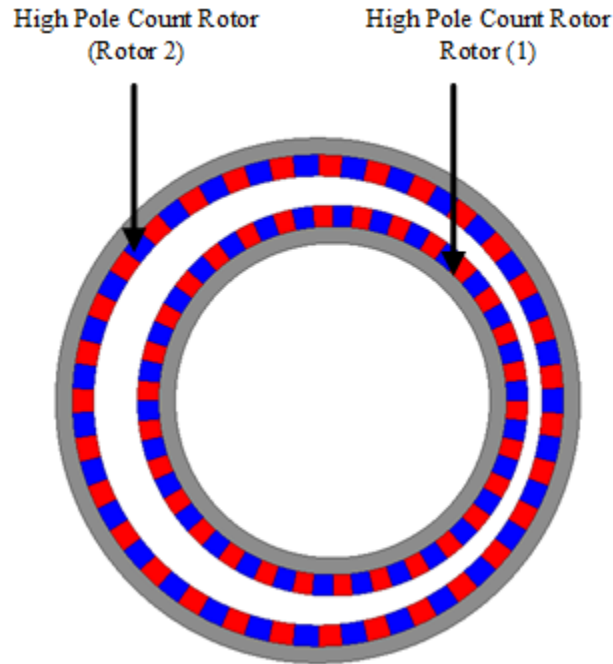


Figure 1.4: Cross section of a cycloidal SPMG.

Cycloidal SPMGs and coaxial SPMGs have significant differences, but both topologies operate based on the same underlying principle. The operating principles of a cycloidal SPMG in detail have been presented in existing literature [12–14]. A cycloidal SPMG has a time-varying, non-uniform air gap that creates the permeance harmonics. The Rotor 2 pole pair count ( $PP_2$ ) is given by 1.4 that is one pole pair more than the Rotor 1 pole pair count ( $PP_1$ ). The gear ratio for the stationary Rotor 2 configuration is given by (1.5),

where  $\omega_{rot}$  is the speed of Rotor 1's rotation around its own axis and  $\omega_{orb}$  is the speed of the orbital revolution of Rotor 1 about the axis of Rotor 2, as explained in [13, 14].

$$PP_2 = PP_1 + 1 \quad (1.4)$$

$$GearRatio_{cycloidalSPMG} = \frac{\omega_{orb}}{\omega_{rot}} = -PP_1 \quad (1.5)$$

### 1.3 High-speed Application Challenges <sup>1</sup>

Much of the existing magnetic gear literature focuses on low speed, high torque applications [1, 2, 11]; however, magnetic gears have also been proposed for higher speed applications [16]. Unfortunately, higher speed operation presents some electromagnetic and mechanical challenges for the conventional SPMGs. Electromagnetically, higher speed rotation leads to higher frequency variation of the magnetic fields and higher eddy current losses, especially in the PMs. This issue can be mitigated by axially segmenting the magnets [17], which is analogous to laminating motor cores. However, this increases the manufacturing complexity. High-speed operation also makes retaining the Rotor 1 PMs more challenging. A sleeve around the PMs can hold them in place, but this increases the effective air gap, which reduces the design's torque, and can incur eddy current losses, if the sleeve is electrically conductive [18]. Alternatively, the PMs could be embedded in the Rotor 1 laminations to form an IPM rotor. However, thin bridges in laminations often provide flux leakage paths, which reduce the air gap flux produced by the PMs [19]. Ad-

---

<sup>1</sup>© 2020 IEEE. Part of this chapter is reprinted with permission from S. Hasanpour, M. C. Gardner, M. Johnson, and H. A. Toliyat, "Comparison of Reluctance and Surface Permanent Magnet Coaxial Magnetic Gears," in *Proc. IEEE Energy Convers. Congr. Expo.*, 2020, pp. 307-314.

ditionally, these thin bridges can experience large mechanical stresses at high speeds [19].

Reluctance topology in MGs has been offered as a solution to the problems of a coaxial SPMG in high-speed applications in the existing literature [20–24]. However, their operating principles have not been established correctly and the conclusion is on better performance of coaxial RMGs than coaxial SPMGs. These two topologies are independently optimized in this study and compared [25]. Also, this study employs a reluctance rotor in a CyMG and investigates the optimal designs' performance in a broad range of gear ratios. The operating principles of the Rel CyMG are established in this study for the first time. Reluctance topologies have significantly lower performance compared to SPM topologies, therefore, a CP rotor is proposed for a CyMG to improve its torque rating while addressing the high-speed operating issues [26]. These topologies are optimized and compared to the SPM CyMGs using multiple metrics.



## 2. MAGNETIC GEAR TOPOLOGIES FOR HIGH-SPEED APPLICATIONS

This study investigates three different topologies and compare them to the basic SP-MGs, Figures 1.2 and 1.4. Two new topologies, Rel CyMGs and CP CyMGs, have been introduced and analyzed in this thesis.

### 2.1 Coaxial Reluctance Magnetic Gear<sup>1</sup>

Coaxial RMGs, as shown in Figure 2.1, are an alternative to coaxial SPMGs at high-speeds [20–25].

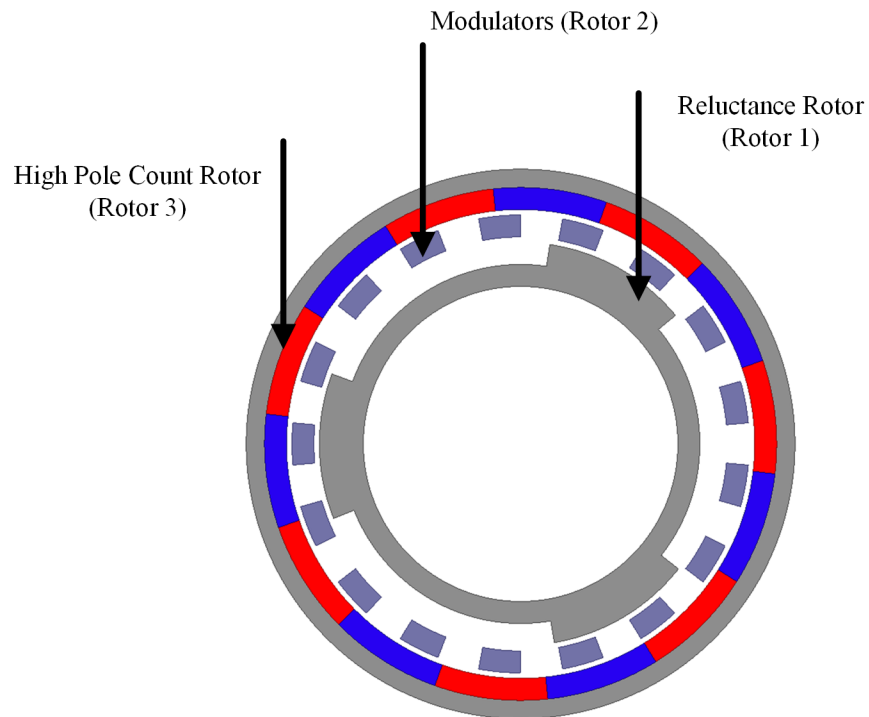


Figure 2.1: Cross section of a coaxial RMG. Reprinted with permission from [25].

<sup>1</sup>© 2020 IEEE. Part of this section is reprinted with permission from S. Hasanpour, M. C. Gardner, M. Johnson, and H. A. Toliyat, "Comparison of Reluctance and Surface Permanent Magnet Coaxial Magnetic Gears," in *Proc. IEEE Energy Convers. Congr. Expo.*, 2020, pp. 307-314.

The coaxial RMG replaces the Rotor 1 PMs with teeth, such that Rotor 1 can be formed from a single stack of laminations, as shown in 2.1. Eliminating the Rotor 1 PMs simplifies the mechanical challenges associated with rotating Rotor 1 at high speeds and eliminates the Rotor 1 PM eddy current losses. Flux switching magnetic gears have also been proposed for high-speed applications [23]. Flux switching magnetic gears are similar to coaxial RMGs but contain extra PMs in the spaces between the modulators, which increases the manufacturing complexity. While previous papers have proposed coaxial RMGs and evaluated a few designs [23, 27–29], this research uses a significant parametric sweep to characterize the capabilities of coaxial RMGs and compare optimal coaxial RMGs against optimal coaxial SPMGs. This study also provides a more accurate description of coaxial RMGs’ operating principles.

## **2.2 Reluctance Cycloidal Magnetic Gear**

Operating at high gear ratios is electromagnetically and mechanically challenging for both coaxial and cycloidal SPMGs. In the most common configuration for both topologies, Rotor 1 accounts for the high-speed motion component. An SPM CyMG is the proposed topology for high gear ratio applications and the PM pole counts on its Rotor 1 is one lower than its maximum gear ratio. Therefore, the high PM counts on Rotor 1 has the similar challenges as discussed earlier.

Figure 2.2 illustrates a Rel CyMG, which is a new magnetic gear topology. In a Rel CyMG, the PMs on Rotor 1 of a SPM CyMG are replaced with teeth. This transformation

is similar to the conversion of a coaxial SPMG into a coaxial RMG [27] and [25].

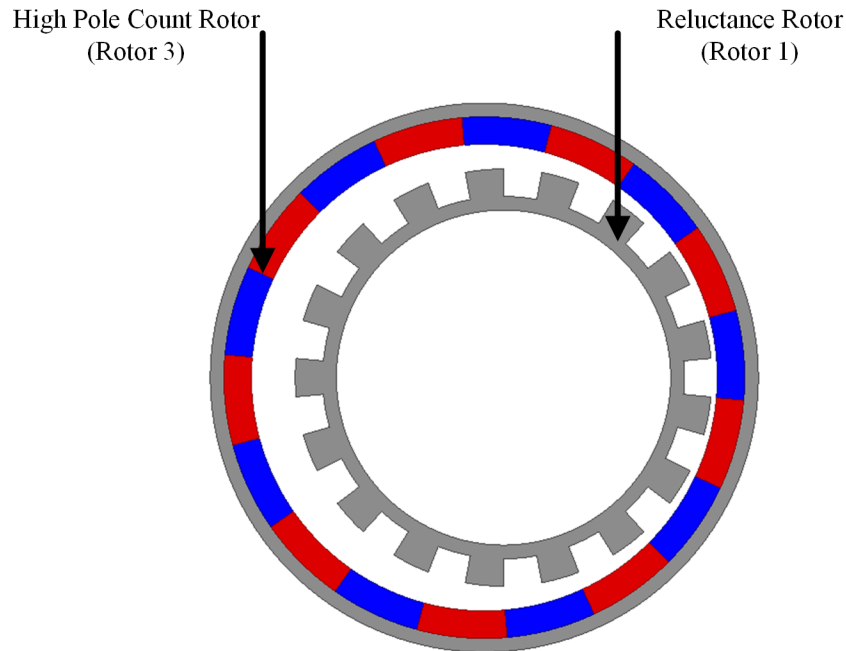


Figure 2.2: Cross section of a reluctance cycloidal magnetic gear.

Rel CyMGs address the mechanical challenges of high-speed Rotor 1 operation in SPM CyMGs by replacing the Rotor 1 surface PMs with a reluctance structure. This gives Rel CyMGs a more mechanically robust rotor (as they have no moving magnets), which is potentially better suited for high-speed operation. However, as shown in [25], replacing PMs in a gear with a reluctance structure yields lower torque density designs due to the resulting decrease in flux density. This research introduces Rel CyMGs and their operating principles and compares the performances of optimal Rel CyMGs, SPM CyMGs, and SPM CoMGs.

### 2.3 Consequent Pole Cycloidal Magnetic Gear <sup>2</sup>

Retaining the PMs on the inner rotor as it simultaneously orbits and rotates in a SPM CyMG is a significant challenge. The inner rotor PMs can be retained with a sleeve, but this increases the effective air gap between the rotors, which decreases the slip torque. The CP topology is an alternative to the SPM topology; all of the PMs on a CP rotor are magnetized in the same direction, and ferromagnetic teeth fill the spaces between PMs. A CP CyMG is potentially more robust and can facilitate the use of a smaller air gap than a SPM CyMG because the CP configuration's PM slots can be designed to naturally retain the PMs, thus eliminating the need for a sleeve around the inner rotor to keep the PMs in place, as shown in Figure 2.3. Additionally, the CP topology may simplify assembly by making it easier to position the PMs by providing slots for the PMs, even if the teeth are not shaped to retain the PMs. The CP topology can further simplify assembly by reducing the piece count, as PM pieces can be replaced with teeth that are part of a single piece (likely a stack of steel laminations).

The CP topology has been employed in motors [30–32], MGM [33, 34], and coaxial MG [35]. Additionally, other studies have proposed inserting PMs between the modulators in a coaxial MG to create a consequent pole configuration on the modulator rotor to increase the torque density [36–39]. However, these designs replace non-magnetic material (the slots between modulators) with PMs, which is a different topology altogether.

---

<sup>2</sup>© 2021 IEEE. Part of this section is reprinted with permission from M. Johnson, S. Hasanpour, M. C. Gardner, and H. A. Toliyat, "Analysis and benchmarking of radial flux cycloidal magnetic gears with reduced permanent magnet piece count using consequent poles," in *Proc. IEEE Energy Convers. Congr. Expo.*, 2021, pp. 4334-4341.

Past studies have anecdotally compared motor [32] or magnetically geared motor [34] designs using CP configurations and claimed that the CP configuration improves the torque density relative to the SPM configuration.

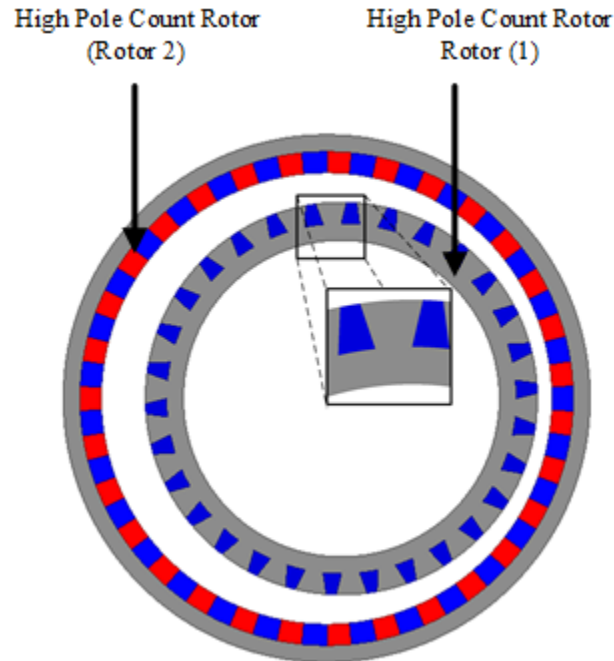


Figure 2.3: Cross section of a consequent pole cycloidal magnetic gear. Reprinted with permission from [26].

However, another study of electric machines claims that the CP configuration is disadvantageous [30]. These conclusions are contradictory, at least in part, due to the use of anecdotal evidence based on a limited number of designs. However, utilizing the CP configuration may affect the optimal design parameters; therefore, the CP and SPM designs should be optimized individually for a fair comparison. This was done for CoMGs with ferrite PMs in [35], which concluded that the CP topology with ferrite PMs achieved

better torque densities than the SPM topology with ferrite PMs. However, the CP topology has not been evaluated for CyMGs. This study introduces CP CyMG and optimizes SPM CyMGs and CP CyMGs for performance comparison.

### 3. OPERATING PRINCIPLES

#### 3.1 Coaxial Reluctance Magnetic Gear <sup>1</sup>

The principle of operation in CoMGs is to modulate the magnetomotive force (MMF) of magnets through the modulators and create a flux distribution in the air gap [16]. In SPM CoMGs, there are two sets of magnets, each creating its own MMF with its specific frequency. However, there is only one set of magnets in coaxial RMGs that can create the MMF, which will be modulated once by the permeance distribution of Rotor 2 and once by the permeance distribution of the Rotor 1 teeth.

The operating principles of coaxial RMGs are similar to those of coaxial SPMGs, which modulate the MMF of magnets through the modulators and create a flux distribution in the air gap [10]. However, there are a few key differences. First, instead of the MMF distribution developed by the Rotor 1 PMs in a coaxial SPMG, the Rotor 1 teeth in a coaxial RMG produce a permeance distribution. Equations (3.1) – (3.3) provide the Rotor 1 permeance ( $P_1$ ), Rotor 2 permeance ( $P_2$ ), and Rotor 3 MMF ( $F_3$ ) functions of a coaxial RMG with  $N_1$  teeth on Rotor 1,  $Q_2$  modulators on Rotor 2, and  $PP_3$  pole pairs on Rotor 3. In these equations,  $P_{1,0}$  and  $P_{2,0}$  represent the constant permeance components,  $P_{1,i}$ ,  $P_{2,j}$ , and  $F_{3,k}$  represent the permeance and MMF spatial harmonic components,  $\omega_1$ ,  $\omega_2$ , and  $\omega_3$  represent the speeds of the three rotors, and  $\theta_{10}$ ,  $\theta_{20}$ , and  $\theta_{30}$  represent the initial positions of the rotors.

---

<sup>1</sup>© 2020 IEEE. Part of this section is reprinted with permission from S. Hasanpour, M. C. Gardner, M. Johnson, and H. A. Toliyat, "Comparison of Reluctance and Surface Permanent Magnet Coaxial Magnetic Gears," in *Proc. IEEE Energy Convers. Congr. Expo.*, 2020, pp. 307-314.

$$P_1(\theta) = P_{1,0} + \sum_{i=1}^{\infty} P_{1,i} \cos(iN_1(\theta - \omega_1 t - \theta_{10})) \quad (3.1)$$

$$P_2(\theta) = P_{2,0} + \sum_{j=1}^{\infty} P_{2,j} \cos(jQ_2(\theta - \omega_2 t - \theta_{20})) \quad (3.2)$$

$$F_3(\theta) = \sum_{k=1}^{\infty} F_{3,k} \cos(kPP_3(\theta - \omega_3 t - \theta_{30})) \quad (3.3)$$

The Rotor 3 PMs' MMF is modulated by the Rotor 2 modulators to produce the flux distribution given by (3.4), where  $\phi_{2,3,0,k}$  is the set of flux spatial harmonics produced by the interaction of  $P_{2,0}$  and  $F_{3,k}$  and  $\phi_{2,3,j,k}$  is the set of flux spatial harmonics produced by the interaction of  $P_{2,j}$  and  $F_{3,k}$ , as defined in (3.5) and (3.6). Similarly, the modulation of the Rotor 3 MMF by the Rotor 1 teeth produces the flux distribution given by (3.7), where  $\phi_{1,3,0,k}$  is the set of flux spatial harmonics produced by the interaction of  $P_{1,0}$  and  $F_{3,k}$  and  $\phi_{1,3,i,k}$  is the set of flux spatial harmonics produced by the interaction of  $P_{1,i}$  and  $F_{3,k}$ , as defined in (3.8) and (3.9).

$$\phi_{2,3}(\theta) = F_3(\theta)P_2(\theta) = \phi_{2,3,0,k}(\theta) + \phi_{2,3,j,k}(\theta) \quad (3.4)$$

$$\phi_{2,3,0,k}(\theta) = \sum_{k=1}^{\infty} F_{3,k}P_{2,0} \cos(kPP_3(\theta - \omega_3 t - \theta_{30})) \quad (3.5)$$



$$\phi_{2,3,j,k}(\theta) = \sum_{j=1}^{\infty} \sum_{k=1}^{\infty} \left( \left( \frac{F_{3,k}P_{2,j}}{2} \right) \cos \left( (kPP_3 \pm jQ_2) \left( \theta - \left( \frac{kP_3\omega_3 \pm jQ_2\omega_2}{kP_3 \pm jQ_2} \right) t - \left( \frac{kPP_3\theta_{30} \pm jQ_2\theta_{2,0}}{kPP_3 \pm jQ_2} \right) \right) \right) \right) \quad (3.6)$$

$$\phi_{1,3}(\theta) = F_3(\theta)P_1(\theta) = \phi_{1,3,0,k}(\theta) + \phi_{1,3,i,k}(\theta) \quad (3.7)$$

$$\phi_{1,3,0,k}(\theta) = \sum_{k=1}^{\infty} F_{3,k}P_{1,0} \cos(kPP_3(\theta - \omega_3 t - \theta_{30})) \quad (3.8)$$

$$\phi_{1,3,i,k}(\theta) = \sum_{i=1}^{\infty} \sum_{k=1}^{\infty} \left( \left( \frac{F_{3,k}P_{1,i}}{2} \right) \cos \left( (kPP_3 \pm iN_1) \left( \theta - \left( \frac{kPP_3\omega_3 \pm iN_1\omega_1}{kPP_3 \pm iN_1} \right) t - \left( \frac{kPP_3\theta_{30} \pm iN_1\theta_{1,0}}{kPP_3 \pm iN_1} \right) \right) \right) \right) \quad (3.9)$$

The gearing action can be achieved by matching the pole counts and speeds of a term from (3.6) with a term from (3.9). This yields the relationship between  $N_1$ ,  $Q_2$ , and  $PP_3$  given by (3.10), where  $k_a$  and  $k_b$  are odd integers, and  $i$  and  $j$  are integers and can be positive, 0, or negative. Then, the speed relationship is given by (3.11), where  $\omega_1$ ,  $\omega_2$ , and  $\omega_3$ , are the speeds of Rotor 1, Rotor 2, and Rotor 3, respectively. Selecting  $k_a = 1$ ,  $k_b = 1$ ,  $j = -1$ , and  $i = 1$  yields (3.12) and (3.13). Then, the gear ratio is given by (3.14) if Rotor 2 is stationary, with the negative sign denoting that Rotors 1 and 3 rotate in opposite directions, or by (3.15) if Rotor 3 is stationary. For this study, Rotor 2 is held stationary and Rotor 3

is used as the low speed rotor, with the gear ratio given by (3.14).

$$|k_a PP_3 + jQ_2| = |k_b PP_3 + iN_1| \quad (3.10)$$

$$\frac{k_a PP_3 \omega_3 + jQ_2 \omega_2}{k_a PP_3 + jQ_2} = \frac{k_b PP_3 \omega_3 + iN_1 \omega_1}{k_b PP_3 + iN_1} \quad (3.11)$$

$$Q_2 = N_1 + 2PP_3 \quad (3.12)$$

$$Q_2 \omega_2 = N_1 \omega_1 + 2PP_3 \omega_3 \quad (3.13)$$

$$GearRatio = \frac{\omega_1}{\omega_3} = \frac{-2PP_3}{N_1} \quad (3.14)$$

$$GearRatio = \frac{\omega_1}{\omega_2} = \frac{Q_2}{N_1} \quad (3.15)$$

Previous papers, [20–24], attempted to derive the gear ratio by multiplying the Rotor 3 MMF by the Rotor 2 permeance function and, then, multiplying the resulting flux distribution by the permeance function of Rotor 1 [20] and [28]. While this yielded the same gear ratio, it is not correct from a physics standpoint. Instead, the operation of the gear is based on coupling a flux harmonic created by the modulation of the Rotor 3 PMs by the Rotor 2 modulators, as defined in (3.6), to a flux harmonic created by the modulation of the Rotor 3 PMs by the Rotor 1 teeth, as defined in (3.9), [25].

In order to illustrate this operating principle, a sample coaxial RMG with the following teeth, modulator, and PM pole counts,  $N_l = 4$ ,  $Q_2 = 22$ , and  $PP_3 = 9$  was simulated and the results are shown in the following figures. Two scenarios were evaluated: the scenario with Rotor 1 and Rotor 3 present without the Rotor 2 modulators and the scenario with

Rotor 2 and Rotor 3 present without the Rotor 1 teeth. Figure 3.1a shows the inner air gap radial flux densities obtained for these two scenarios, and Figure 3.1b shows the normalized FFT of the inner air gap radial flux densities. Both scenarios produce a large 9<sup>th</sup> harmonic component, which corresponds to the 9 pole pair counts on Rotor 3,  $PP_3$ . The 13<sup>th</sup> harmonic component corresponding to  $|PP_3 - Q_2|$  or  $|PP_3 + N_l|$ . In this case, it is the interaction of these 13<sup>th</sup> harmonic components that produces the gearing behavior.

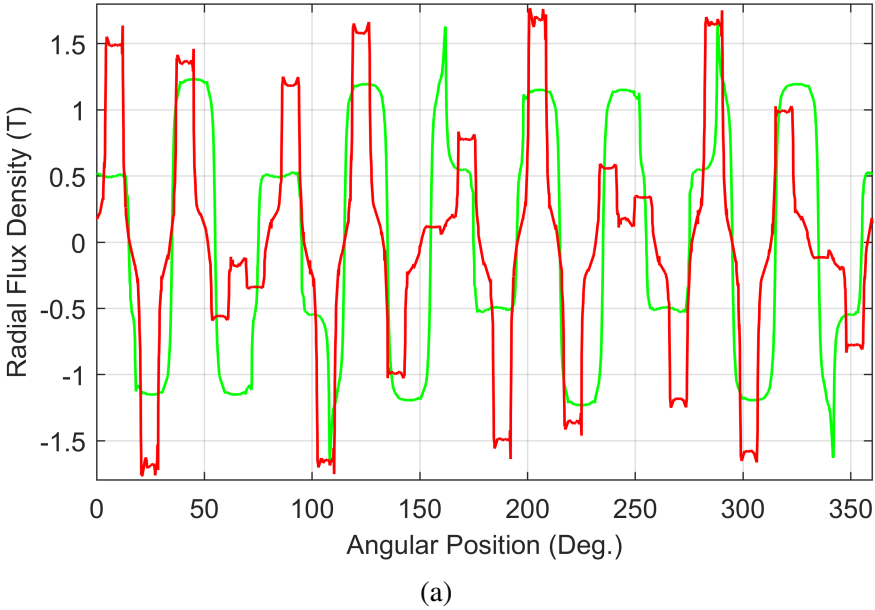


Figure 3.1

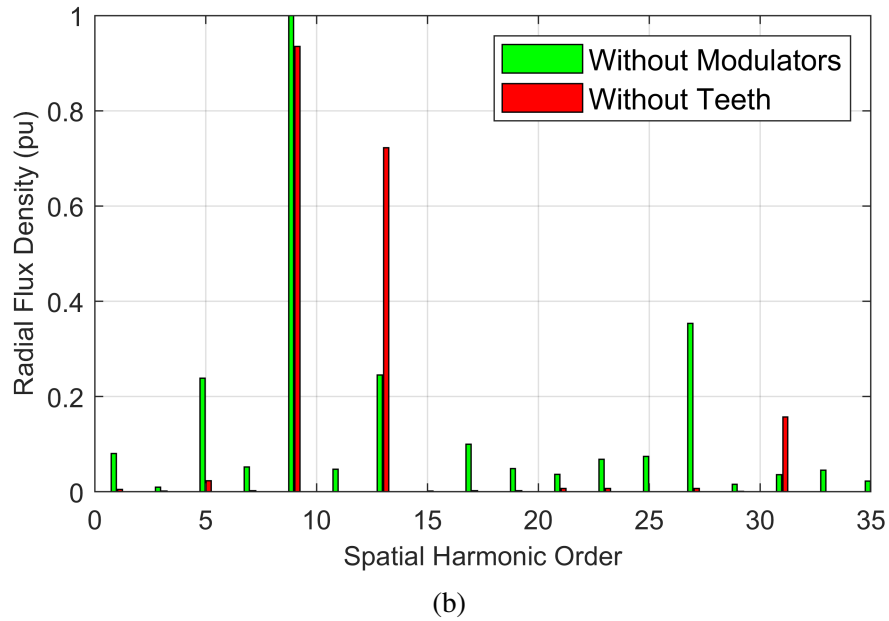
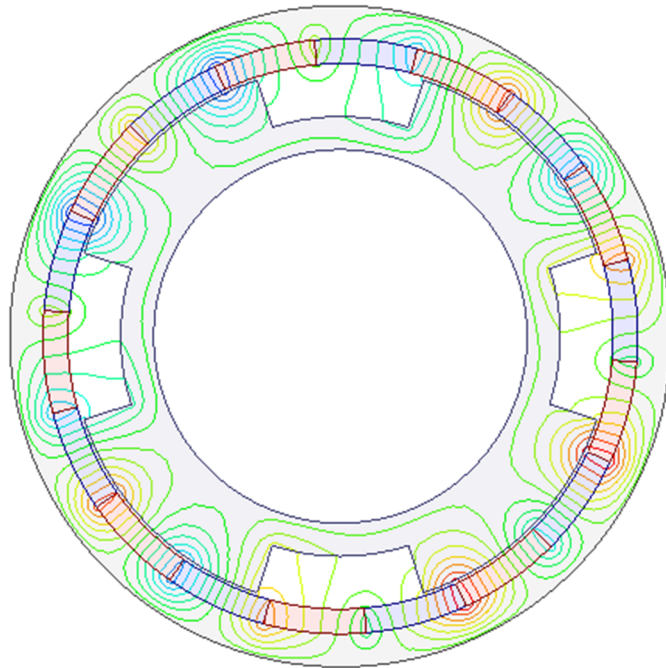
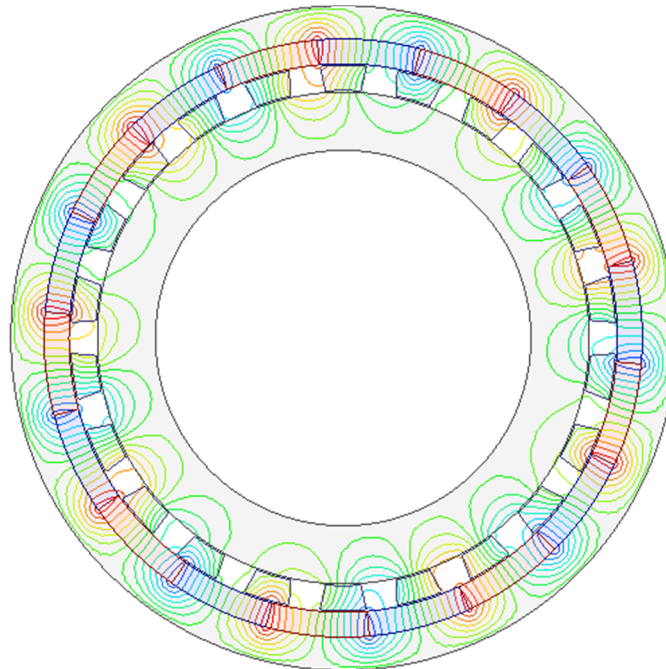


Figure 3.1: (a) Distribution of radial flux density in the inner air gap and (b) normalized FFT of the radial flux density in the inner air gap for the scenario 1 without Rotor 2 modulators and scenario 2 without Rotor 1 teeth in a coaxial reluctance magnetic gear. Reprinted with permission from [25].

Figure 3.2a illustrates the flux lines for the scenario without the Rotor 2 modulators that represents a noticeable flux line count in the air gap resulted by leakage and elimination of the modulators. Figure 3.2b illustrates the flux lines for the scenario without the Rotor 1 teeth, where the modulators provide a path from the flux created by the magnets to Rotor 1.



(a)



(b)

Figure 3.2: Flux lines for a structure with (a) a structure with no modulators and (b) a structure with no Rotor 1 teeth in a reluctance coaxial magnetic gear. Reprinted with permission from [25].

### 3.2 Reluctance Cycloidal Magnetic Gear

Rel CyMGs and SPM CyMGs have similar operating principles; however, a Rel CyMG's Rotor 1 teeth produce a permeance function instead of the MMF distribution produced by a Rel CyMG's Rotor 1 PMs. This is analogous to the replacement of an SPM CoMG's Rotor 1 PMs with teeth and slots to form a coaxial RMG [25]. The MMF produced by a Rel CyMG's Rotor 2 PMs is modulated once by the permeance function of the air gap to produce the flux distribution given by (3.16).  $\phi_{AG,2,0,k}$  is the set of flux spatial harmonics produced by the interaction of  $P_{AG,0}$  and  $F_{2,k}$ .  $\phi_{AG,2,j,k}$  is the set of flux spatial harmonics produced by the interaction of  $P_{AG,j}$  and  $F_{2,k}$ , as defined in (3.18). Similarly, the Rotor 1 teeth permeance modulates the Rotor 2 MMF to create the flux distribution given by (3.19).  $\phi_{1,2,0,k}$  is the set of flux spatial harmonics produced by the interaction of  $P_{1,0}$  and  $F_{2,k}$ .  $\phi_{1,2,i,k}$  is the set of flux spatial harmonics produced by the interaction of  $P_{1,i}$  and  $F_{2,k}$ , as defined in (3.21).  $N_1$  and  $PP_2$  represent the Rel CyMG Rotor 1 teeth and Rotor 2 PM pole pair counts.  $P_{AG,0}$  and  $P_{1,0}$  represent the air gap permeance and Rotor 1 permeance constant components.  $P_{AG,j}$ ,  $P_{1,i}$ , and  $F_{2,k}$  represent the air gap permeance, Rotor 1 permeance, and Rotor 2 MMF spatial harmonic components.  $\omega_{orb}$ ,  $\omega_{rot}$ , and  $\omega_2$  represent the inner rotor orbital speed, inner rotor rotational speed, and outer rotor rotational speed.  $\theta_{orb0}$ ,  $\theta_{rot0}$ , and  $\theta_{20}$  represent the initial angular positions of the inner rotor orbital motion, inner rotor rotational motion, and outer rotor rotational motion.

$$\phi_{AG,2}(\theta) = F_2(\theta)P_{AG}(\theta) = \phi_{AG,2,0,k}(\theta) + \phi_{AG,2,j,k}(\theta) \quad (3.16)$$

$$\phi_{AG,2,0,k}(\theta) = \sum_{k=1}^{\infty} ((F_{2,k}P_{AG,0})\cos(kPP_2(\theta - \omega_2t - \theta_{20}))) \quad (3.17)$$

$$\begin{aligned} \phi_{AG,2,j,k}(\theta) = \sum_{j=1}^{\infty} \sum_{k=1}^{\infty} & \left( \left( \frac{F_{2,k}P_{AG,j}}{2} \right) \cos \left( (kPP_2 \pm j) \left( \theta - \right. \right. \right. \\ & \left. \left. \left. \left( \frac{kPP_2\omega_2 \pm j\omega_{orb}}{kPP_2 \pm j} \right) t - \left( \frac{kPP_2\theta_{20} \pm j\theta_{orb,0}}{kPP_2 \pm j} \right) \right) \right) \right) \end{aligned} \quad (3.18)$$

$$\phi_{1,2}(\theta) = F_2(\theta)P_1(\theta) = \phi_{1,2,0,k}(\theta) + \phi_{1,2,i,k}(\theta) \quad (3.19)$$

$$\phi_{1,2,0,k}(\theta) = \sum_{k=1}^{\infty} ((F_{2,k}P_{1,0})\cos(kPP_2(\theta - \omega_2t - \theta_{20}))) \quad (3.20)$$

$$\begin{aligned} \phi_{1,2,i,k}(\theta) = \sum_{i=1}^{\infty} \sum_{k=1}^{\infty} & \left( \left( \frac{F_{2,k}P_{1,i}}{2} \right) \cos \left( (kPP_2 \pm iN_1) \left( \theta - \right. \right. \right. \\ & \left. \left. \left. \left( \frac{kPP_2\omega_2 \pm iN_1\omega_{rot}}{kPP_2 \pm iN_1} \right) t - \left( \frac{kPP_2\theta_{20} \pm i\theta_{rot,0}}{kPP_2 \pm iN_1} \right) \right) \right) \right) \end{aligned} \quad (3.21)$$

The gearing action is achieved by selecting the teeth and PM pole pair counts to match the pole count and speed of one harmonic in (3.18) with those of one harmonic in (3.21). This yields the relationship between  $N_1$  and  $PP_2$ , Rel CyMG given by (3.22), where  $k_a$  and  $k_b$  are odd integers, and  $i$  and  $j$  are integers and can be positive, 0, or negative. The speed relationship given by (3.23). Selecting  $k_a = 1$ ,  $k_b = -1$ ,  $j = -1$ , and  $i = 1$  yields (3.24) and (3.25). The maximum achievable gear ratio is given by (3.26), when Rotor 2 is stationary. The negative sign in (3.26) denotes that Rotor 1's rotation about its own axis is

in the opposite direction of its orbital revolution around Rotor 2's axis.

$$|k_a PP_2 + j| = |k_b PP_2 + iN_1| \quad (3.22)$$

$$\frac{k_a PP_2 \omega_2 + j \omega_{orb}}{k_a PP_2 + j} = \frac{k_b PP_2 \omega_2 + iN_1 \omega_{rot}}{k_b PP_2 + iN_1} \quad (3.23)$$

$$2PP_2 = N_1 + 1 \quad (3.24)$$

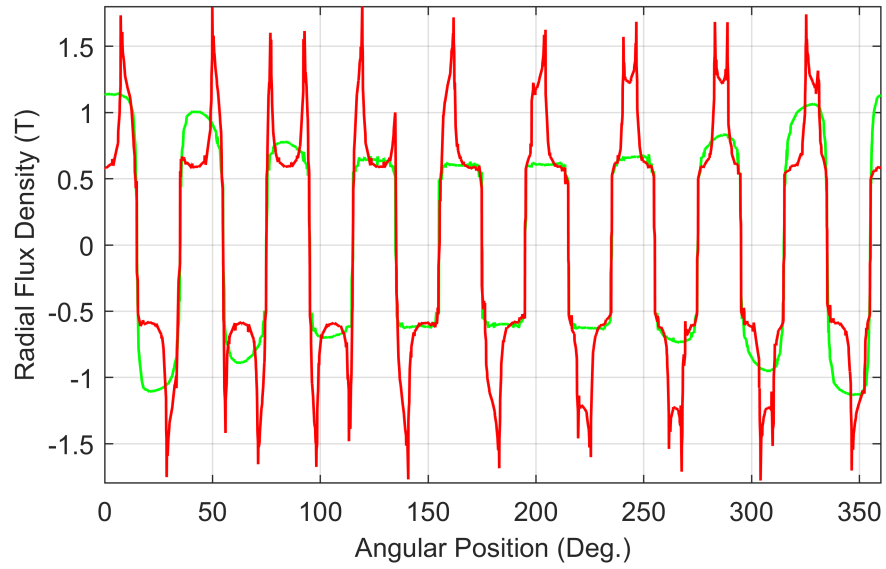
$$2PP_2 \omega_2 = N_1 \omega_{rot} + \omega_{orb} \quad (3.25)$$

$$Gear\ Ratio = \frac{\omega_{orb}}{\omega_{rot}} = -N_1 \quad (3.26)$$

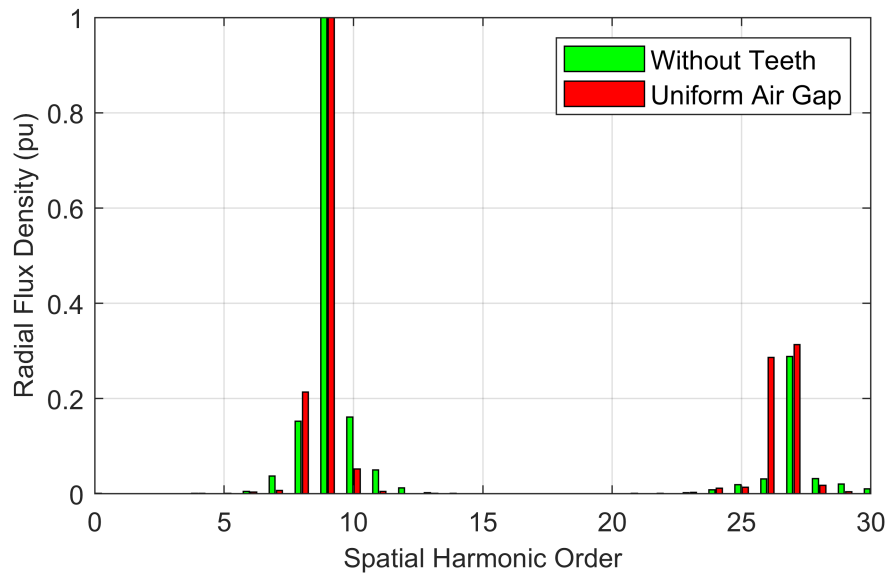
The figures below demonstrate the operating principle of a Rel CyMG with  $N_1 = 17$  and  $PP_2 = 9$ , resulting in a gear ratio of 17:1. In order to illustrate this operating principle, two scenarios were evaluated: the scenario with the Rotor 1 teeth present but no axis offset and the scenario with an axis offset but no Rotor 1 teeth. Figure 3.3a shows the air gap radial flux densities obtained for these two scenarios, and Figure 3.3b shows the normalized FFTs of these air gap radial flux densities. Both scenarios produce a large 9<sup>th</sup> harmonic component corresponding to  $PP_2$  and also an 8<sup>th</sup> harmonic component corresponding to  $|PP_2 - 1|$  or  $|PP_2 + N_1|$ . In this case, it is the interaction of these 8<sup>th</sup> harmonic components



that produces the gearing behavior.



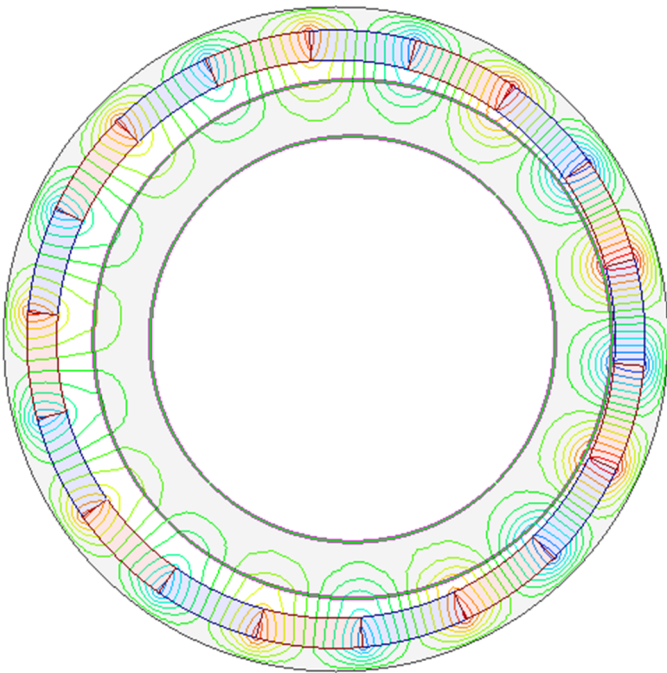
(a)



(b)

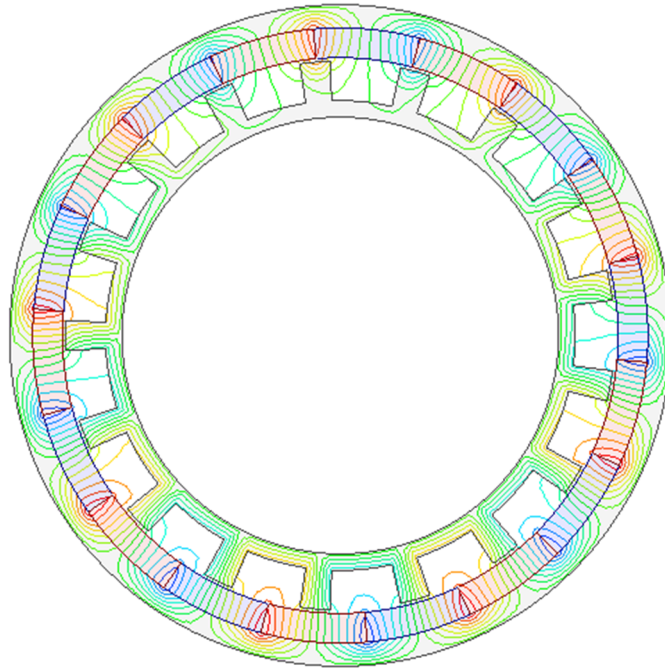
Figure 3.3: Air gap radial flux density (a) distribution and (b) FFT for a reluctance cycloidal magnetic gear with  $N_1 = 17$  and  $PP_2 = 9$  with an axis offset but no Rotor 1 teeth and with the Rotor 1 teeth present but a uniform air gap.

Figure 3.4a illustrates the flux lines for the scenario with an axis offset but no Rotor 1 teeth. Figure 3.4b illustrates the flux lines for the scenario with the Rotor 1 teeth present but no axis offset. Figure 3.4 represents the operating principle of Rel CyMG, where the effective torque is produced in the thin air gap part of the gear that a significant portion of the magnet fluxes close their path through Rotor 1.



(a)

Figure 3.4



(b)

Figure 3.4: Flux lines for a structure with (a) an axis offset but no Rotor 1 teeth and (b) the Rotor 1 teeth present but no axis offset in a reluctance cycloidal magnetic gear.

#### 4. COMPARISON OF COAXIAL RELUCTANCE AND SURFACE PERMANENT MAGNET MAGNETIC GEARS\* <sup>1</sup>

The performance of optimal coaxial RMGs are compared to optimal coaxial SPMGs, Figure 4.1. The operating principles of both topologies were illustrated in the previous chapters. This chapter uses significant 2D and 3D parametric sweeps to characterize the capabilities of coaxial RMGs and compare optimal coaxial RMGs against optimal coaxial SPMGs.

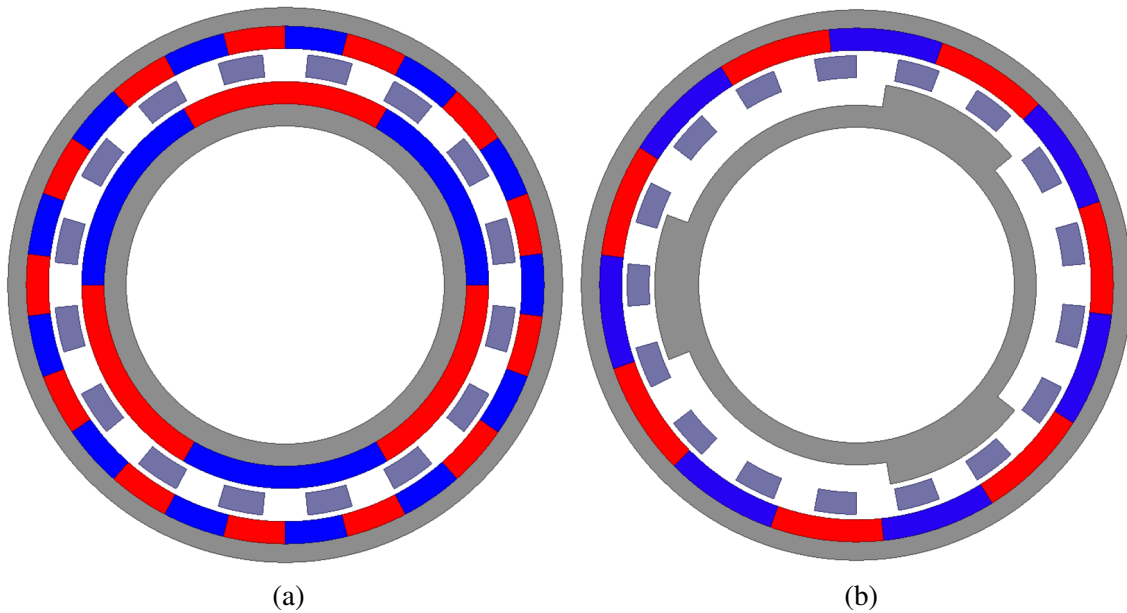


Figure 4.1: Cross-sections of (a) a coaxial SPMG and (b) a coaxial RMG. Reprinted with permission from [25].

<sup>1</sup>© 2020 IEEE. Part of this chapter is reprinted with permission from S. Hasanpour, M. C. Gardner, M. Johnson, and H. A. Toliyat, "Comparison of Reluctance and Surface Permanent Magnet Coaxial Magnetic Gears," in *Proc. IEEE Energy Convers. Congr. Expo.*, 2020, pp. 307-314.

#### 4.1 Design Study Methodology

Both the coaxial SPMG and the coaxial RMG topologies were evaluated using 2D FEA simulations at the slip torque alignment. The ferromagnetic components (back irons, Rotor 1 teeth, and modulators) are made of M47 steel (26 gauge), and NdFeB N42 is used for the magnets. Table 4.1 shows the design parameter values evaluated for each topology.

Table 4.1: Design parameters sweep ranges for the coaxial RMG and the coaxial SPMG. Reprinted with permission from [25].

Name	Description	Values	Units
$G_{Int}$	Integer part of the gear ratio	4, 6, 10, 16	
$R_{Out}$	Outer radius	100	mm
$T_{BI1}$	Rotor 1 back iron thickness	5, 10, 20	mm
$T_{BI3}$	Rotor 3 back iron thickness	5, 10, 20	mm
$T_{Mods}$	Modulators thickness	5, 10, 20	mm
$T_{PM1}$	SPMG Rotor 1 PM thickness	3, 6, 9, 12, 15	mm
$k_{PM}$	SPMG PM thickness ratio	0.5, 0.75, 1	
$T_{TH}$	RMG Rotor 1 teeth thickness	3, 6, 9, 12, 15	mm
$T_{PM3}$	RMG Rotor 3 PM thickness	3, 6, 9, 12, 15	mm
$\alpha_{TH}$	RMG teeth tangential fill factor	0.35, 0.4, ... 0.55	
$\alpha_{Mods}$	Modulator tangential fill factor	0.5	
$\alpha_{PM}$	PM tangential fill factor	1	
$T_{AG}$	Air gap thickness	0.5	mm
$L_{Stack}$	Stack length	20, 30, 50, 70	mm

Table 4.2 summarizes the values considered for the coaxial RMG tooth count and the coaxial SPMG Rotor 1 pole pair count for each  $G_{Int}$  value without including unnecessary suboptimal cases with high pole counts and high gear ratios.

Table 4.2: Rotor 1 tooth count for coaxial RMG and pole pair count for coaxial SPMG sweep ranges. Reprinted with permission from [25].

$G_{Int}$	Coaxial RMG	Coaxial SPMG
4	3, 4, ... 10	3, 4, ... 18
6	3, 4, ... 7	3, 4, ... 13
10	3, 4, 5, 6	3, 4, ... 9
16	3, 4, 5	3, 4, 5, 6

Reference [24] optimizes the shape and skew of the coaxial RMG teeth to reduce torque ripple; however, this study only evaluates arc-shaped modulators and magnets, as the alterations in [24] do not significantly increase the designs' slip torques. The different torque densities evaluated in this study are VTD, the Rotor 3 slip torque divided by the gear's total active volume (4.1), ST, the Rotor 3 slip torque divided the gear's total active mass (4.2), and PM ST , the Rotor 3 slip torque divided by the gear's total PM mass (4.3).

$$VTD = \frac{T_{slip}}{ActiveVolume} \quad (4.1)$$

$$ST = \frac{T_{slip}}{ActiveMass} \quad (4.2)$$

$$PMST = \frac{T_{slip}}{ActivePMMass} \quad (4.3)$$

After all designs specified in Tables 4.1 and 4.2 were evaluated using magnetostatic 2D FEA, the optimal designs were evaluated using magnetostatic 3D FEA at the stack lengths specified in Table 4.1 to investigate the end effect impacts on the torque. Additionally, 2D transient FEA was used to evaluate the electromagnetic efficiencies of the optimal designs. The gear ratio for both topologies is defined as the ratio of the Rotor 1 speed to the Rotor 3 speed with the modulators fixed, so (3.14) gives the gear ratio for coaxial RMGs. For coaxial SPMGs, (1.3) gives the gear ratio.

The Rotor 3 PM pole pair counts are derived from the parameters in Table 4.1 using (4.4) for coaxial SPMGs and (4.5) for coaxial RMGs to avoid integer gear ratios, which tend to result in designs with large torque ripple [1,40,41]. Substituting the  $PP_{3, coaxial SPMG}$  of equation (4.4) into (1.1) gives an even number of modulators for any combination of  $PP_1$  and  $G_{Int}$ , which ensures that the design has some symmetry. This symmetry cancels out unbalanced magnetic forces on the rotors. However, based on (4.5) and (3.13), a coaxial RMG design will only have symmetry if  $N_l$  is even.

$$PP_{3, coaxial SPMG} = \begin{cases} G_{Int}PP_1 + 1, & \text{for } (G_{Int} + 1)PP_1 \text{ odd} \\ G_{Int}PP_1 + 2, & \text{for } (G_{Int} + 1)PP_1 \text{ even} \end{cases} \quad (4.4)$$

$$PP_{3, coaxial RMG} = \begin{cases} 0.5(G_{Int}N_1 + 1), & \text{for } G_{Int}N_1 \text{ odd} \\ 0.5(G_{Int}N_1 + 2), & \text{for } G_{Int}N_1 \text{ even} \end{cases} \quad (4.5)$$

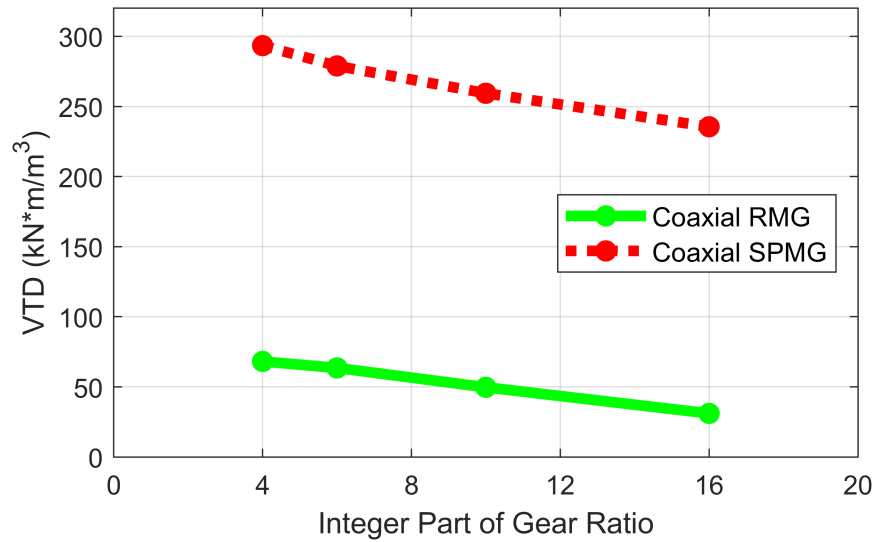
The PM thickness ratio ( $k_{PM}$ ) relates the thickness of the magnets on Rotor 3 ( $T_{PM3}$ ) to the thickness of the magnets on Rotor 1, ( $T_{PM1}$ ) for coaxial SPMGs according to (4.6). Rotor 1 has fewer poles than Rotor 3, so the optimal designs have thicker magnets on Rotor 1 [40, 42]; however, if the Rotor 1 magnets are too much thicker than the Rotor 3 magnets, then the Rotor 3 magnets may be demagnetized. Thus,  $k_{PM}$  is varied between 0.5 and 1.

$$T_{PM3} = k_{PM}T_{PM1} \quad (4.6)$$



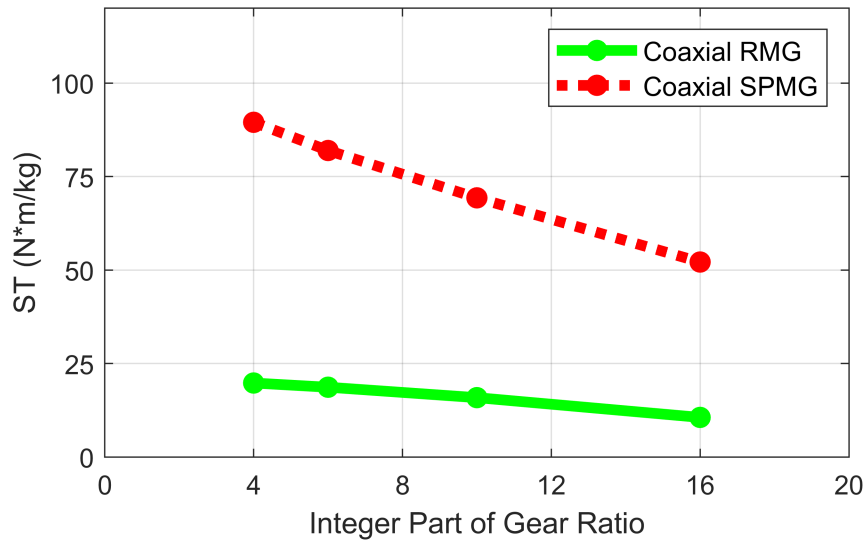
## 4.2 Results

Figure 4.2 illustrates that coaxial SPMGs outperform coaxial RMGs in terms of VTD, ST, and PM ST. While the coaxial RMG is expected to achieve lower VTD and ST than the coaxial SPMG, the reduced PM ST contradicts the assertions of a previous paper [43]. Even though the coaxial RMG has no PMs on Rotor 1, the associated reduction in torque outweighs the reduction in PM mass, so coaxial RMGs actually use PM material less effectively than coaxial SPMGs. Thus, a coaxial RMG can require at least 3 times as much PM material to get the same torque as a coaxial SPMG design based on Figure 4.2c, which implies the higher cost of coaxial RMGs than coaxial SPMGs, as long as the magnet cost rate is significantly greater than that of the steel, used for back irons, teeth, and modulators.

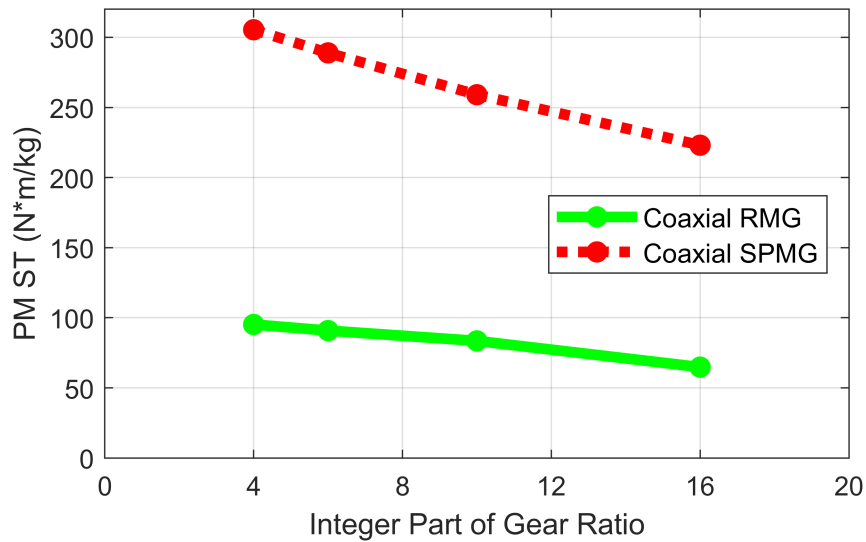


(a)

Figure 4.2



(b)

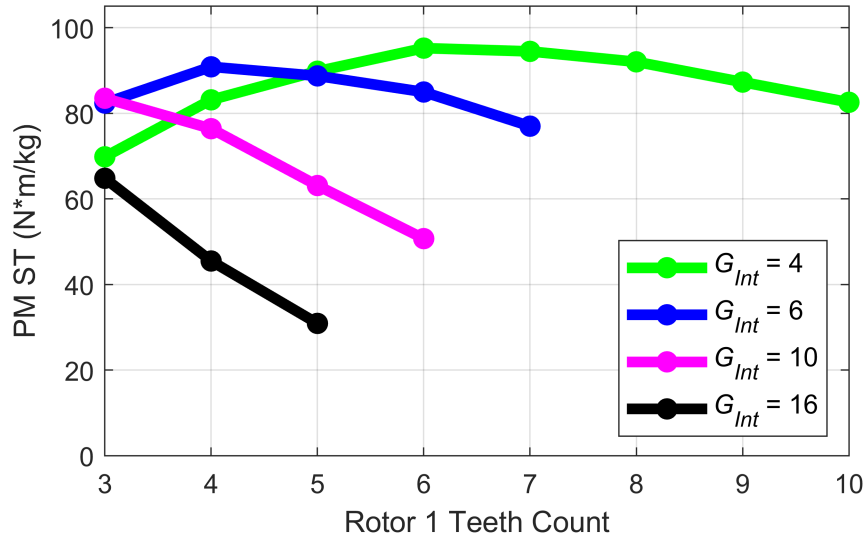


(c)

Figure 4.2: Impact of gear ratio on the achievable (a) VTD, (b) ST, and (c) PM ST for coaxial RMGs and coaxial SPMGs based on 2D simulations. Reprinted with permission from [25].

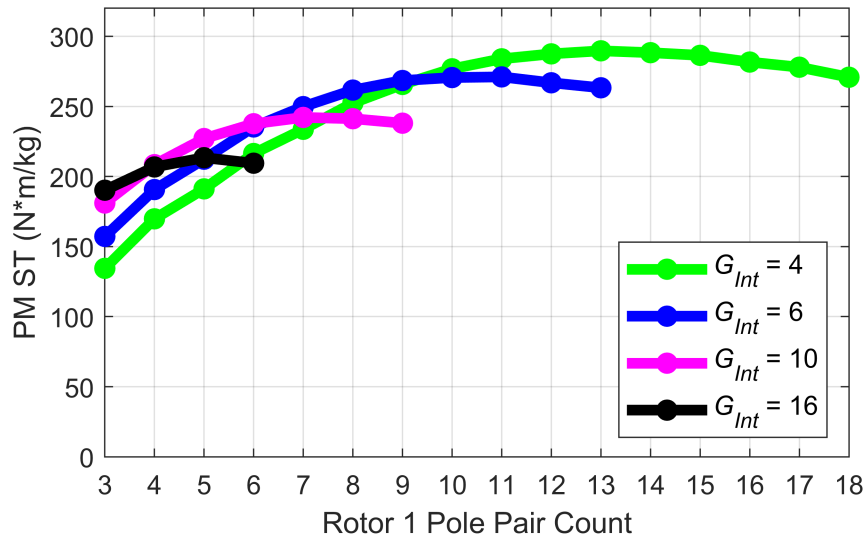
Figure 4.3 shows that, similarly to coaxial SPMG designs, coaxial RMG designs with larger gear ratios are optimized with fewer Rotor 1 teeth. However, for a given gear ratio,

the optimal coaxial RMG Rotor 1 teeth count is much lower than the optimal coaxial SPMG Rotor 1 pole pair count, which means that the optimal Rotor 3 pole pair and Rotor 2 modulator counts for a given gear ratio will also be lower for a coaxial RMG than for a coaxial SPMG. For a coaxial SPMG, increasing the gear ratio tends to reduce the optimal  $PP_1$  and increase the optimal  $PP_3$ , coaxial SPMG, resulting in PM pole counts that are farther from the optimal values that would be selected for a similar design with a 1:1 gear ratio. However, the coaxial RMG has only one set of magnets to be optimized for any certain gear ratio, avoiding the conflict between the optimal values of  $PP_1$  and  $PP_3$ , coaxial SPMG that reduces the torque densities of SPMGs with higher gear ratio. Therefore, the optimal  $PP_3$  value for a coaxial RMG can be maintained by reducing  $N_1$  as the gear ratio increases. However, reducing  $N_1$  to a value of 1 or 2 results in an integer gear ratio, which can produce excessive torque ripples [1], so these designs were not simulated, even though they might produce the optimal PM STs for coaxial RMGs with larger gear ratios at this outer radius.



(a)

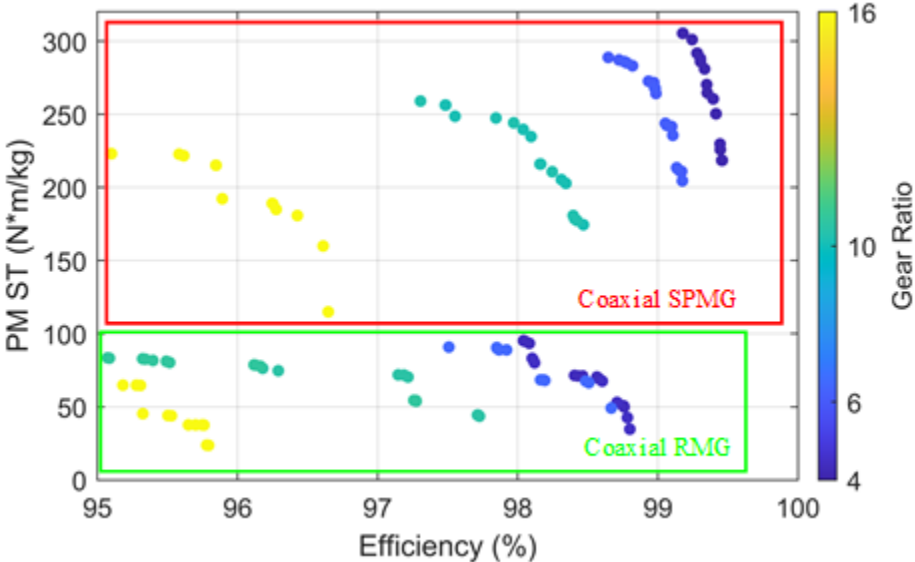
Figure 4.3



(b)

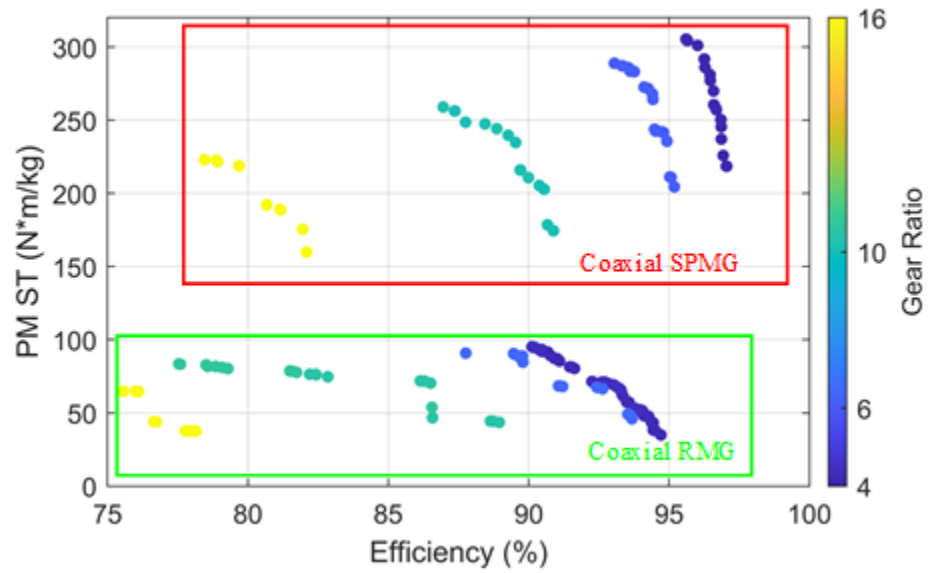
Figure 4.3: Impact of (a) coaxial RMG Rotor 1 teeth count and (b) coaxial SPMG Rotor 1 pole pair count on the achievable PM ST of designs with  $G_{Int}$  based on 2D simulations. Reprinted with permission from [25].

A previous paper suggested that the elimination of the PM eddy currents from Rotor 1 may make a coaxial RMG more efficient than a coaxial SPMG [27]. This is not generally accurate, as demonstrated by Figure 4.4, which illustrates the Pareto optimal fronts of the coaxial RMGs and coaxial SPMGs that maximize full load electromagnetic efficiency and PM ST with Rotor 3 speeds of 100, 1000, and 5000 rpm. At each speed, the optimal coaxial SPMG designs are significantly more efficient than the optimal coaxial RMG designs. Of course, the losses in either type of gear could be reduced by segmenting the PMs or by using a less lossy grade of steel. These changes might affect coaxial RMGs and coaxial SPMGs differently, due to different loss distributions. Nonetheless, the coaxial RMG's efficiency is limited by the fact that it requires significantly more steel and PM material to achieve the same torque as an optimal coaxial SPMG.

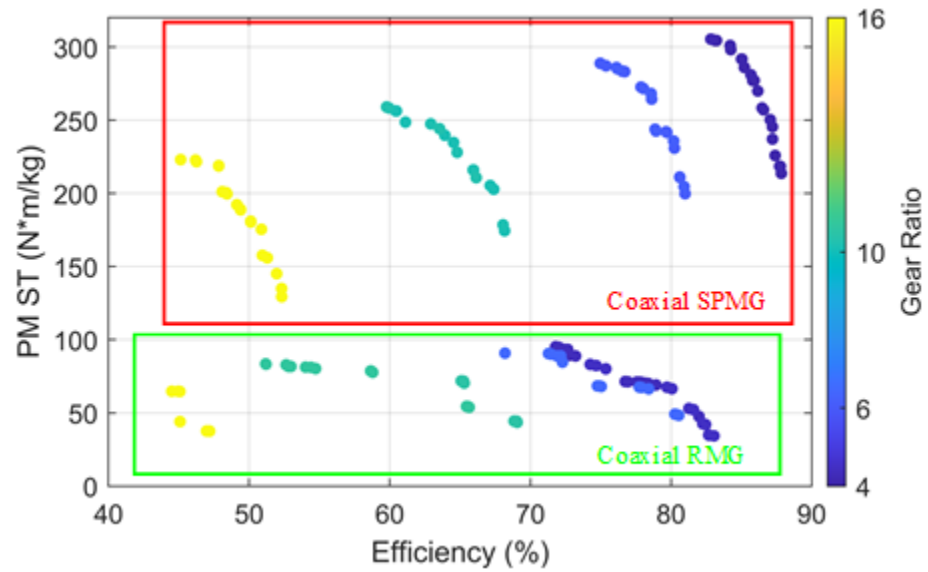


(a)

Figure 4.4



(b)

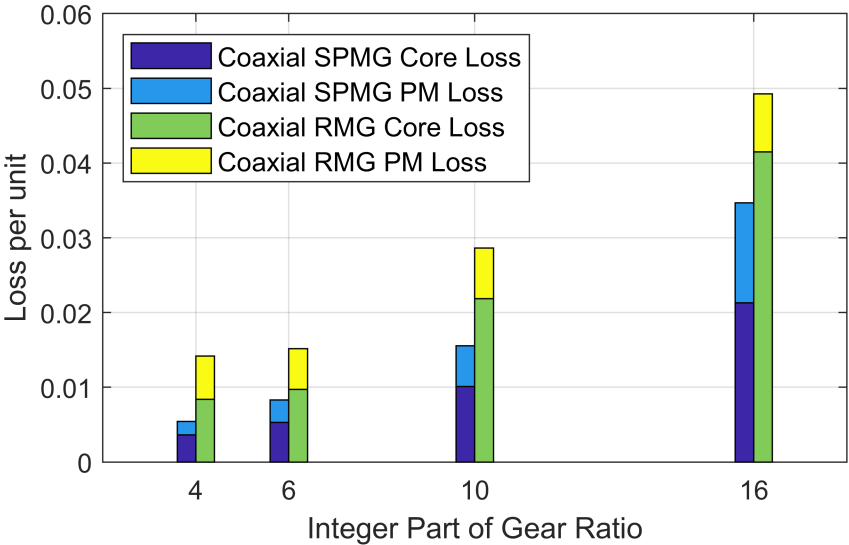


(c)

Figure 4.4: Pareto optimal fronts maximizing PM ST and full load electromagnetic efficiency at Rotor 3 speeds of (a) 100 rpm, (b) 1000 rpm, and (c) 5000 rpm for coaxial RMGs and coaxial SPMGs with different gear ratios based on 2D simulations. Reprinted with permission from [25].

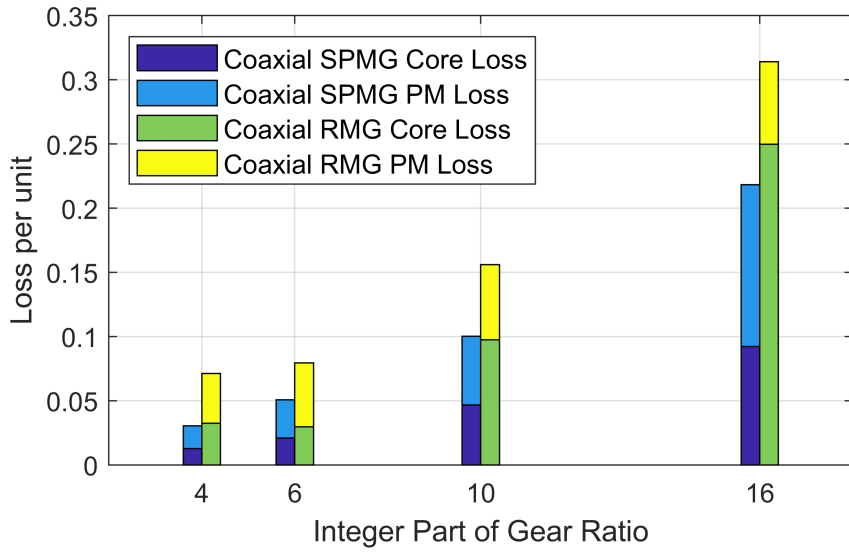
Figure 4.5 shows how the losses in both topologies correspond to the change of Rotor

3 speed in the most efficient designs that were simulated. The loss per unit parameter has been defined as the ratio of the losses to the output power. As the speed increases, both gears experience higher losses, but the loss distribution is different. While the presence of the Rotor 1 PMs in coaxial SPMGs does result in an additional source of losses, the overall efficiencies of the coaxial SPMGs are higher than those of the coaxial RMGs because the coaxial SPMGs can produce significantly more torque with the same amount of active material.

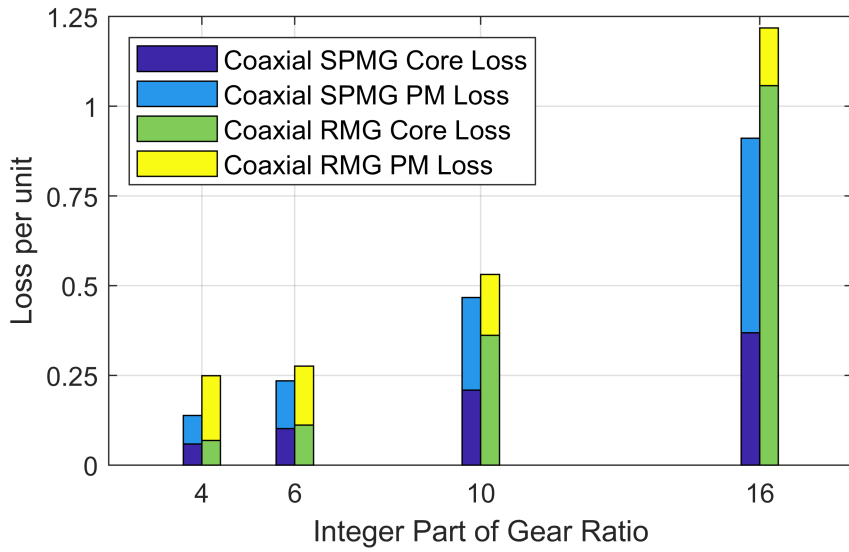


(a)

Figure 4.5



(b)



(c)

Figure 4.5: Corresponding loss amplitude for the designs with maximum efficiency at Rotor 3 speeds of (a) 100 rpm, (b) 1000 rpm, and (c) 5000 rpm, for coaxial RMGs and coaxial SPMGs with different gear ratios, based on 2D simulations. Reprinted with permission from [25].

The PMs experience eddy current losses, which increase quadratically with the speed.



The core losses in the back irons, modulators, and Rotor 1 teeth have two components, eddy current losses and hysteresis losses, which are proportional to the square of the frequency and to the frequency itself, respectively. Since the coaxial RMG has no Rotor 1 PMs, the most efficient coaxial RMG design experiences a lower percentage of its losses as PM losses than the optimal coaxial SPMG design. However, the coaxial RMG tends to suffer significantly larger per unit core losses because it requires significantly more core material to produce the same torque as a coaxial SPMG. Thus, even at a Rotor 3 speed of 5000 rpm, the most efficient coaxial RMG is still less efficient than the most efficient coaxial SPMG.

While [27] compares two non-optimized designs and concludes that the torque ripple in the coaxial RMG is higher than it is in the coaxial SPMG, the choice of an integer gear ratio results in very large torque ripples, which may not be representative of designs with non-integer gear ratios. To determine whether this is the case for optimized designs, the torque ripple is evaluated for the coaxial RMG and coaxial SPMG designs with the maximum VTD or PM ST for  $G_{Int} = 4$ , using 2D FEA. Rotor 2 is fixed, and Rotors 1 and 3 are rotated at the maximum torque orientation according to the gear ratio. Figure 4.6 shows the torque on both rotors and reveals that the torque ripple on Rotor 1 tends to be much larger than the torque ripple on Rotor 3, even though the average torque on Rotor 1 is much lower than the average Rotor 3 torque, as found in [41]. Additionally, the optimal coaxial RMG designs have much more significant torque ripples than the optimal coaxial SPMG designs.

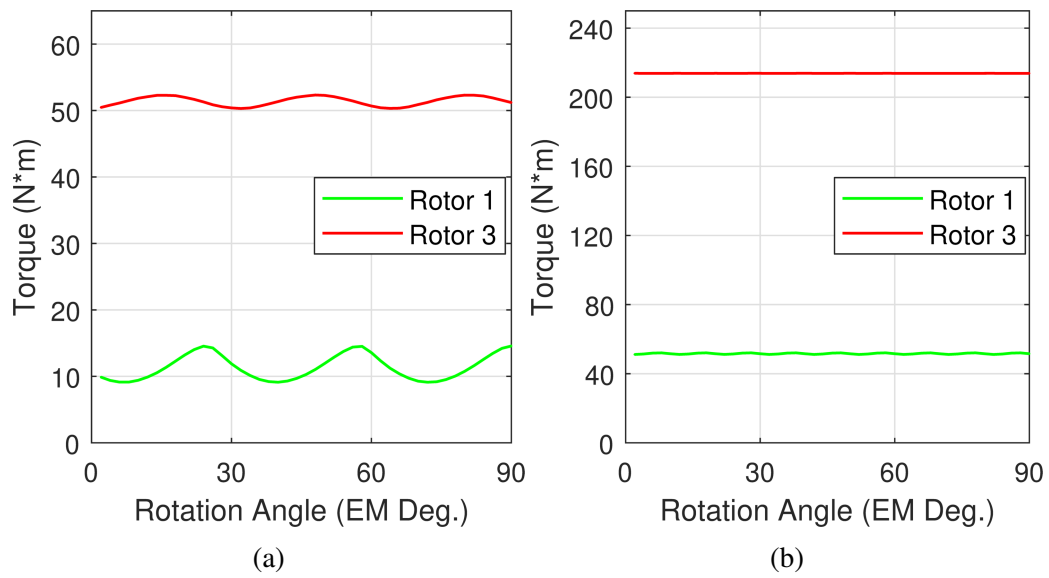


Figure 4.6

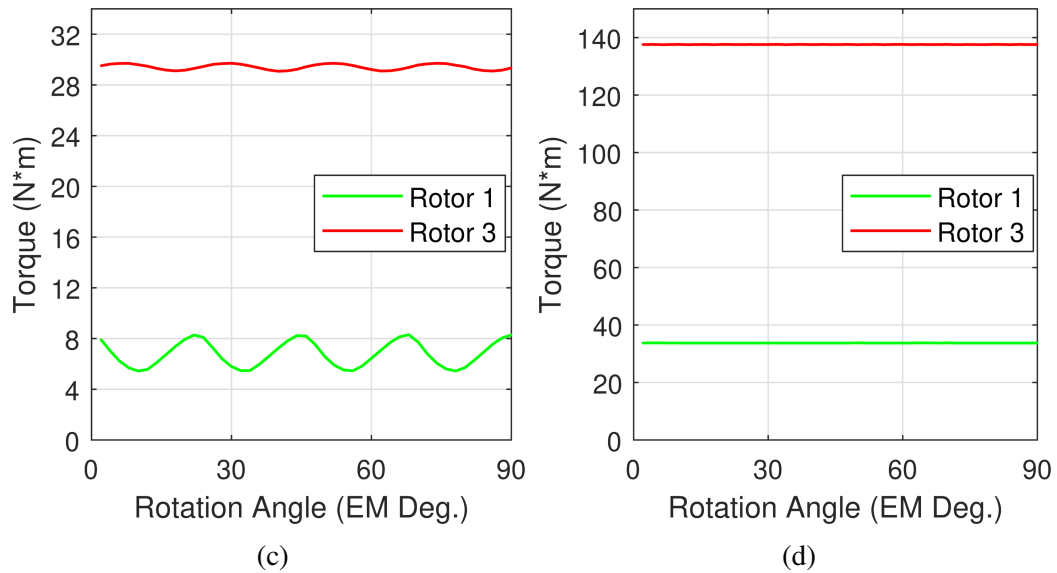


Figure 4.6: Rotor 1 and Rotor 3 torque ripple characteristic for continuous operation at the maximum torque orientation of (a) the coaxial RMG with maximum VTD, (b) the coaxial SPMG with maximum VTD, (c) the coaxial RMG with maximum PM ST, and (d) the coaxial SPMG with maximum PM ST based on 2D simulations. Reprinted with permission from [25].

Figure 4.7 illustrates the corresponding torque ripple percentages for the coaxial RMG and SPMG designs with the maximum PM ST in Figure 4.3. The torque ripple percentage is defined as the ratio of the peak-to-peak torque ripple of each rotor to its average torque. For both topologies, the torque ripple tends to decrease as the number of Rotor 1 pole pairs or teeth increases. In a design with a fixed gear ratio, as the Rotor 1 pole count or teeth count increases,  $Q_2$  and  $P_3$  will also increase, so there will be lower torque ripple percentages due to the higher values of the LCM of the pole counts of the two rotating rotors [1]. Thus, one reason that the coaxial RMG designs of Figure 4.6 have higher torque ripples than the coaxial SPMG designs is that the optimal coaxial RMG Rotor 1 tooth counts tend to be lower than the optimal coaxial SPMG Rotor 1 pole pair counts.

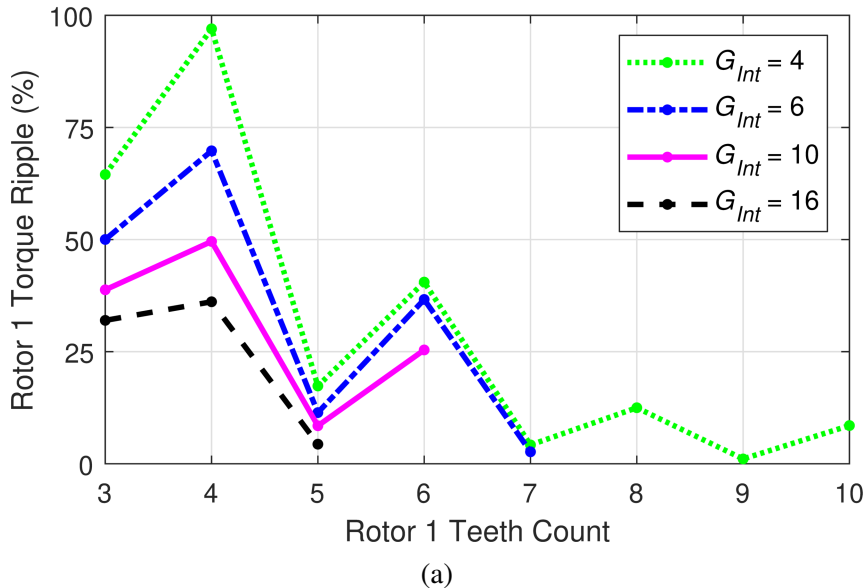
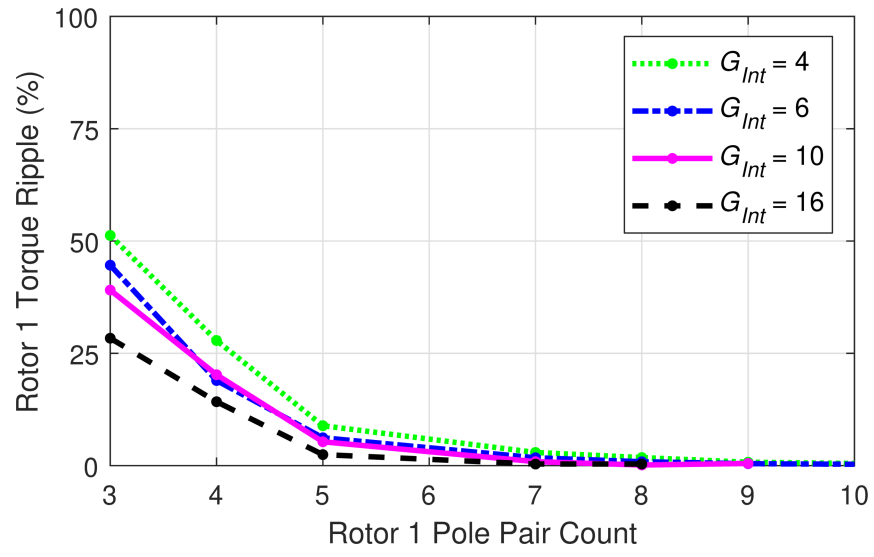
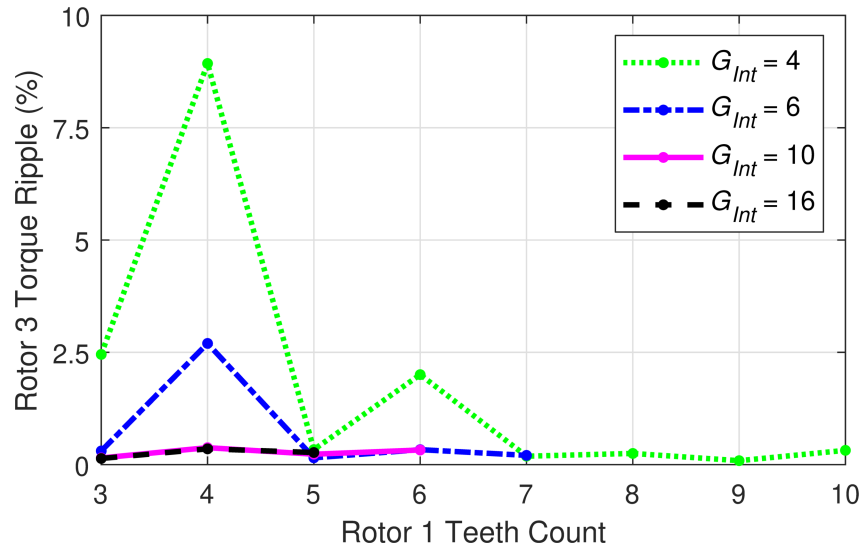


Figure 4.7



(b)



(c)

Figure 4.7

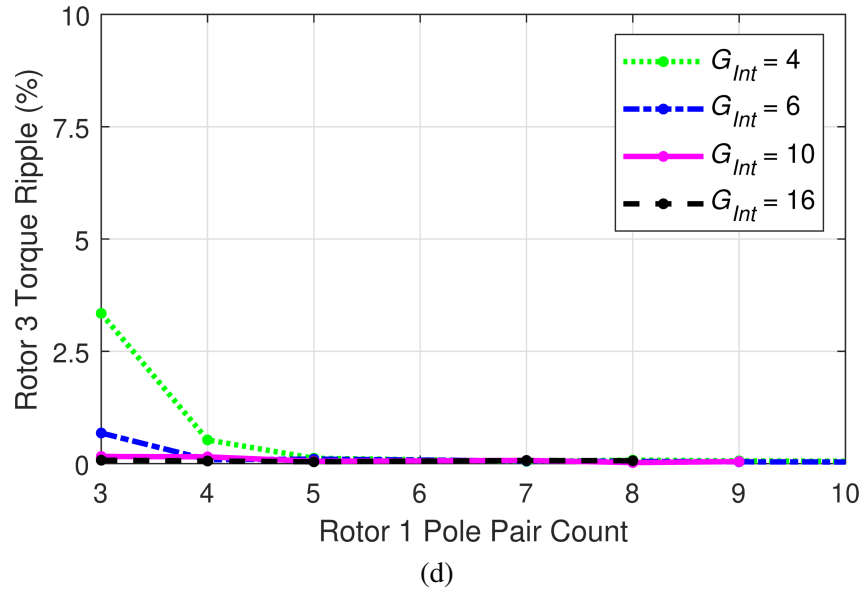


Figure 4.7: Corresponding Rotor 1 torque ripple percentages for the coaxial (a) RMG and (b) SPMG designs with maximum PM ST and corresponding Rotor 3 torque ripple percentages for the same coaxial (c) RMG and (d) SPMG designs based on 2D simulations. Reprinted with permission from [25].

In Figures 4.7a and 4.7c, the coaxial RMG designs with even Rotor 1 tooth counts exhibit significantly larger torque ripples than the designs with odd tooth counts. Based on (3.12) and (4.5), these designs with even Rotor 1 tooth counts have symmetry, while the designs with odd tooth counts do not have symmetry. Designs with symmetry tend to experience larger torque ripple percentages [1]. For both topologies, lower gear ratios tend to produce higher torque ripple percentages for a fixed Rotor 1 tooth count or pole count due to the lower LCM of the pole counts [1]. As the gear ratio or the pole counts increase, both topologies tend to exhibit very small torque ripples.

Comparing Figures 4.7b and 4.7d with Figures 4.7a and 4.7c reveals that, for both

topologies at any gear ratio, Rotor 3 exhibits a much smaller torque ripple percentage than Rotor 1 because of higher pole counts and larger average torques. In both topologies, the Rotor 3 torque ripple percentage becomes negligible as the gear ratio or Rotor 1 teeth or pole count is increased.

The opposing sets of magnets facing each other in coaxial SPMGs produce significant axially escaping flux, which reduces the torque [44]. Thus, since coaxial RMGs only have a single set of PMs, coaxial RMGs might experience less of a reduction in torque than coaxial SPMGs when simulated in 3D. To investigate this hypothesis, a subset of the designs with maximum PM ST and minimum torque ripple for both topologies were simulated as 3D models. The stack length was varied from 20 to 70 mm, according to Table 4.1. Figure 4.8 shows the designs with maximum PM ST and their corresponding ratio of 3D torque over 2D torque for different gear ratios and stack lengths. Figures 4.8a and 4.8b indicate that higher PM ST is obtained in designs with lower gear ratios. Comparing Figures 4.8c and 4.8d disproves the hypothesis that the coaxial RMGs may suffer significantly less end effects than coaxial SPMGs with the same gear ratios and stack lengths. For the designs with a stack length of 20 mm, the coaxial RMG torque predicted by the 3D model is less than 75% of the 2D model prediction, while most of the coaxial SPMGs experience less than a 20% reduction when the 3D model is used. The optimal coaxial RMG design for any gear ratio has fewer Rotor 3 pole pairs than the optimal coaxial SPMG design. The lower the pole count, the further the flux must travel to close its path, which results in more torque reduction in 3D. However, due to the coaxial

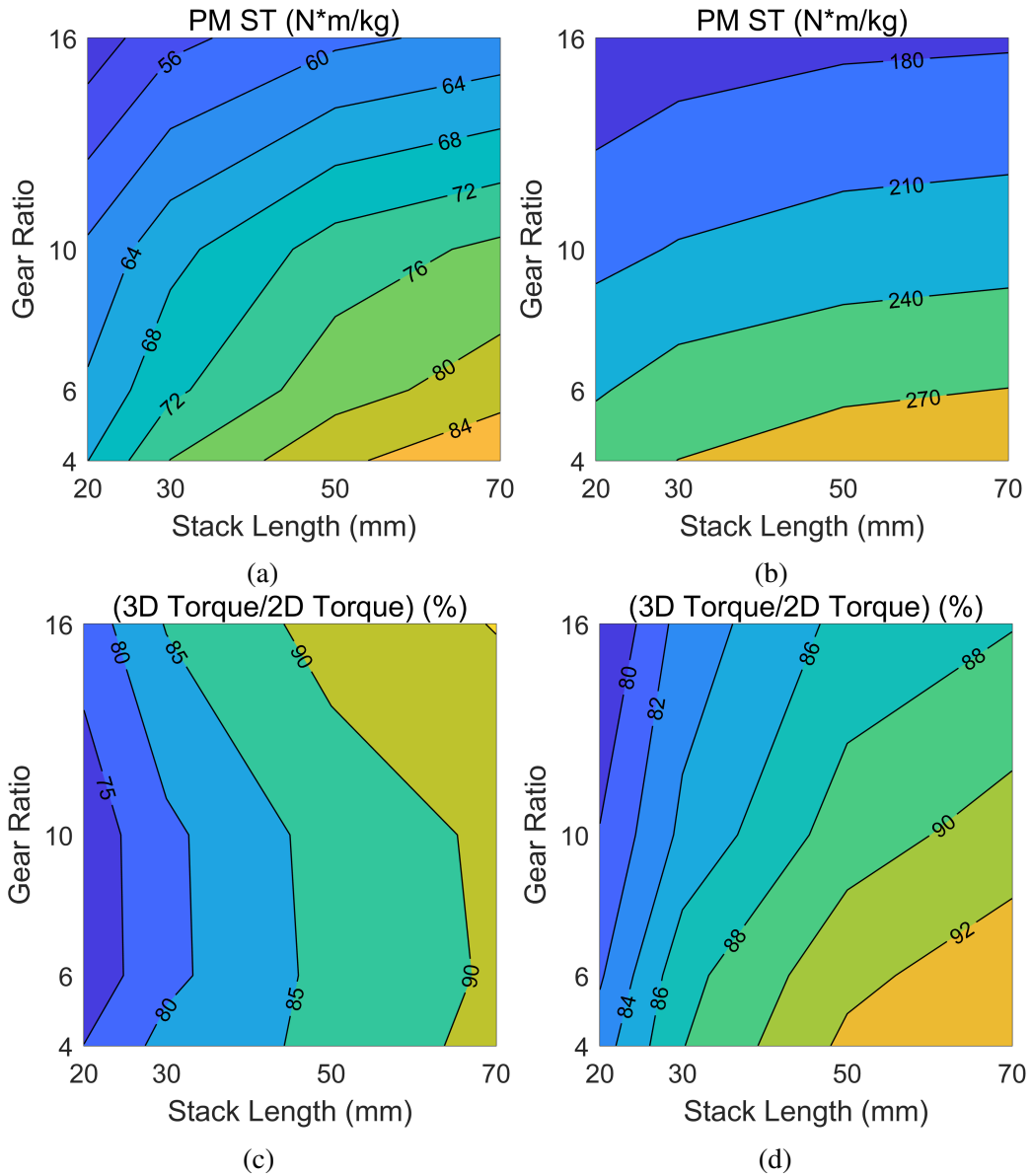


Figure 4.8: Variation of the maximum achievable PM ST based on 3D simulations for coaxial (a) RMGs and (b) SPMGs and the corresponding ratio of 3D simulation torque to 2D simulation torque for these coaxial (c) RMGs and (d) SPMGs. Reprinted with permission from [25].

RMGs' lower VTDs, they may require longer stack lengths than coaxial SPMGs to achieve a target torque for a fixed outer diameter; in this case, the longer stack length required by a coaxial RMG would make its end effects less significant.

Figures 4.2 and 4.3 also indicate that the coaxial RMG experiences a slightly smaller reduction in performance than the coaxial SPMG as the gear ratio increases, at least in the range where the optimal coaxial RMG Rotor 1 teeth count was simulated. Thus, especially at large radii, the coaxial RMG might become a more reasonable option for situations requiring a very large gear ratio in a single stage. Therefore, to obtain the results shown in Figure 4.9, the gear ratio of 30 was added and the outer radius was increased to 300 mm. Figure 4.9 shows that the coaxial RMG's PM ST varies less with gear ratio than the coaxial SPMG's PM ST. As the integer portion of the gear ratio increases from 4 to 30, the achievable PM ST decreases by approximately 8 for the coaxial RMG and 36 for the coaxial SPMG. The semi-constant performance of coaxial RMGs for any gear ratio might be interesting for specific applications. However, even at the gear ratio of approximately 30, the coaxial SPMG can still achieve significantly higher torque densities than the coaxial RMG.



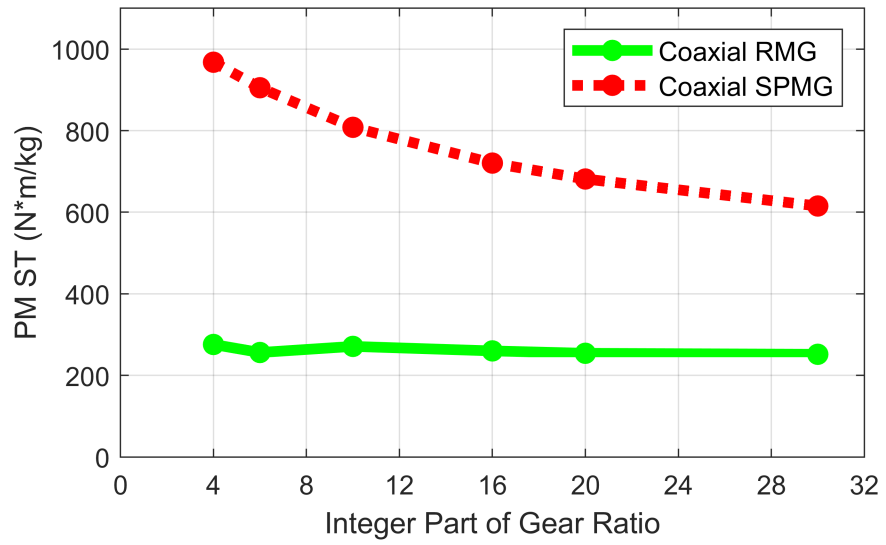


Figure 4.9: Impact of gear ratio on PM ST at a 300mm outer radius based on 2D simulations. Reprinted with permission from [25].

### 4.3 Conclusion

The coaxial RMG topology replaces the magnets on the high-speed rotor with a reluctance structure. The operating principle of a coaxial RMG is similar to that of a coaxial SPMG, and its governing equations are derived in this study. The performance capabilities of the coaxial RMG and SPMG topologies are compared. An extensive parametric evaluation was used to independently optimize the coaxial RMG and SPMG topologies for maximum VTD, PM ST, and ST based on 2D and 3D FEA simulations. It is shown that the magnet utilization of an optimized coaxial RMG is significantly less than that of an optimized coaxial SPMG, so the coaxial RMG may use on the order of 3 times as much magnet material to achieve a target torque. Also, due to its low torque density, a coaxial RMG may require about 5 times as much active volume as a coaxial SPMG to achieve the same torque. Furthermore, the efficiency comparison for the optimal designs of both topologies shows that the coaxial SPMGs outperform the coaxial RMGs across a wide range of speeds. The magnet utilization and efficiency results disagree with the proposed benefits of coaxial RMGs for high speeds touted based on comparisons of nonoptimized designs in other papers. The coaxial RMGs remove a set of magnets, but their inability to achieve a comparable torque density to coaxial SPMGs makes them require thicker magnets or a longer stack length. The transient simulations show that removing the magnets from the high-speed rotor does not improve the efficiency because the coaxial RMGs require more core material to provide a desired torque.

Additionally, the torque ripples of both structures are shown for the optimal VTD and

PM ST designs. The optimal coaxial RMG designs tend to have lower Rotor 1 teeth counts compared to the Rotor 1 pole counts of the optimal coaxial SPMGs. Thus, the coaxial RMGs have fewer poles on Rotor 3, which reduces the LCM of the pole counts and produces higher torque ripples on the rotors. Additionally, the lower pole counts of coaxial RMGs produces longer flux paths. Thus, even though coaxial RMGs lack the opposing sets of magnets, which produce axially escaping flux, coaxial RMGs suffer comparable torque reductions from end effects as coaxial SPMGs with similar diameters and stack lengths.

Simulations also revealed that the torque densities of coaxial RMGs vary less with gear ratio than those of coaxial SPMGs. Nonetheless, even at a gear ratio of 30 and a large outer radius, coaxial SPMGs were still able to achieve a better magnet utilization than coaxial RMGs.

Based on the results, it is evident that the coaxial SPMG topology can outperform the coaxial RMG topology in terms of torque density, efficiency, and torque ripple. Although the coaxial SPMG has magnets on the high-speed rotor, which incur eddy current losses and result in potential mechanical challenges at high speeds, the coaxial SPMG can provide a target torque in a smaller volume and a lighter mass with a more efficient design, which also uses the magnets more effectively. Thus, coaxial RMGs may only be suitable for applications where environmental or mechanical constraints prohibit the use of magnets on the high-speed rotor.

5. CYCLOIDAL RELUCTANCE MAGNETIC GEARS FOR HIGH GEAR RATIO APPLICATIONS

This study compares the performances of optimal SPM CoMGs, SPM CyMGs, and Rel CyMGs as shown in Figure 5.1, across a range of gear ratios using a GA and parametric 2D FEA simulations.

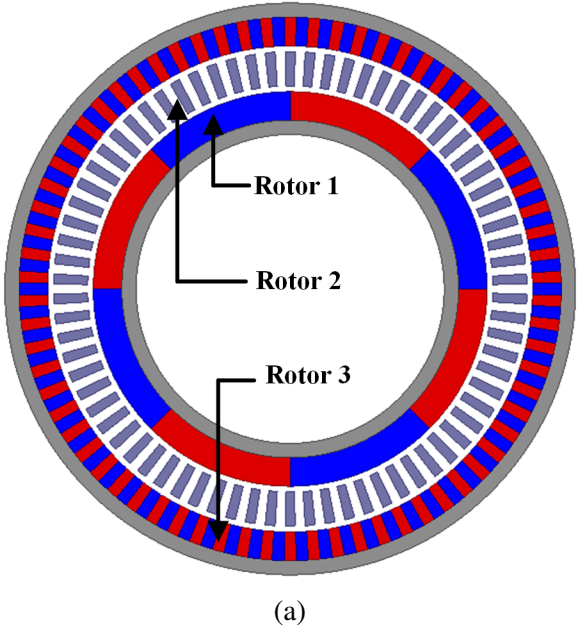
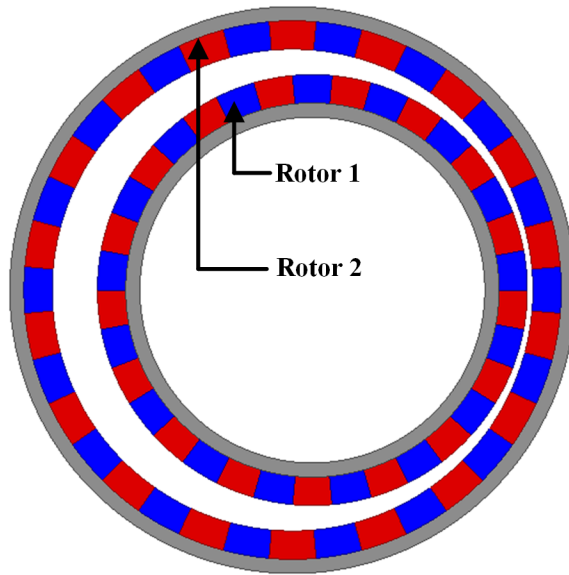
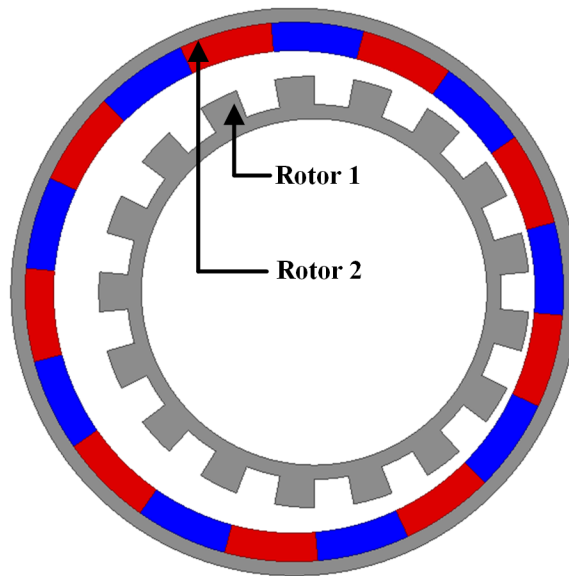


Figure 5.1



(b)



(c)

Figure 5.1: Cross-sections of (a) an SPM CoMG, (b) a SPM CyMG, and (c) a Rel CyMG for gear ratios of 17.5:1, 17:1, and 17:1, respectively.

## 5.1 Design Study Methodology

A GA was used to independently optimize SPM CoMGs, SPM CyMGs, and Rel CyMGs for ST and PM ST across gear ratios ranging from approximately 5:1 to 51:1, considering odd gear ratios to obtain feasible Rotor 2 pole pair counts in Rel CyMGs. In each optimization, the GA used 2D FEA to optimize a population of approximately 1000 designs over 100 generations with the objective of maximizing ST and PM ST across this range of gear ratios. The minimum air gap was fixed at 1 mm; however, the Rel CyMG designs were also optimized using a 0.75 mm minimum air gap because Rel CyMGs do not have any PMs on Rotor 1, thus they do not require a PM retention sleeve on Rotor 1, which might enable the use of a smaller effective air gap. Table 5.1 summarizes these different scenarios. A broad range of values was considered for each design parameter as listed in Table 5.2. NdFeB N45 UH was used for the PMs and Hiperco 50 was used for the back irons, modulators, and teeth.

The gear ratio in SPM CoMG topologies is defined as the ratio of the Rotor 1 speed to the Rotor 2 speed with the Rotor 3 fixed, given by (1.2). The PM pole pair count on Rotor 1 of SPM CoMGs was considered to vary in the range of 3 to 15. To avoid integer gear ratios, which results in designs with significant torque ripple [3, 40, 41], the PM pole pair counts on Rotor 3 were derived using (4.4). All the considered designs have some symmetry, which cancels out unbalanced magnetic forces on the rotors, since utilizing equations (1.1) and (4.4) ensure an even number of modulators for any design combination. CoMGs with only 1 or 2 pole pairs with Rotor 1 were not included because

they could not simultaneously achieve non-integer gear ratios and symmetry.

Table 5.1: Legend for Different Design Configurations Characterized in Figures 5.2 and 5.3





				
	Rel CyMG	Rel CyMG	SPM CyMG	SPM CoMG
Air Gap (mm)	0.75	1	1	1

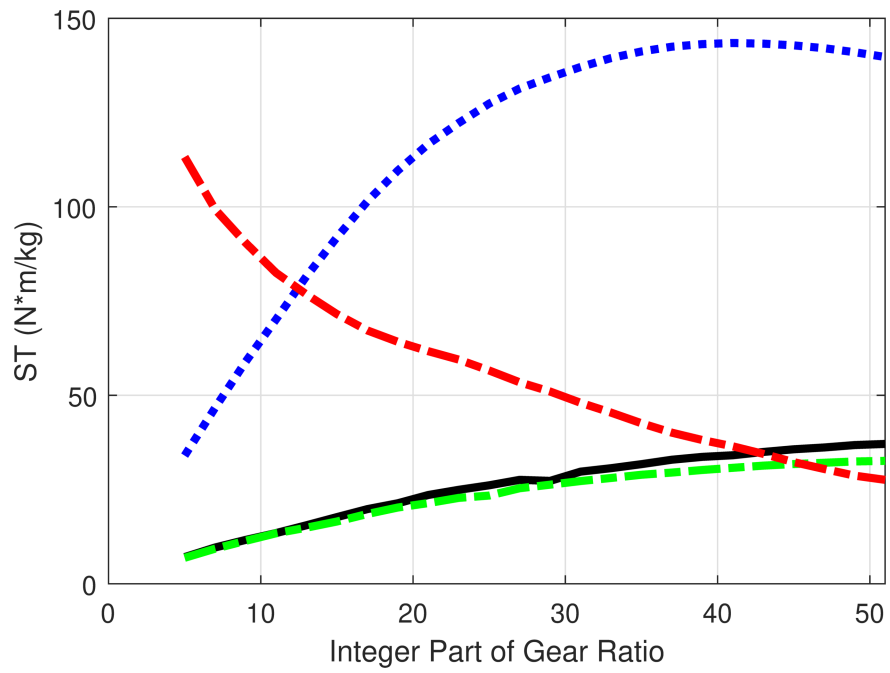
Table 5.2: GA Parameter Value Ranges.

Name	Description	Values	Units
$G_{Int}$	SPM CoMG integer part of the gear ratio	5, 7, ...51	
$G$	Rel CyMG and SPM CyMG gear ratio	5, 7, ...51	
$R_{Out}$	Outer radius	100	mm
$T_{BI,In}$	Inner rotor back iron radial thickness	2 – 15	mm
$T_{PM,In}$	SPM CyMG and SPM CoMG inner rotor PM radial thickness	3 – 20	mm
$T_{TH,In}$	Rel CyMG inner rotor teeth radial thickness	3 – 20	mm
$\alpha_{PM,In}$	SPM CyMG and SPM CoMG inner rotor PM tangential fill factor	0.1 – 1	
$\alpha_{TH,In}$	SPM CyMG and SPM CoMG inner rotor PM tangential fill factor	0.1 – 1	
$T_{off}$	Rel CyMG and SPM CyMG Axis offset	0.5 – 20	mm
$T_{Mods}$	SPM CoMG modulators radial thickness	3 – 20	mm
$\alpha_{Mods,In}$	SPM CoMG modulators tangential fill factor	0.7 – 1.3	
$T_{PM,Out}$	Outer rotor PM radial thickness	3 – 20	mm
$\alpha_{PM,Out}$	Outer rotor PM tangential fill factor	0.01 – 1	
$T_{BI,Out}$	Outer back iron radial thickness	2 – 15	mm

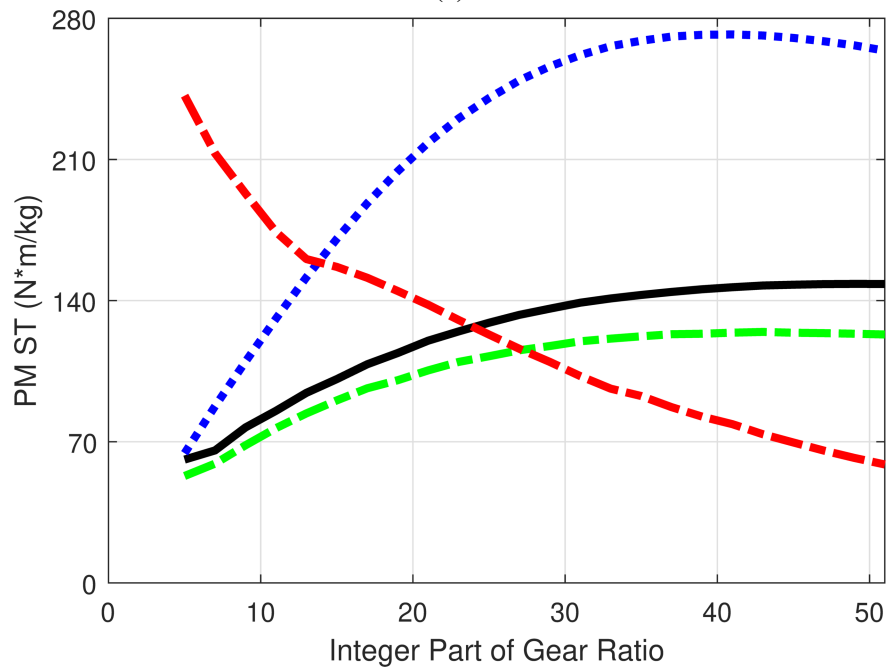
## 5.2 Results

Figure 5.2 illustrates that an SPM CoMG can achieve higher ST and PM ST than an SPM CyMG or a Rel CyMG at low gear ratios; however, as the gear ratio increases, the maximum achievable ST and PM ST decrease for the SPM CoMG and increase for the SPM CyMG and Rel CyMG. The higher achieved PM STs at high gear ratios by SPM CoMGs demonstrate their lower cost as they use the magnets more effectively. SPM CoMGs perform better at lower gear ratios because their pole pair counts can be optimized based on the selected (approximate) gear ratio and lower gear ratios result in more similar pole counts on both rotors. More similar pole counts enable better simultaneous optimization of both rotors. However, the performance of an SPM CoMG decreases as the gear ratio increases because larger gear ratios result in increasingly dissimilar pole counts on both rotors, which leads to increasingly suboptimal pole counts on both rotors. The optimal SPM CoMG Rotor 1 pole count decreases to mitigate the extent to which the Rotor 3 pole count exceeds its optimal value as the gear ratio increases. This decreasing optimal Rotor 1 pole pair count (combined with the fact that pole pair count is a discrete value) results in the jagged portion of the optimal SPM CoMG Rotor 3 pole pair count curve in the low gear ratio region of Figure 5.3a. Once the optimal Rotor 1 pole pair count decreases to the minimum considered value, which is typically greater than 1 [45] (in this study it is 3), the optimal Rotor 3 pole pair count increases linearly with gear ratio to extremely high and suboptimal values, as shown in Figure 5.3a.



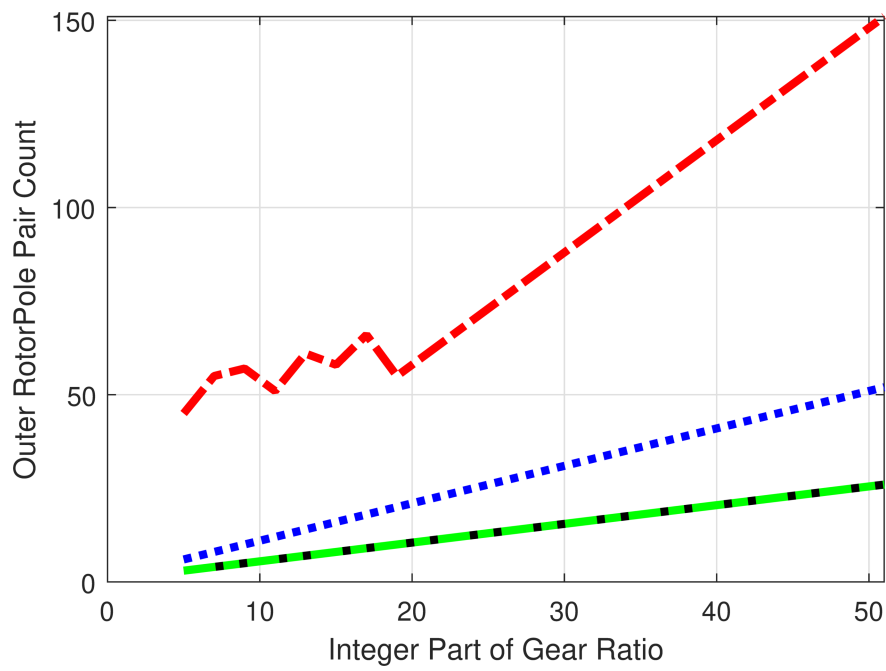


(a)

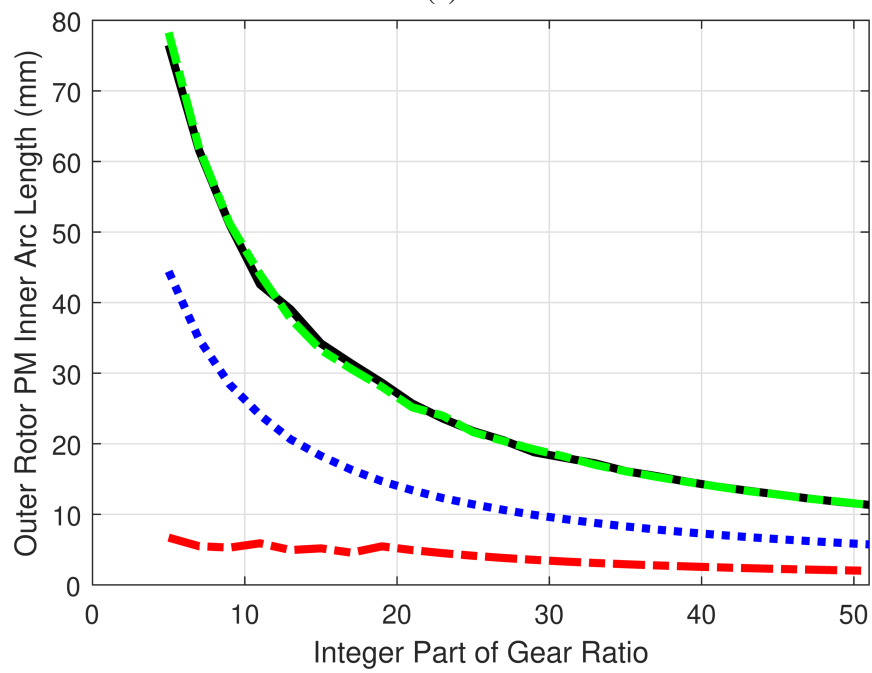


(b)

Figure 5.2: Impact of gear ratio on the achievable (a) ST and (b) PM ST of SPM CoMGs, SPM CyMGs, and Rel CyMGs.



(a)



(b)

Figure 5.3

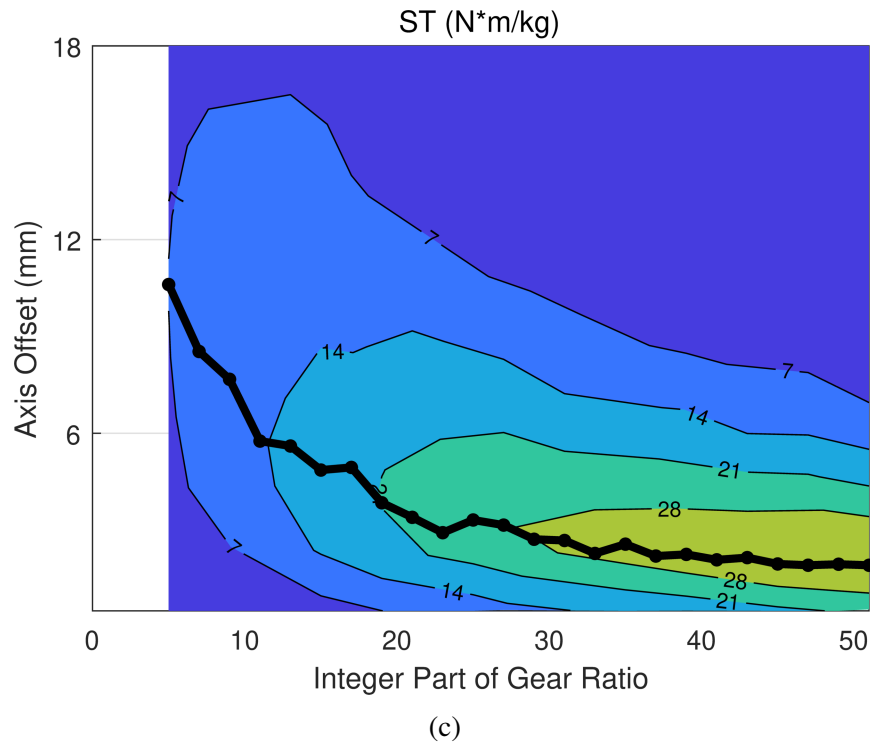


Figure 5.3: Outer rotor PM (a) pole pair counts and (b) inner arc lengths for the maximum ST designs in Fig. 3(a). (c) Variation of maximum ST with gear ratio and axis offset for Rel CyMG designs with a 1 mm air gap. The black line indicates the optimal axis offset for each gear ratio.

Alternatively, in a SPM CyMG or a Rel CyMG,  $P_{l,SPMCyMG}$  or  $N_l$  is equivalent to the gear ratio, as indicated by (1.5) and (3.26), so these parameters cannot be optimized at a given gear ratio and increase linearly with gear ratio, as indicated in Figure 5.3a. Consequently, at a given radius and air gap, there is a nontrivial optimal  $P_{l,SPMCyMG}$  and  $N_l$  value (gear ratio) for SPM CyMGs and Rel CyMGs, respectively. As the gear ratio increases, the SPM CyMG quickly begins to achieve higher ST and PM ST than the SPM CoMG. Although the Rel CyMG never achieves a higher ST or PM ST than the SPM CyMG, it also does eventually achieve a higher ST and PM ST than the SPM CoMG at

higher gear ratios. The optimal gear ratios for the SPM CyMG and the Rel CyMG and the gear ratios at which they begin to outperform the SPM CoMG depend on other design constraints such as the radius and the air gap. The Rel CyMG designs with 0.75 mm air gaps slightly outperform the Rel CyMG designs with 1 mm air gaps, but the smaller air gap does not help enough to overcome the decrease in ST and PM ST caused by removing the Rotor 1 PMs.

Figures 5.3a and 5.3b show the corresponding outer rotor PM pole pair counts and PM arc lengths for the optimal designs in Figure 5.2a. Because  $P_{l,SPMCoMG}$  was restricted to values of 3 or higher in order to eliminate torque ripple issues [45], the SPM CoMG designs have significantly higher outer rotor PM counts than the cycloidal designs. As the gear ratio increases, all three topologies eventually experience a decrease in ST and PM ST once their outer rotor pole arcs become sub-optimally small and experience excessive leakage flux. Also, extremely small PMs are prone to breaking during assembly. Figure 5.3c shows the optimal Rel CyMG axis offset between Rotors 1 and 2 corresponding to the maximum ST designs shown in Figure 5.2a. The pole pair counts increase with the gear ratio. Assuming a fixed outer radius, this means that the PMs have to be tangentially thinner. Consequently, the optimal axis offset decreases as the gear ratio increases, to create a smaller average effective air gap and reduce the increase in leakage flux per pole caused by smaller pole arcs. As the gear ratio of a SPM CoMG increases, its ST and PM ST decrease dramatically, which is quite different than those of SPM CyMGs and Rel CyMGs. Therefore, the following studies only consider SPM CyMGs and Rel CyMGs

with the parameter ranges mentioned in Table 5.2. Additionally, Rel CyMGs with 1 mm air gap were not considered for the comparisons below because the smaller air gap enabled the Rel CyMGs to achieve slightly higher torque densities.

Previous literature illustrated advantages of employing Halbach arrays in magnetic gears, such as increasing torque density [46–50], efficiency [47], and reducing torque ripple [47–50]. Therefore, a GA was used to maximize the ST and PM ST of SPM CyMGs and Rel CyMGs utilizing a Halbach array with two pieces per pole over the same range of gear ratios and parameter values as presented in Table 5.2. Also, since Halbach arrays achieve higher torque densities without back irons [49], air core (0 mm back irons thickness) designs were considered in addition to the back iron thicknesses in Table 5.2. Table 5.3 presents the different scenarios for Figures 5.4, 5.5, and 5.6.

Table 5.3: Legend for Different Design Configurations Characterized in Figures 5.4-5.6.





	Rel CyMG (0.75 mm air gap)	SPM CyMG (1 mm air gap)
Conventional PMs		
Halbach Array PMs		

Figure 5.4 shows the maximum ST and PM ST values achieved for each different scenario across the range of considered gear ratios. Using Halbach arrays improves the achievable ST in both topologies, shown in Figure 5.4a, since this PM arrangement favors air core designs to minimize the total weight of a design. The flux path in a topology with

a Halbach array and an air core passes through the tangentially magnetized PMs instead of the back iron. Therefore, the PMs tend to be thicker in designs with Halbach arrays to facilitate this flux path [51], which results in lower PM STs as shown in Figure 5.4b. However, as the gear ratio and, thus, the pole counts increase, the optimal designs require thinner back irons. Similarly, in designs with high gear ratios and Halbach arrays, thinner tangentially magnetized PMs are able to facilitate the flux paths. These thinner PMs are optimal for maximizing PM ST.

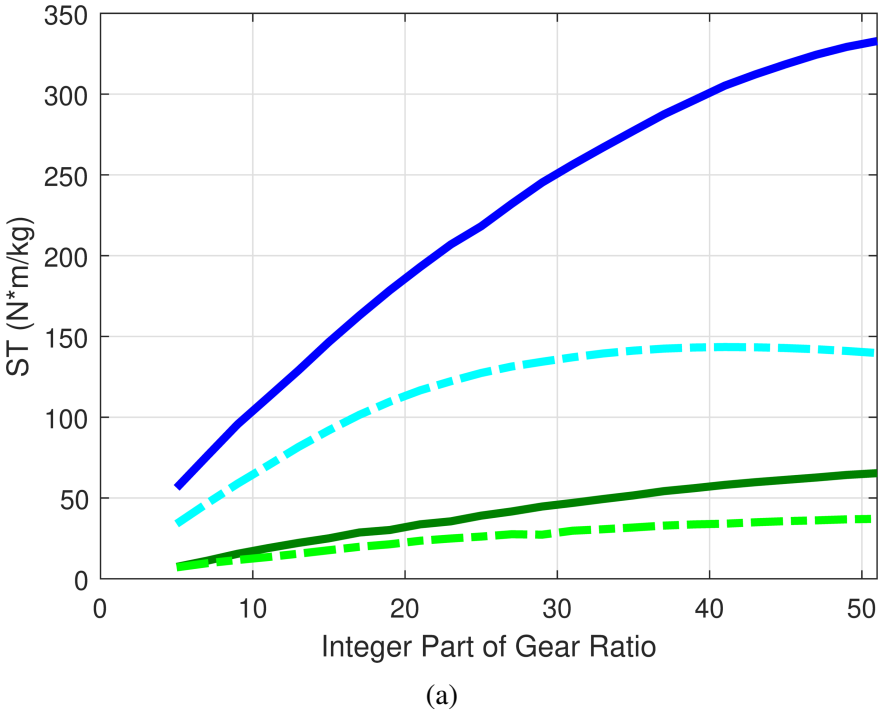


Figure 5.4

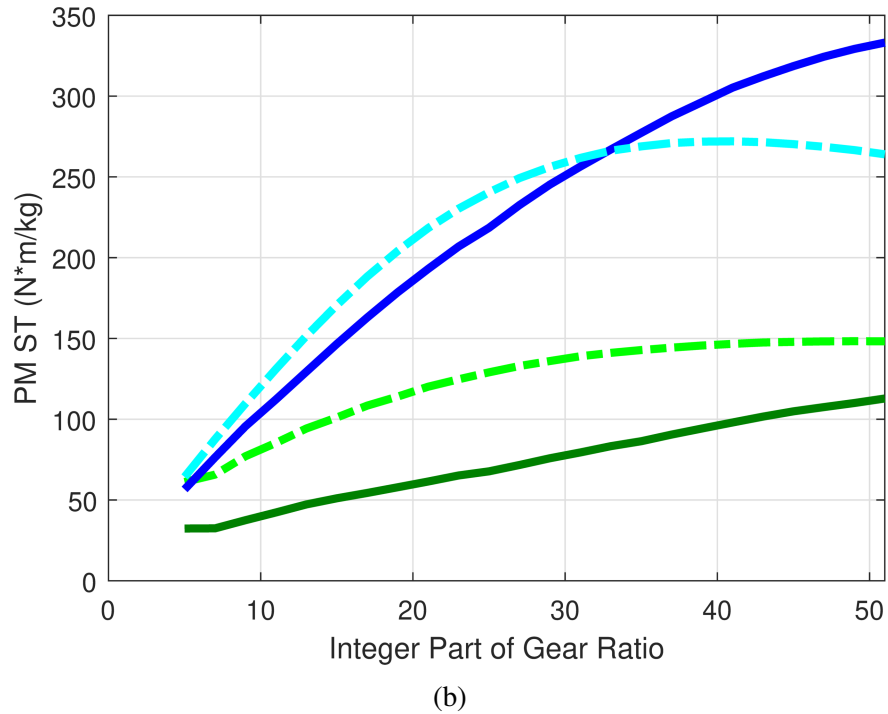


Figure 5.4: Impact of gear ratio and Halbach array utilization on the achievable (a) ST and (b) PM ST of SPM CyMGs and Rel CyMGs.

Figure 5.5 illustrates the corresponding torque ripple percentage, the ratio of the peak-to-peak low-speed shaft torque ripple to the average low-speed shaft torque, for the maximum ST and PM ST designs shown in Figure 5.4. Figures 5.5a and 5.5b show that the torque ripple decreases at higher gear ratios for both topologies due to having more PMs involved in torque production. Also, at the higher gear ratios, the higher STs mean that a shorter stack length is required to provide the target torque, which reduces the torque ripple presented in the gear. The maximum PM ST designs exhibit higher torque ripples than the maximum ST designs, especially at lower gear ratios, due to the smaller effective air gap resulting from the thinner PMs in the maximum PM ST designs. These thinner ef-

fective air gaps do not filter out the higher order harmonics, which cause the torque ripple, as effectively.

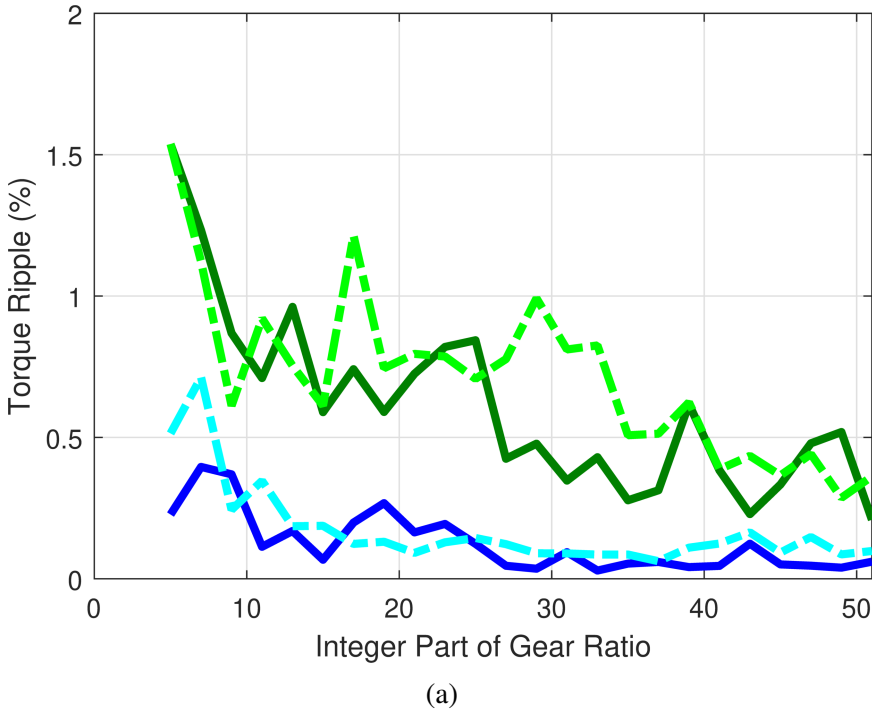
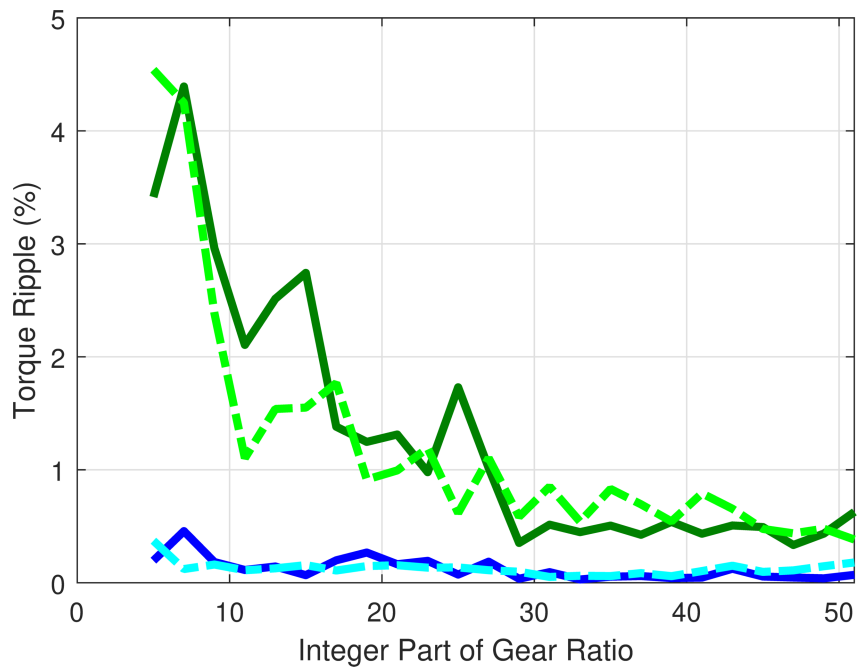


Figure 5.5



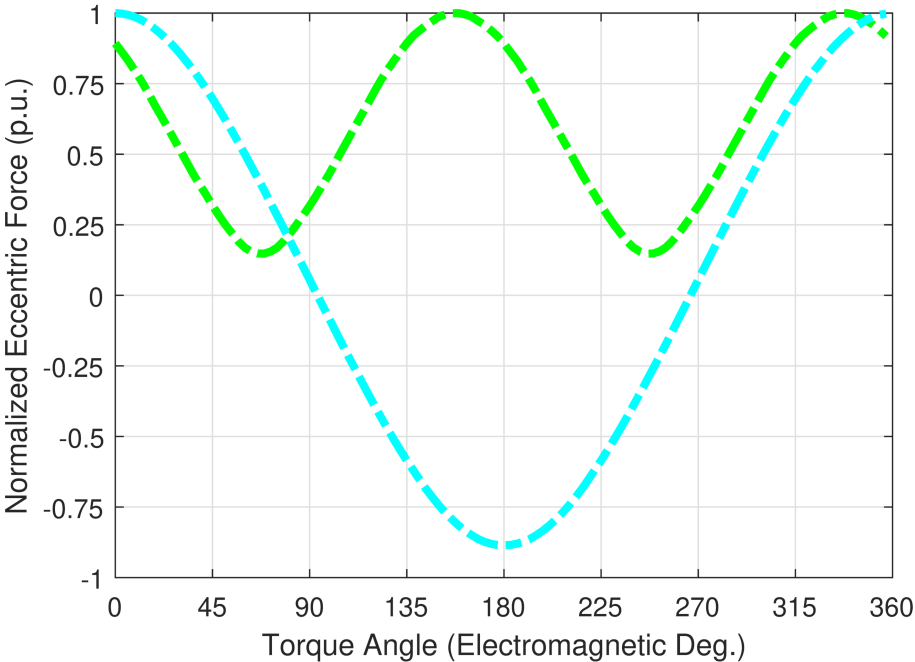


(b)

Figure 5.5: Rotor 1 torque ripple characteristic at the maximum torque orientation of SPM CyMGs and Rel CyMGs with maximum (a) ST and (b) PM ST.

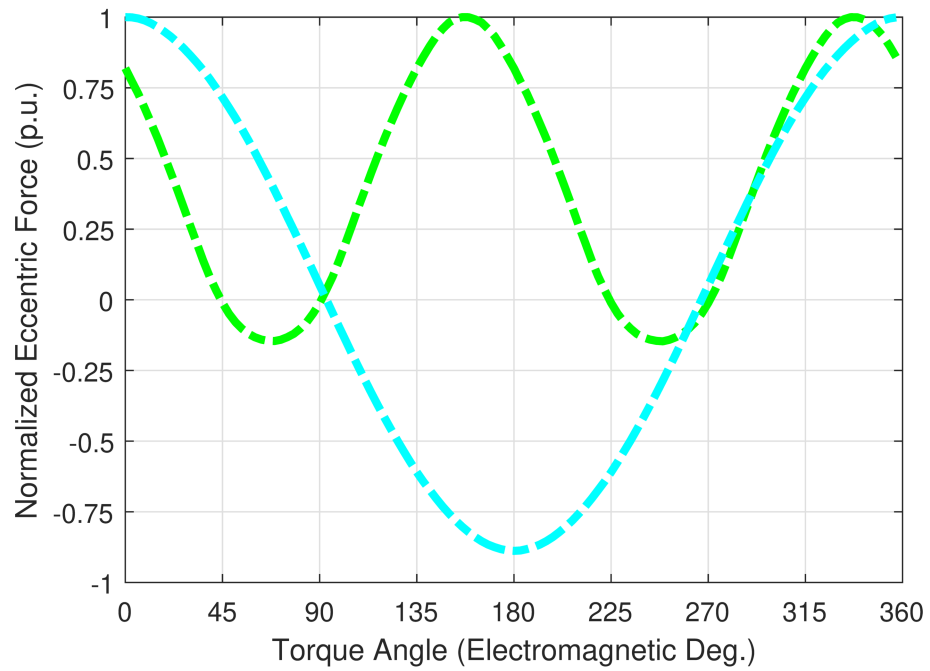
Figure 5.6 demonstrates eccentric magnetic force on Rotor 1, which is in the direction of the minimum air gap, of the SPM CyMG and Rel CyMG with the maximum ST and PM ST shown in Figure 5.4. The values for force in Figures 5.6a and 5.6b are normalized by each design's maximum value. The eccentric forces in a Rel CyMG with maximum ST are positive values for any electromagnetic angle. Rel CyMGs eliminate PMs on Rotor 1; this eliminates any repulsive forces between Rotors 1 and 2. Therefore, Rel CyMGs experience positive forces in the direction of the minimum air gap as the ferromagnetic teeth are attracted to the PMs on Rotor 2. Also, the eccentric force waveforms for Rel CyMGs in Figure 5.6 peak twice in one electromagnetic cycle because the ferromagnetic

teeth are attracted to the PMs regardless of the polarity of PMs. The offset in the maximum values of eccentric force between SPM CyMGs and Rel CyMGs shows that the largest eccentric forces in Rel CyMGs occur when the teeth near the minimum air gap are aligned with the center of a Rotor 2 PM. The non-zero eccentric force in the maximum PM ST Rel CyMG at its maximum torque angle ( $45^\circ$  electromagnetic angle) might be a potential advantage for Rel CyMGs as it helps to balance the pin reaction forces, which are in the direction of the maximum air gap [6]. The net forces on Rotor 1 increase the bearing loads [6, 15, 51, 52]; therefore, reducing these forces can improve the reliability and efficiency of CyMGs, where friction losses in the bearings significantly reduce efficiency.



(a)

Figure 5.6



(b)

Figure 5.6: The normalized magnetic eccentric force exerted on the inner rotor as a function of torque angle for the SPM CyMG and Rel CyMG designs with the maximum (a) STs and (b) PM STs.

### 5.3 Conclusion

This study introduces the Rel CyMG topology and its operating principles. A GA was used to parametrically optimize SPM CoMGs, SPM CyMGs, and Rel CyMGs for maximum ST and PM ST based on 2D FEA simulations over a broad range of parameter value ranges, as summarized in Table 5.2. The simulation results reveal the following conclusions.

- Optimal SPM CyMGs significantly outperform the other two topologies at higher gear ratios in terms of ST and PM ST.
- Rel CyMGs outperform SPM CoMGs at higher gear ratios.
- Rel CyMGs require half the outer rotor PM pole pair count of SPM CyMGs to achieve a given gear ratio, which simplifies assembly.
- The PMs on the outer rotor of Rel CyMGs are wider than those of SPM CyMGs for the same gear ratio and radius, which can be an advantage in the manufacturing process, especially for high-gear ratio designs.
- Rel CyMGs achieve poor specific torques; however, they may be more mechanically robust because all the PMs are stationary.
- Halbach arrays reduce the overall active weight of SPM and Rel CyMGs required to achieve a target torque.

- However, Halbach arrays reduce the PM ST for both SPM and Rel CyMG designs, except at very high gear ratios.
- The optimal SPM CyMGs experience less torque ripple than the optimal Rel CyMGs.
- The eccentric forces on the inner rotor of a Rel CyMG corresponding to the maximum ST are positive over the full 360° electromagnetic angle as the reluctance rotor is always attracted to the outer rotor with PMs in the direction of the minimum air gap.
- The non-zero eccentric forces at the maximum torque angle in the Rel CyMG designs reflect a potential advantage to balance the pin reaction forces, which are a challenge in CyMG designs.

6. ANALYSIS AND BENCHMARKING OF RADIAL FLUX CYCLOIDAL  
MAGNETIC GEARS WITH REDUCED PERMANENT MAGNET PIECE  
COUNT USING CONSEQUENT POLES\* <sup>1</sup>

This study focuses on optimizing and comparing the performances of cycloidal MGs with the different rotor combinations, as shown in Figure 6.1 and listed in Table 6.1. The CP and SPM cycloidal MGs with NdFeB PMs were optimized and compared across a broad range of gear ratios using a GA and 2D FEA. Then, 3D FEA is used to evaluate the end effects of the optimal designs.

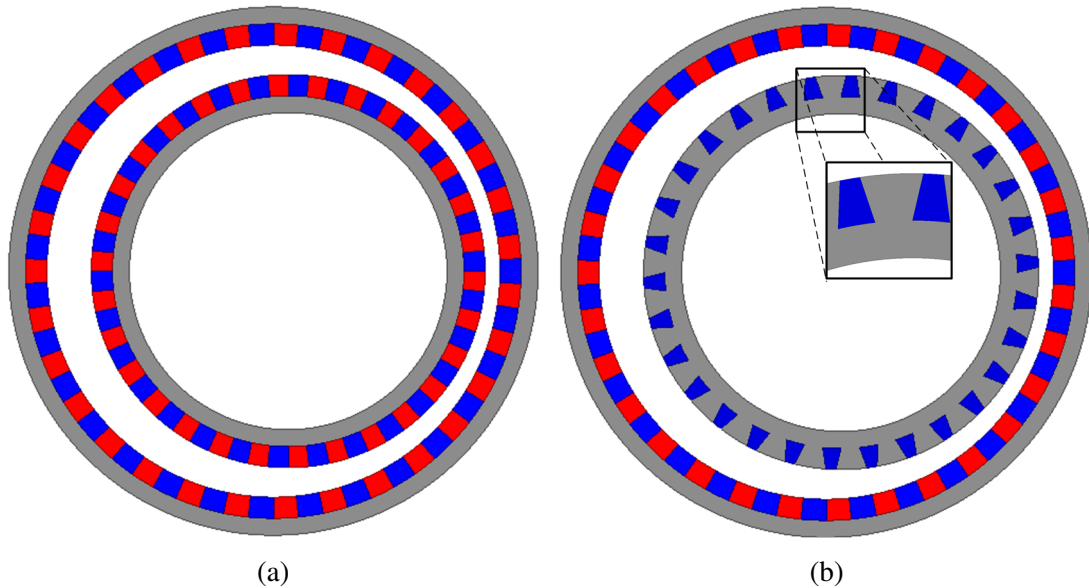


Figure 6.1

<sup>1</sup>© 2021 IEEE. Part of this chapter is reprinted with permission from M. Johnson, S. Hasanpour, M. C. Gardner, and H. A. Toliyat, "Analysis and benchmarking of radial flux cycloidal magnetic gears with reduced permanent magnet piece count using consequent poles," in *Proc. IEEE Energy Convers. Congr. Expo.*, 2021, pp. 4334-4341.

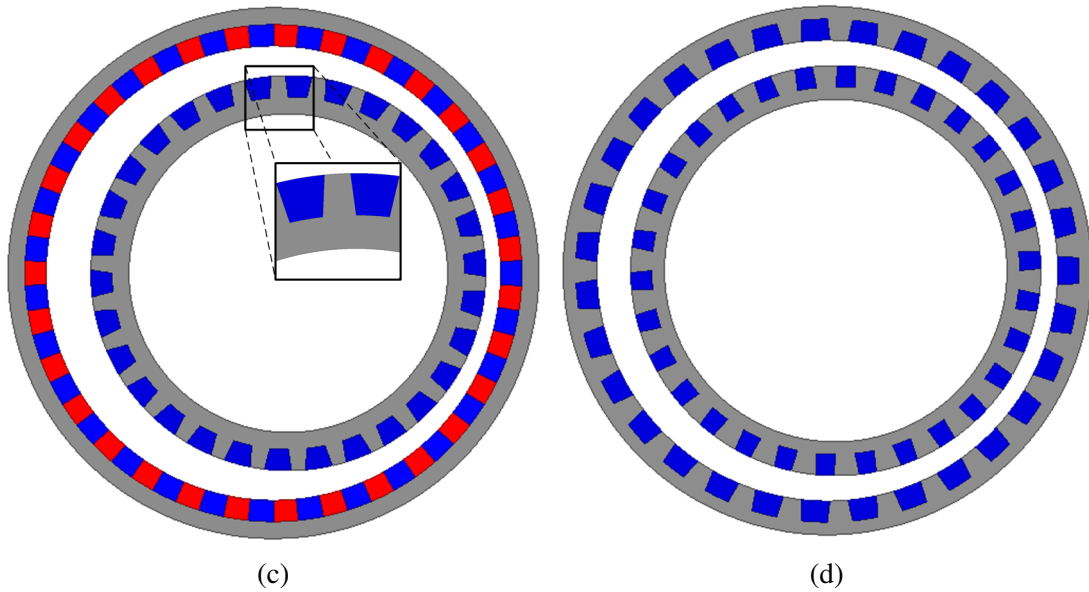


Figure 6.1: Cross-sections of (a) an SPM-SPM cycloidal MG, (b) a CP-SPM cycloidal MG with the inner rotor teeth shaped to retain the PMs, (c) a CP-SPM cycloidal MG with the inner rotor teeth not shaped to retain the PMs, and (d) a CP-CP cycloidal MG. Reprinted with permission from [26].

## 6.1 Design Study Methodology

The SPM-SPM cycloidal MG with SPM inner rotor and SPM outer rotor, CP-SPM cycloidal MG with CP inner rotor and SPM outer rotor, and CP-CP cycloidal MG with CP inner rotor and CP outer rotor, shown in Figure 6.1, were optimized to independently maximize PM ST and VTD across gear ratios ranging from 30:1 to 80:1 using a GA with 2D FEA. For each optimization, the GA used 100 generations with approximately 1000 individuals in each generation. For a CP inner rotor, the PM grip is defined as half of the difference obtained by subtracting the length of the chord connecting a PM's outer corners from the length of the chord connecting its inner corners. The teeth in a CP inner rotor

with a positive PM grip, such as the design illustrated in Figure 6.1b, can retain the inner rotor PMs, which eliminates the need for a sleeve and may simplify the assembly. A CP inner rotor with a negative PM grip, such as the design depicted in Figure 6.1c, does not offer any inherent PM retention benefits. For the CP-SPM and CP-CP topologies, two different inner rotor conditions were evaluated and optimized:

1. A 0.25 mm inner rotor PM grip with a 0.75 mm magnetic air gap (no PM retention sleeve present)
2. An unconstrained inner rotor PM grip with a 1 mm magnetic air gap (including a PM retention sleeve)

Table 6.1 summarizes these different scenarios. Table 6.2 lists the parameters considered in this study and their respective ranges.

Table 6.1: Legend for Different Design Configurations Characterized in the following Figures. Reprinted with permission from [26].






					
	SPM-SPM	CP-SPM	CP-SPM	CP-CP	CP-CP
Air Gap (mm)	1	0.75	1	0.75	1
Inner Rotor PM Grip (mm)	N/A	0.25	Any	0.25	Any



Table 6.2: GA Parameter Value Ranges. Reprinted with permission from [26].

Name	Description	Values	Units
$P_{In}$	Inner pole pair count	30 – 80	
$R_{Out}$	Outer radius	100	mm
$T_{BI,In}$	Inner back iron radial thickness	0, 2 – 5	mm
$T_{PM,In}$	Inner PM radial thickness	2 – 20	mm
$\alpha_{PM,In,In}$	Inner rotor PM inner pitch	0.05 – 0.95	
$\alpha_{PM,In,Out}$	Inner rotor PM outer pitch	0.05 – 0.95	
$T_{off}$	Axis offset	0.5 – 10	mm
$T_{PM,Out}$	Outer PM radial thickness	2 – 20	mm
$\alpha_{PM,Out,In}$	Outer rotor PM inner pitch	0.05 – 0.95	
$\alpha_{PM,Out,Out}$	Outer rotor PM outer pitch	0.05 – 0.95	
$T_{BI,Out}$	Outer back iron radial thickness	0, 2 – 5	mm

There are a few considerations for the range of parameters in Table 6.2:

- As very thin back irons would be difficult to fabricate, only air cores (0 mm thickness) and back irons thicker than 2 mm were considered.
- For most optimizations; for some PM ST optimizations, the PM thickness was constrained to 2 – 10 mm because it was clear that the optimal PM thicknesses were much smaller than 10 mm.
- For CP rotors; SPM rotors were constrained to have normalized pitches in the range of 0.125 to 0.5.

- For CP rotors with arbitrary PM grip; for SPM rotors, each PM has the same inner and outer pitch.
- All PM pitch values are normalized pitches based on the definition given in (6.1).

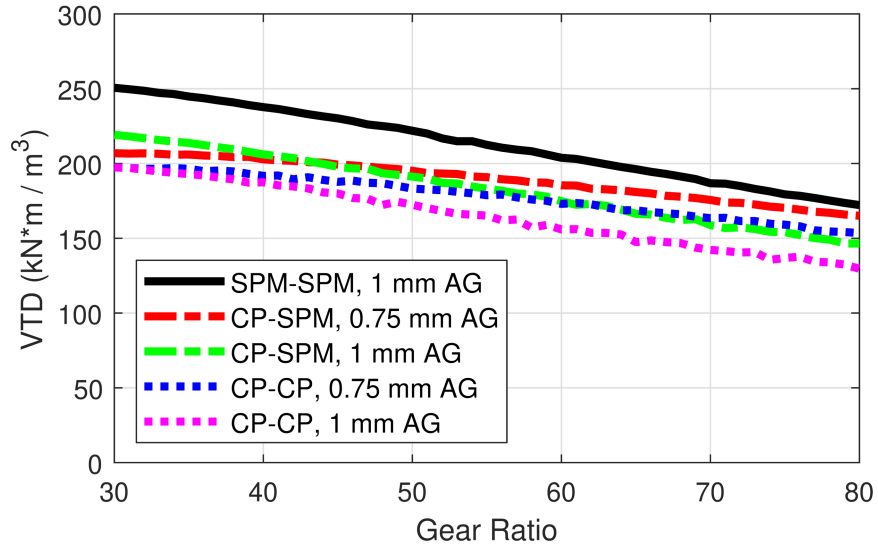
For CP rotors using the arbitrary grip scenario, the PMs' normalized inner and outer pitches were allowed to vary independently. The normalized PM pitch ( $\alpha_{PM}$ ) is defined as the ratio of the PM arc length to the arc length of one pole pair, as given by

$$\alpha_{PM} = \frac{PMArcLength}{PolePairArcLength} \quad (6.1)$$

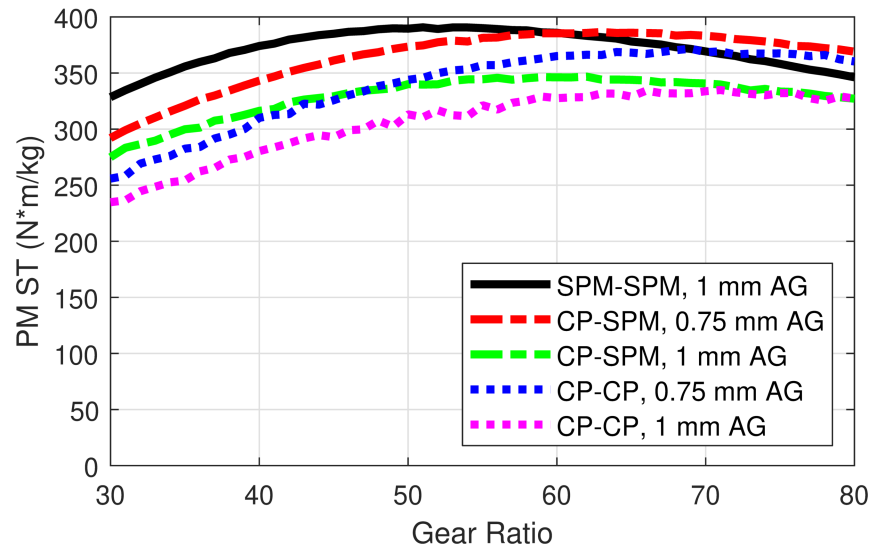
For CP inner rotors using the fixed 0.25 mm PM grip, the normalized inner PM pitch was allowed to vary, while the normalized outer PM pitch was set to achieve the 0.25 mm PM grip. The normalized pitch of the PMs on an SPM rotor was allowed vary between 0.125 and 0.5 (half of a pole pair arc). All designs were simulated using NdFeB N52H for the PMs and M15 (29 gauge) for the back irons and CP teeth.

## 6.2 Results

Figures 6.2a and 6.2b show the maximum VTD and PM ST values achieved for each of the different design configuration scenarios across the range of considered gear ratios. As illustrated in Figures 6.2a and 6.2b, at lower gear ratios, the optimal SPM-SPM cycloidal MGs perform better than the CP-SPM and CP-CP cycloidal MGs in terms of both VTD and PM ST. However, at higher gear ratios, the CP-SPM and CP-CP scenarios with thinner air gaps achieve higher PM STs, as shown in Figure 6.2b. Within the considered gear ratio range the CP-SPM and CP-CP cycloidal MGs never match the SPM-SPM cycloidal MGs in terms of VTD, but the CP-SPM cycloidal MGs do get very close at the very high gear ratios, as shown to the right of Figure 6.2a, and would likely surpass the SPM-SPM cycloidal MGs in terms of VTD if even higher gear ratios were considered. However, because the CP rotor configuration replaces NdFeB PMs with soft magnetic material, it is not surprising that the CP-SPM and CP-CP topologies do not yield higher VTDs than the SPM-SPM topology. Thus, these results indicate that the CP-SPM and CP-CP topologies are more appropriate for applications where particularly large gear ratios are required or reducing the cost is more important than reducing the volume. Figure 6.2c depicts the corresponding VTD values for the designs with the maximum PM ST values, which are shown in 6.2b. Relative to the SPM-SPM topology, using the CP-SPM topology to increase the PM ST at high gear ratios does result in a lower VTD, but this penalty is less than 15%.

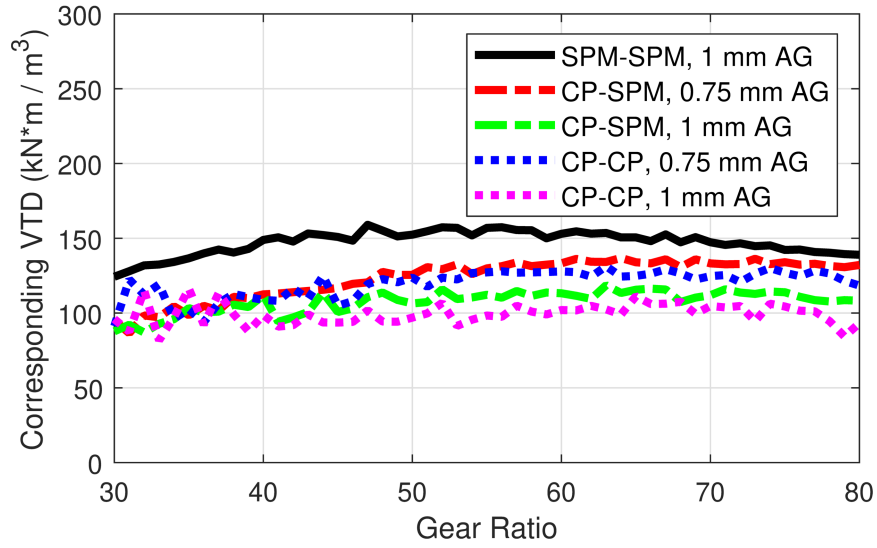


(a)

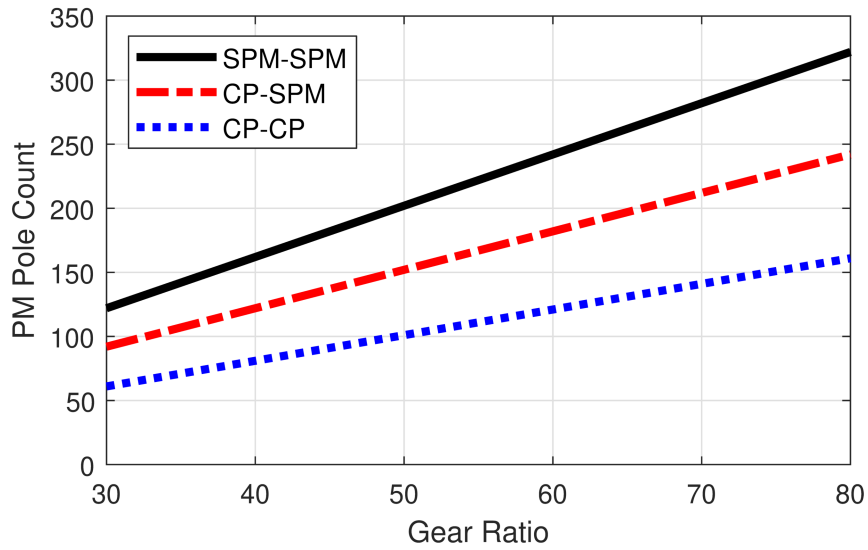


(b)

Figure 6.2



(c)



(d)

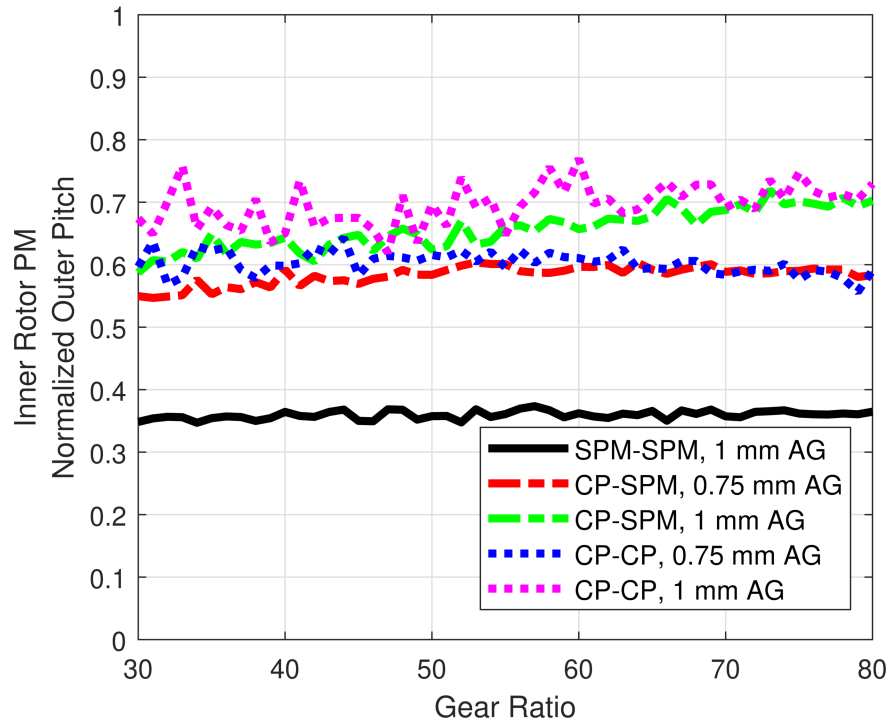
Figure 6.2: The maximum (a) VTDs and (b) PM STs achieved for each GA optimization scenario across a range of gear ratios. The (c) VTDs of the designs achieving the maximum PM STs and (d) the PM pole counts required to achieve a range of gear ratios for each of the different topologies. Reprinted with permission from [26].

Based on (1.5), a higher gear ratio requires a higher PM pole pair count, which makes

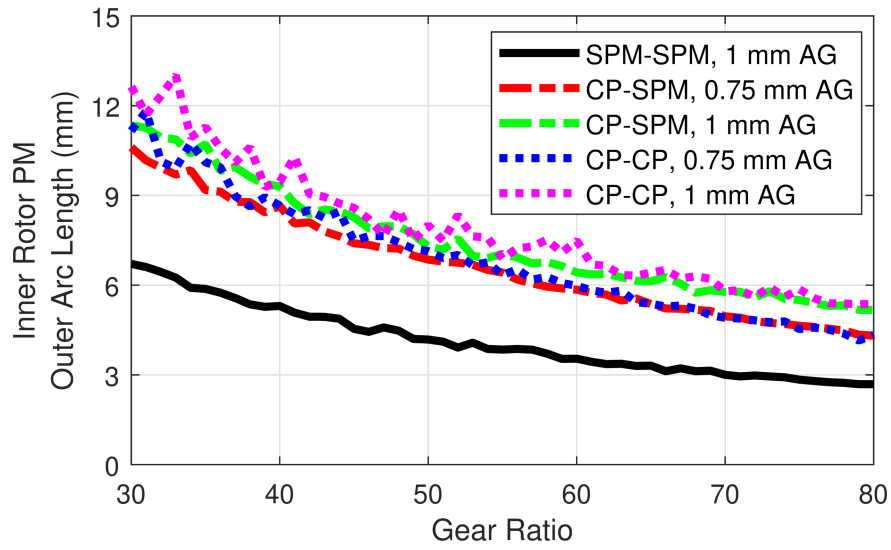
the pole arcs of the PM pieces shorter and increases the tangential leakage flux. A CP rotor replaces half of the PMs on an SPM rotor with ferromagnetic teeth and, consequently, only uses half as many PM poles as the SPM rotor. Figure 6.2d compares the number of PM poles required for each topology to achieve the various gear ratios. This demonstrates one of the main advantages of using CP rotors. Relative to the SPM-SPM topology, the CP-SPM topology requires almost 25% fewer PM poles, and the CP-CP topology only requires half as many PM poles as the SPM-SPM topology. This reduction in piece count, along with the PM insertion slots created by the CP teeth, can potentially reduce assembly costs.

In addition to reducing the piece count, replacing half of the PM poles on a rotor with ferromagnetic teeth also allows the arc lengths of the remaining PMs on a CP rotor to be increased beyond half of the pole pair arc length with a corresponding decrease in teeth arc lengths. On the other hand, it is not possible to increase the arc lengths of all of the PMs on an SPM rotor beyond half of the pole pair arc length. Figure 6.3a shows the corresponding normalized PM pitches at the outer radius of the inner rotor for the maximum PM ST designs. The CP-SPM and CP-CP cycloidal MGs with the maximum PM ST values favor normalized PM pitches larger than 0.5, indicating that the PMs are wider than the teeth. Consequently, the PM arc lengths of the optimal CP cycloidal MGs are longer than those of the optimal SPM cycloidal MGs at the same gear ratio, as shown in Figure 6.3b. The CP rotor's ability to facilitate the use of larger magnet pieces may help with manufacturing considerations, especially at high gear ratios, where the PMs

can become extremely small. Note that, as illustrated in Figures 6.1b and 6.1c, the PM pitch can be different at the inner and outer edges of a CP cycloidal MG's inner rotor PMs. The CP-SPM and CP-CP designs using the arbitrary PM grip scenario converge to designs with significantly negative grips, as shown in Figure 6.3c. Thus, the positive PM grip constraints are magnetically suboptimal. However, the smaller magnetic air gap resulting from the elimination of the PM retention sleeve (which is enabled by positive PM grips) allows these designs to outperform the negative PM grip designs with larger air gaps, especially at larger gear ratios. Figure 6.3d shows the corresponding PM arc lengths at the inner radius of the outer rotor PMs. As on the inner rotor, using a CP outer rotor results in larger optimal PM arc lengths, which can simplify manufacturing, particularly at high gear ratios.



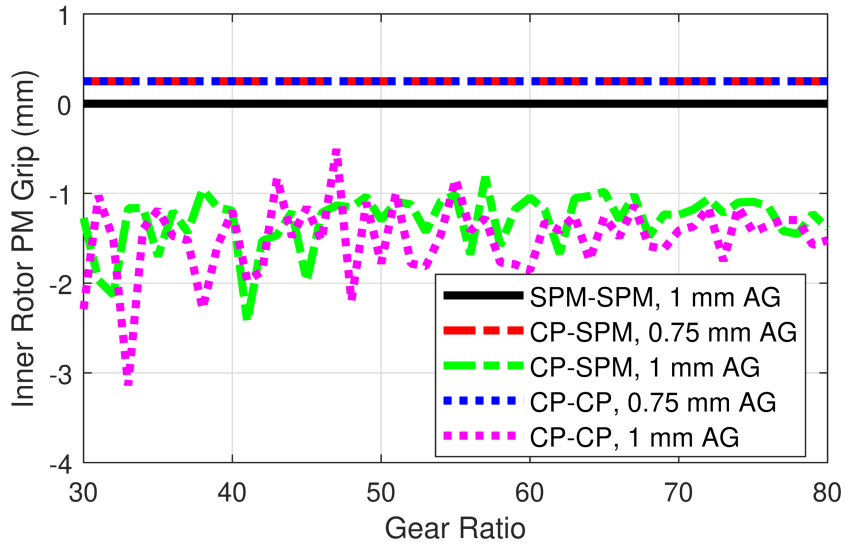
(a)



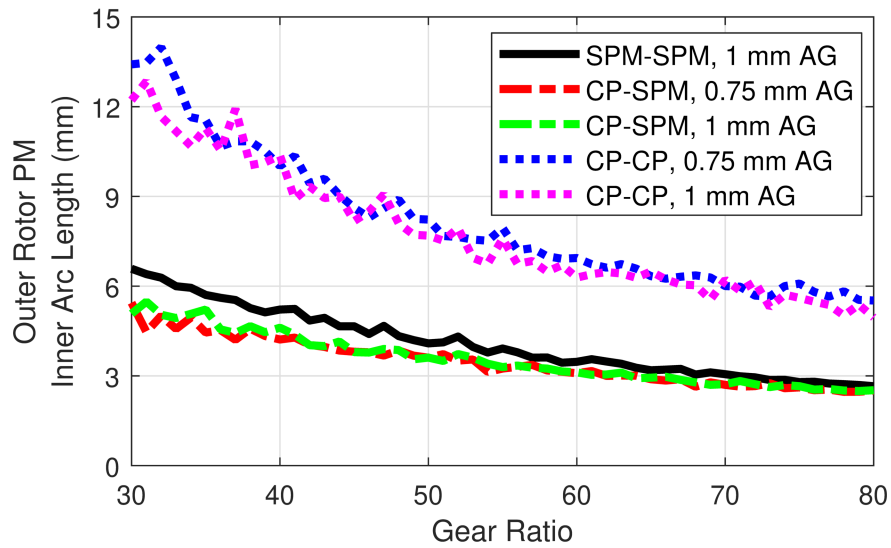
(b)

Figure 6.3





(c)



(d)

Figure 6.3: The corresponding (a) inner rotor PM normalized outer pitch, (b) inner rotor PM outer arc length, (c) inner rotor PM grip, and (d) outer rotor PM inner arc length for the designs with the maximum PM ST values given in Figure 6.2b. Reprinted with permission from [26].

Figure 6.4 displays the cross sections of the optimal designs with maximum VTD for

each topology, corresponding to the results in Figure 6.2a. Similarly, Figure 6.5 depicts the cross sections of the maximum PM ST designs, corresponding to the results in Figure 6.2b. Comparing the maximum PM ST designs reveals that the PM pieces on the CP rotors are wider than those on the SPM rotors. The ability of CP rotors to use wider PM pieces at a given gear ratio and achieve smaller air gaps result in a higher optimum gear ratio with respect to maximizing PM ST, as compared to SPM rotors. Figure 6.4 demonstrates that optimization of a topology for VTD leads to designs with thicker PMs, especially on the inner rotor. Utilizing thicker PMs on the outer rotor decreases the air gap radius (assuming a fixed outer radius), which reduces its slip torque. Thus, there is a tradeoff between the increased flux density benefits of increasing the thickness of the outer rotor PMs and the deleterious consequences of the associated reduction in the air gap radius. Increasing the thickness of the PMs on the inner rotor does not reduce the air gap radius (assuming a fixed outer radius).

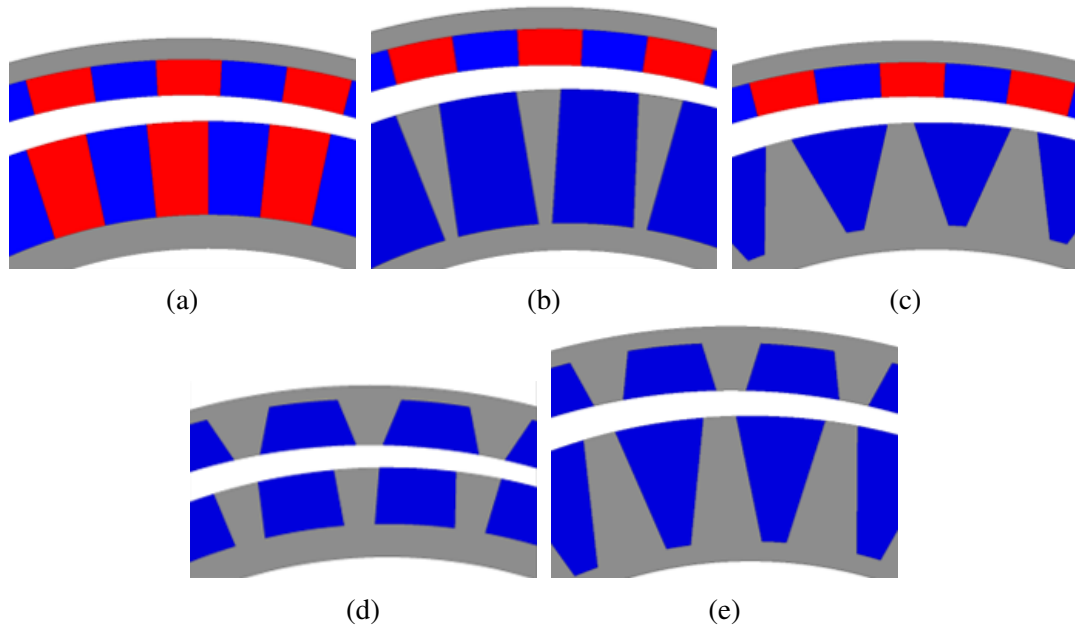


Figure 6.4: Cross-sectional portions of (a) the SPM-SPM cycloidal MG, (b) the CP-SPM cycloidal MG with a 0.25 mm inner rotor PM grip, (c) the CP-SPM cycloidal MG with an arbitrary inner rotor PM grip, (d) the CP-CP cycloidal MG with a 0.25 mm inner rotor PM grip, and (e) the CP-CP cycloidal MG with an arbitrary inner rotor PM grip that achieve the maximum VTD. Reprinted with permission from [26].

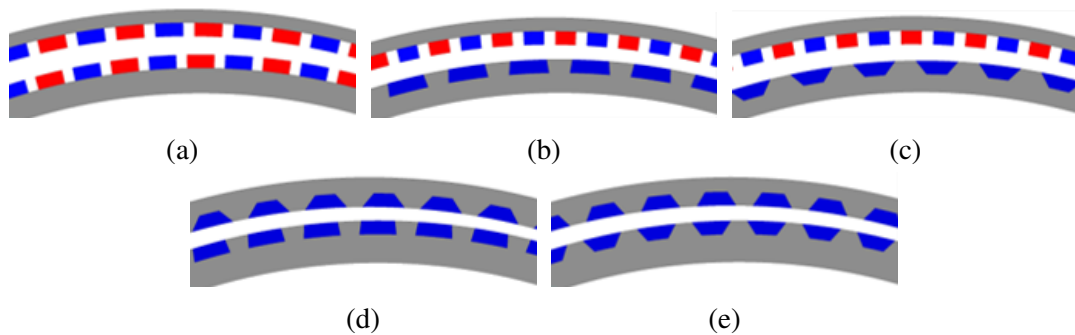


Figure 6.5: Cross-sectional portions of (a) the SPM-SPM cycloidal MG, (b) the CP-SPM cycloidal MG with a 0.25 mm inner rotor PM grip, (c) the CP-SPM cycloidal MG with an arbitrary inner rotor PM grip, (d) the CP-CP cycloidal MG with a 0.25 mm inner rotor PM grip, and (e) the CP-CP cycloidal MG with an arbitrary inner rotor PM grip that achieve the maximum PM ST. Reprinted with permission from [26].

The magnetic forces acting on the inner rotor are also key aspects of the design [6, 15, 51, 52]. These forces increase the load upon the bearing between the high-speed shaft and the inner rotor [6], reducing its expected lifetime and increasing losses. As the electromagnetic losses in CyMGs are relatively small [6], [53], the friction losses tend to be the dominant source of losses [6]. Consequently, these forces can have a large impact on efficiency. Figures 6.6 and 6.7 show the normalized torques and magnetic forces exerted on the inner rotor as a function of the torque angle (the difference in the electromagnetic angles of the rotors where the air gap is smallest) for the designs with the highest VTDs and PM STs for each topology. For comparison purposes, each torque or force versus torque angle curve for a given design in Figures 6.6 and 6.7 is normalized by its own maximum value and not by the overall maximum value in the graph.

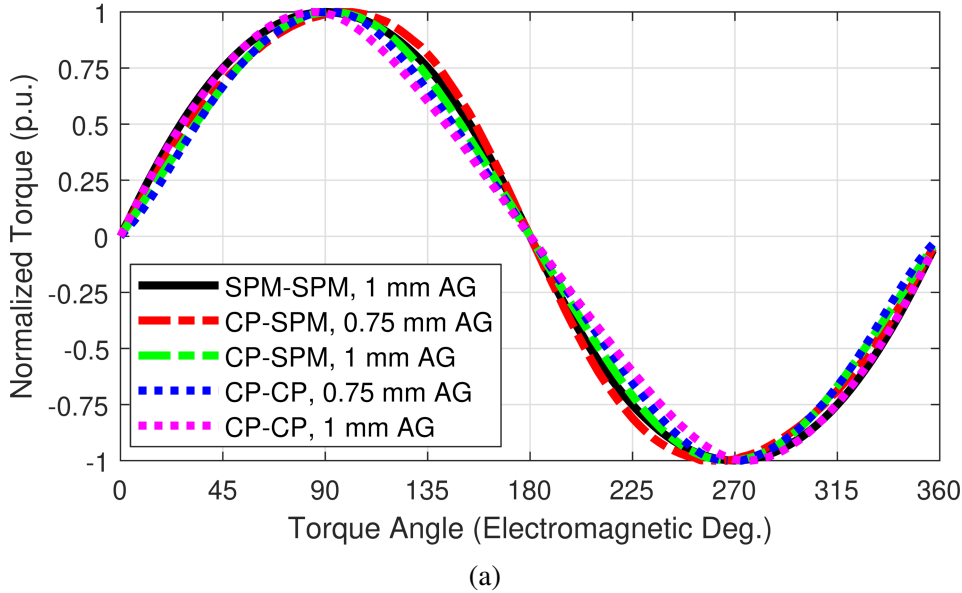
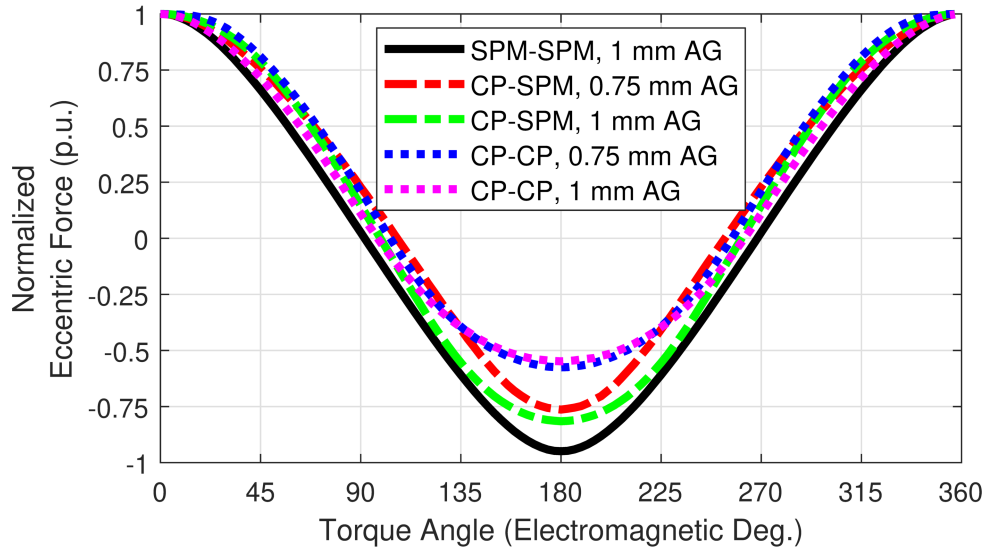
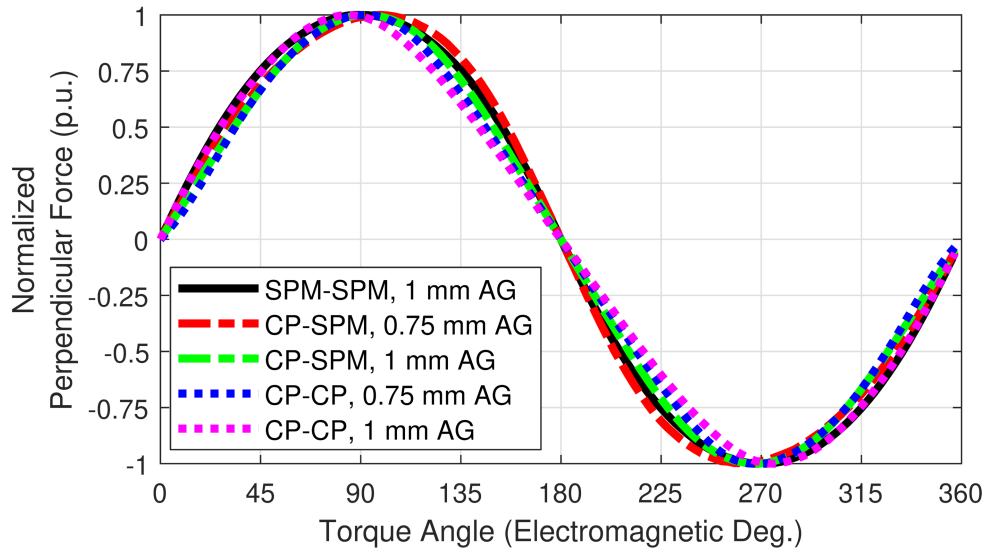


Figure 6.6

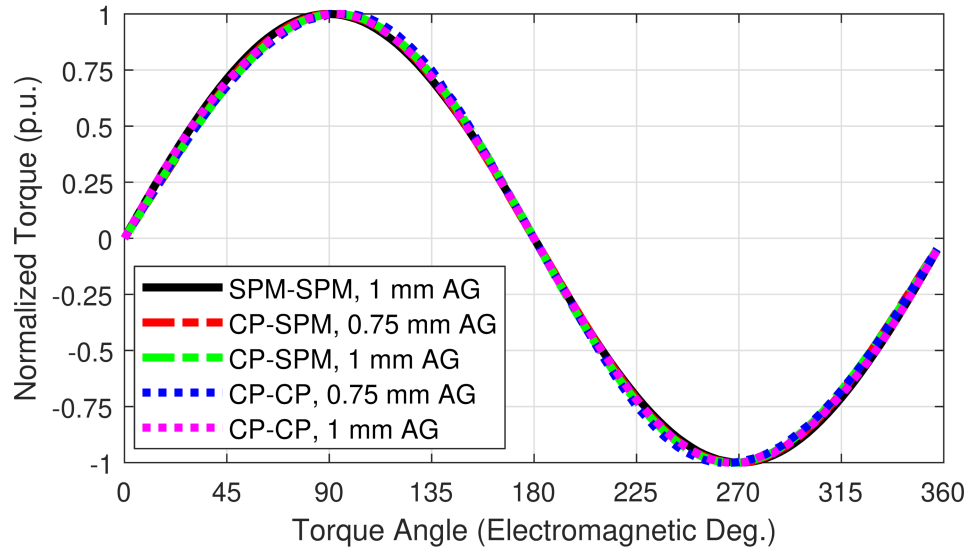


(b)

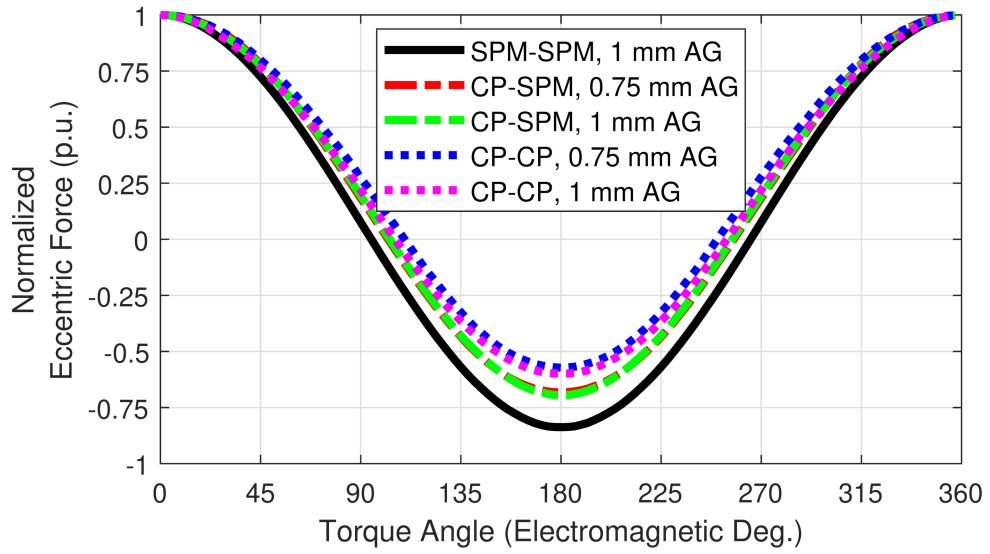


(c)

Figure 6.6: The normalized magnetic (a) torque, (b) eccentric force, and (c) perpendicular force exerted on the inner rotor as a function of torque angle for the cycloidal MG designs with the highest VTDS for each topology. Reprinted with permission from [26].

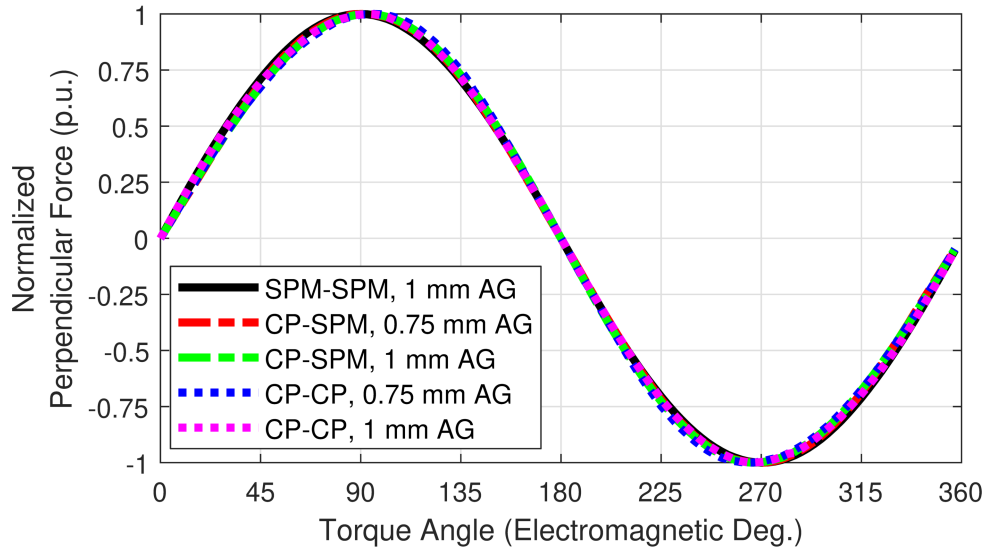


(a)



(b)

Figure 6.7



(c)

Figure 6.7: The normalized magnetic a) torque, (b) eccentric force, and (c) perpendicular force exerted on the inner rotor as a function of torque angle for the cycloidal MG designs with the highest PM STs for each topology. Reprinted with permission from [26].

The eccentric forces shown in Figures 6.6b and 6.7b are the magnetic forces in the direction of the axis offset. The perpendicular forces shown in Figures 6.6c and 6.7c are the magnetic forces in the direction perpendicular to the axis offset. The torques shown in Figures 6.6a and 6.7a are approximately sinusoidal, although the torques of the maximum VTD designs with CP rotors tend to be slightly less sinusoidal than those of the other designs. The eccentric forces are also sinusoidal with a maximum at the zero torque angle. However, the eccentric forces have a non-zero average with respect to torque angle, and the average eccentric forces of the designs with CP rotors are larger than those of the SPM-SPM designs. This means that the designs with CP rotors have a larger eccentric force at high loads. This is noteworthy because this eccentric force could be used to

partially mitigate the pin reaction forces [6]. The perpendicular forces shown in Figures 6.6c and 6.7c are responsible for generating the torques, and have a similar profile to the torques shown in Figures 6.6a and 6.7a. Figures 6.8 and 6.9 compare the no load eccentric forces and peak load perpendicular forces for each of the maximum VTD and PM ST designs characterized in Figures 6.2a and 6.2b, each scaled to the stack length required to produce a 100 N·m slip torque, based on 2D FEA. For the same slip torque, both the perpendicular and eccentric forces of the optimal designs tend to decrease slightly as the gear ratio increases. The perpendicular forces at the maximum torque angle are relatively consistent across all topologies. However, the CP-CP topology has larger eccentric forces at no load than the other topologies.

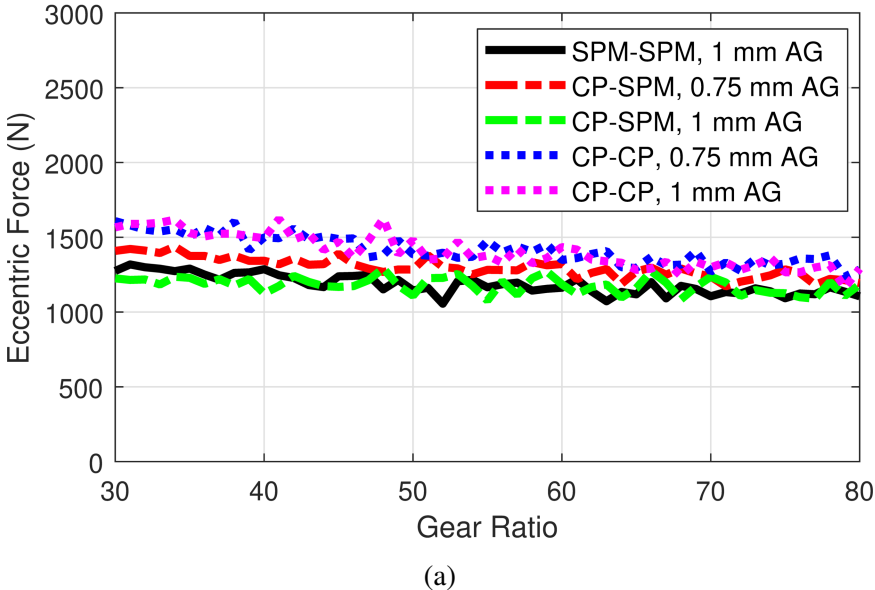
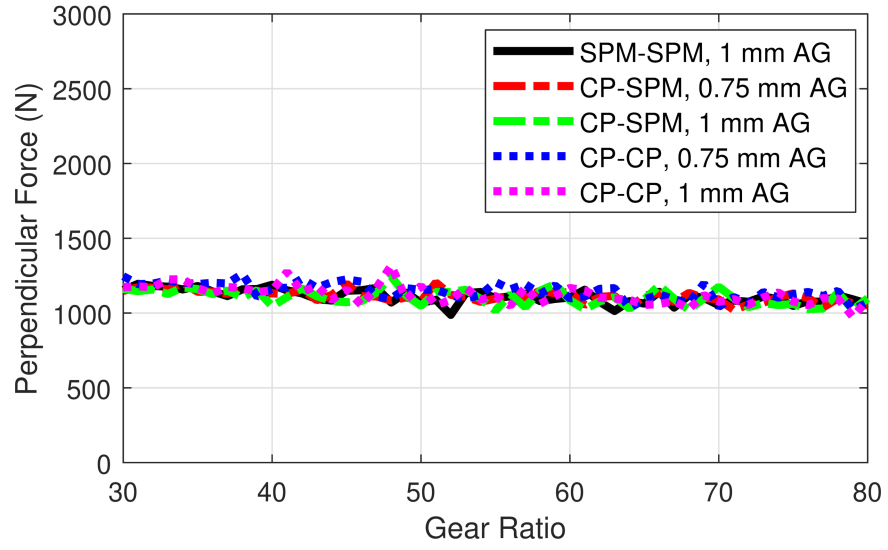


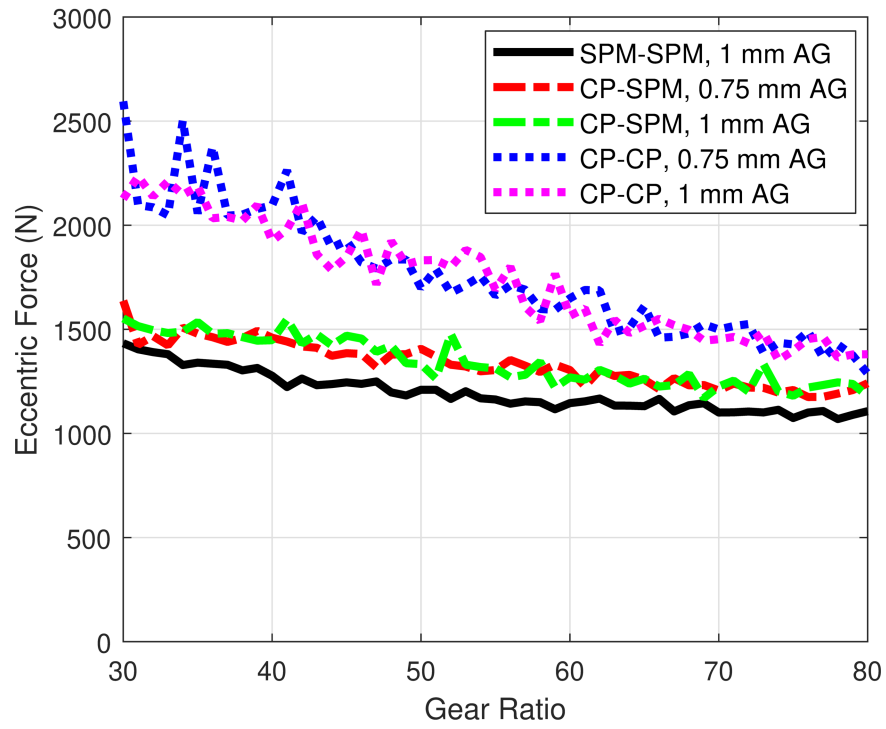
Figure 6.8



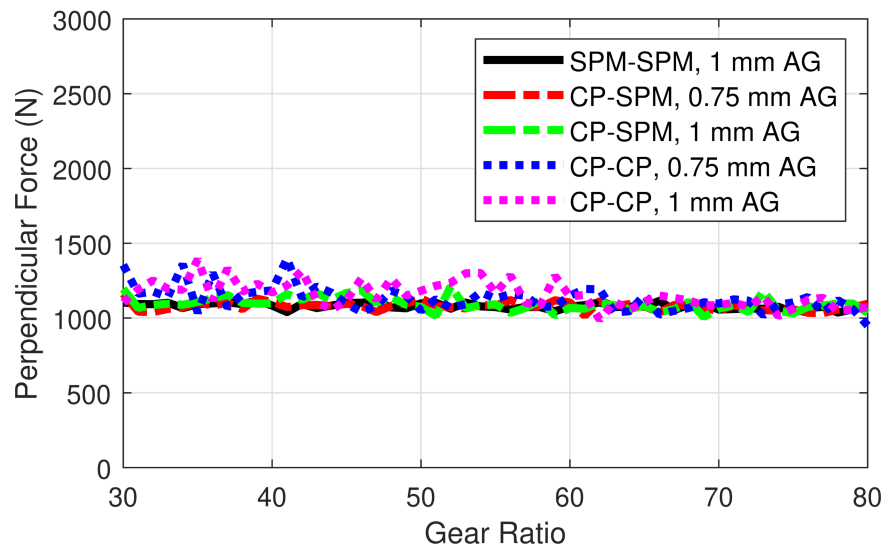


(b)

Figure 6.8: Inner rotor (a) No load eccentric forces and (b) peak load perpendicular forces for the cycloidal MG designs with the highest VTDs for each topology at each gear ratio (corresponding to the designs characterized in Figure 6.2a). Reprinted with permission from [26].



(a)



(b)

Figure 6.9: Inner rotor (a) No load eccentric forces and (b) peak load perpendicular forces for the cycloidal MG designs with the highest PM STs for each topology at each gear ratio (corresponding to the designs characterized in Figure 6.2b). Reprinted with permission from [26].

Another important consideration is end effects. It is well established that end effects are often very significant for coaxial magnetic gears [54]. However, end effects can also be significant for cycloidal MGs [55]. While the previous results are based on 2D FEA, Figure 6.10 shows the significance of the end effects for the optimal VTD and PM ST designs depicted in Figures 6.2a and 6.2b at a 25 mm stack length, based on 3D FEA. The maximum VTD designs tend to suffer more significant end effects than the maximum PM ST designs. Additionally, the CP-CP designs tend to suffer more significant end effects than the CP-SPM and SPM-SPM designs, and the SPM-SPM designs tend to experience less significant end effects than the CP-CP and CP-SPM designs.

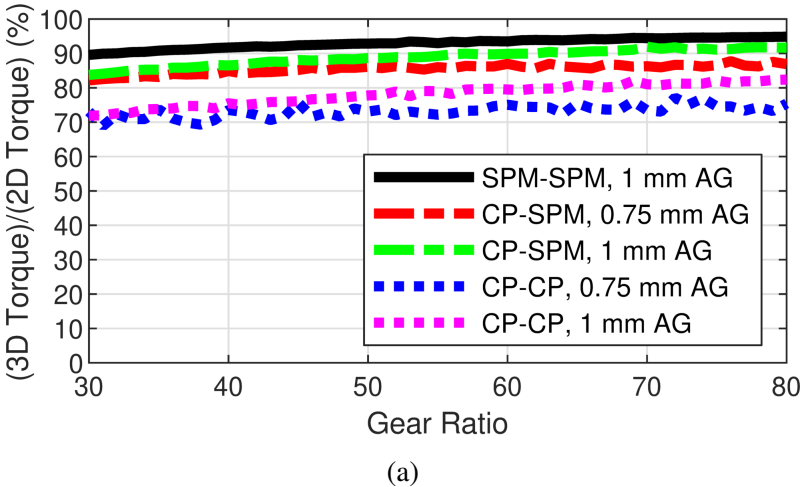


Figure 6.10

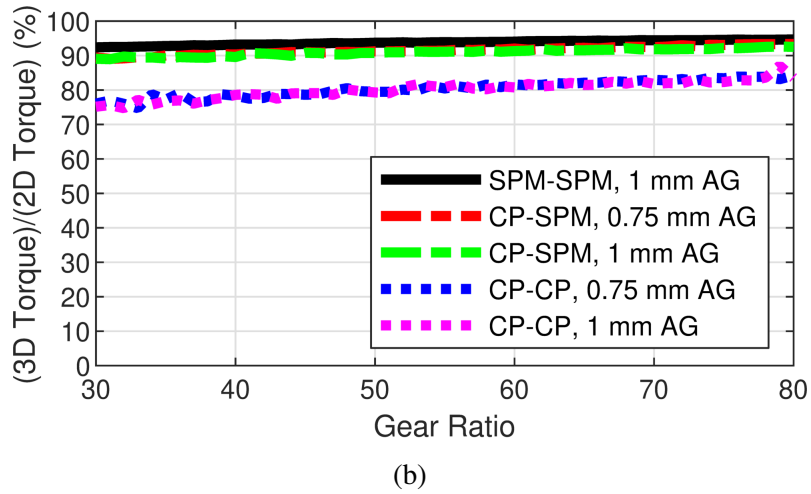


Figure 6.10: Significance of 3D effects on slip torque for (a) the maximum VTD designs and (b) the maximum PM ST designs of each topology at a stack length of 25 mm. Reprinted with permission from [26].

### 6.3 Conclusion

This study uses 2D FEA simulations to compare CyMGs with different combinations of SPM rotors and CP rotors, as summarized in Table 6.1. A basic analysis of the different topologies along with a review of the simulation results supports the following general conclusions within the evaluated design space:

- Cycloidal MGs with CP rotors require less PM pieces than cycloidal MGs with SPM rotors, which may simplify manufacturing.
- Cycloidal MGs with CP rotors require less PM pieces than cycloidal MGs with SPM rotors, which may simplify manufacturing.
- Cycloidal MGs with CP rotors provide inherent PM insertion slots, which may sim-

plify manufacturing relative to cycloidal MGs with SPM rotors.

- Cycloidal MGs with CP rotors achieve lower VTD values than cycloidal MGs with SPM rotors.
- Cycloidal MGs with CP rotors can use PMs with wider arc lengths than cycloidal MGs with SPM rotors. The use of wider PMs provides some potential practical manufacturing advantages and results in cycloidal MGs with CP rotors exhibiting a higher optimum gear ratio for maximizing PM ST than cycloidal MGs with SPM rotors.
- Cycloidal MGs with CP inner rotors can be designed to inherently retain the PMs, thus potentially eliminating the need for a PM retention sleeve and enabling the use of a smaller effective air gap.
- If using a CP inner rotor eliminates the need for a PM retention sleeve and enables the use of a smaller effective air gap, cycloidal MGs with CP inner rotors can achieve higher PM STs than cycloidal MGs with SPM inner rotors at higher gear ratios.
- Optimized cycloidal MGs with CP rotors do not necessarily achieve higher PM STs than optimized cycloidal MGs with SPM rotors if they use the same air gap, except possibly at gear ratios beyond the range evaluated in this study and much higher than the optimal gear ratios.
- Cycloidal MGs with CP rotors experience slightly higher eccentric magnetic forces at no load than cycloidal MGs with SPM rotors.

- Cycloidal MGs with CP rotors experience higher eccentric magnetic forces at full load than cycloidal MGs with SPM rotors.
- Cycloidal MGs with CP rotors and SPM rotors experience very similar perpendicular magnetic forces.
- CP-CP cycloidal MGs optimized with 2D FEA exhibit a larger slip torque reduction when evaluated with 3D FEA due to end effects than CP-SPM and SPM-SPM cycloidal MGs optimized with 2D FEA.

## 7. PROTOTYPE CONSEQUENT POLE CYCLOIDAL MAGNETIC GEAR

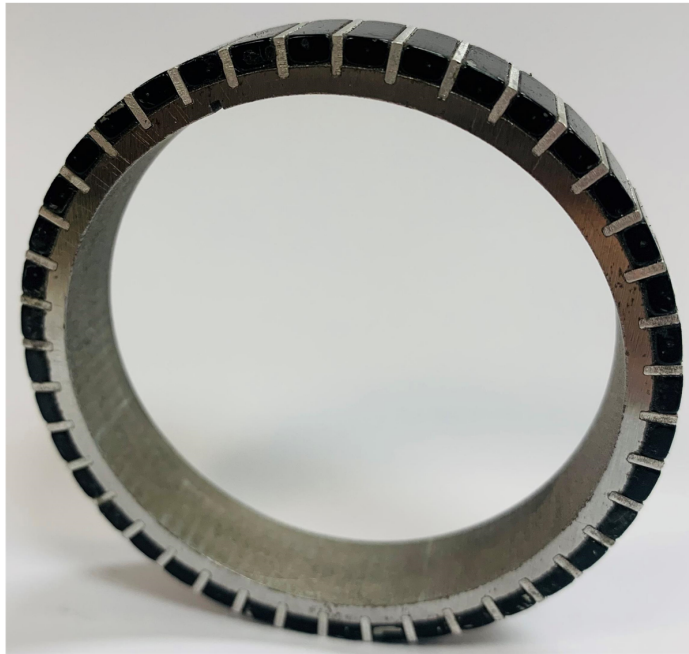
The previous section introduces CP CyMGs and illustrates the potential performance of CyMGs with reduced PM piece counts using CP topology. In this section, a prototype is designed, fabricated, and tested to validate the FEA model of the CP CyMG and compare it with the SPM CyMG. A prototype was fabricated to validate the FEA models for the CP CyMG. The prototype utilized the existing structural parts and the outer rotor of a 20:1 SPM CyMG prototype in addition to off-the-shelf PMs to facilitate rapid and reduced cost fabrication. Therefore, minimizing the fabrication time and cost were prioritized over maximizing the torque of the CP CyMG prototype. Table 7.1 summarizes the final prototype design details for the SPM CyMG and the CP CyMG. NdFeB N52 H was used for the PMs and M15 steel was used for the back irons in the SPM CyMG. The CP CyMG prototype shared the outer rotor of the SPM CyMG prototype; however, the PMs and the back iron of the inner rotor were made from NdFeB N50 and 1018 mild steel, respectively.

Table 7.1: PROTOTYPES ACTIVE DESIGN PARAMETER VALUES.

Parameter	SPM CyMG	CP CyMG
Inner rotor pole pair count	20	
Outer rotor pole pair count	21	
Outer diameter	81 mm	
Outer rotor back iron radial	2.5 mm	
Outer rotor PM thickness	2.5 mm	
Outer rotor PM outer edge width	4.6 mm	
Outer rotor axial length	11.26 mm	
Minimum effective air gap thickness	1.5 mm	
Axis offset	1.5 mm	
Inner rotor PM thickness	2.5 mm	2 mm
Inner rotor PM inner edge width	3.7 mm	6 mm
Inner rotor back iron radial	2.5 mm	3 mm
Inner rotor axial length	11.26 mm	10 mm

Figures 7.1a and 7.1b show the inner rotors of the cycloidal SPMG and the cycloidal CPMG, respectively. Both rotors are part of cycloidal MGs with gear ratio 20:1. The CP rotor has fewer PM piece counts than the SPM rotor, which allows the PMs be wider and makes the assembly process easier.





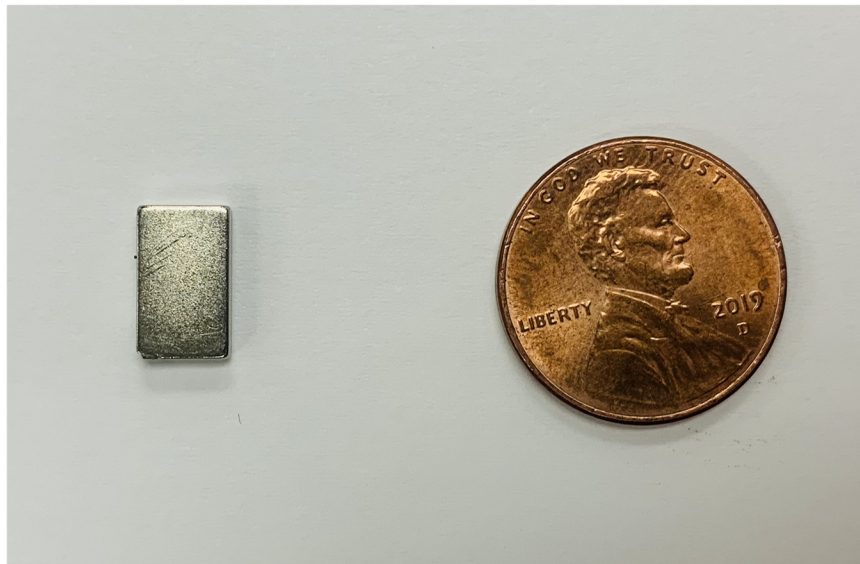
(a)



(b)

Figure 7.1: Inner rotor of the (a) SPM CyMG and (b) CP CyMG prototypes.

The inner rotor PMs, Figure 7.2a, were inserted into the CP back iron, Figure 7.2b, and fixed using epoxy to ensure a safe operation at high speeds. PMs are magnetized in one direction and they are assembled on the back iron with their North pole facing the air gap. Figure 7.3 presents the inner and the outer rotors of the CP CyMG prototype.



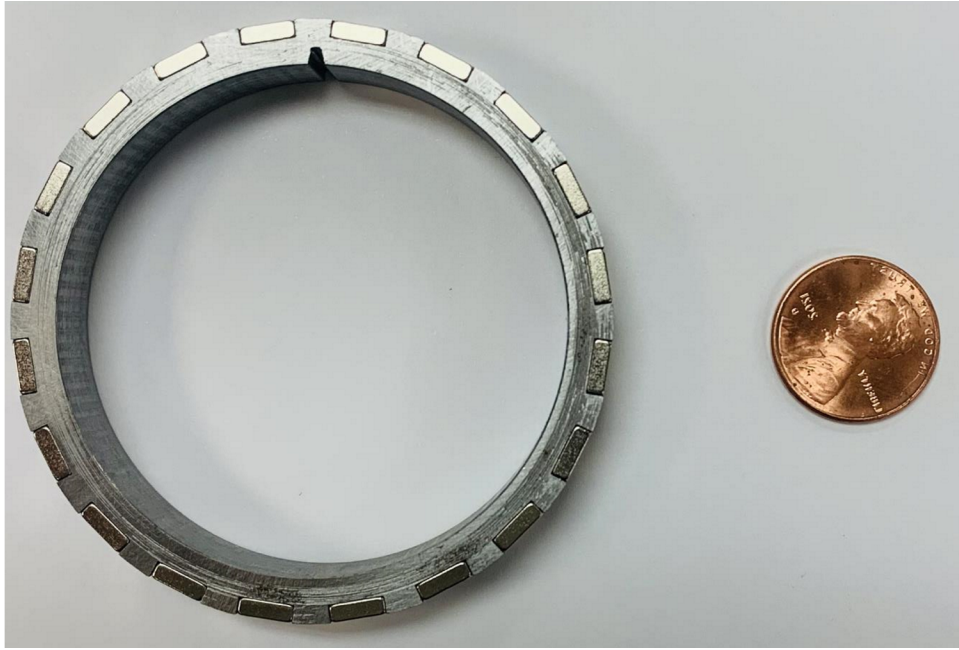
(a)

Figure 7.2



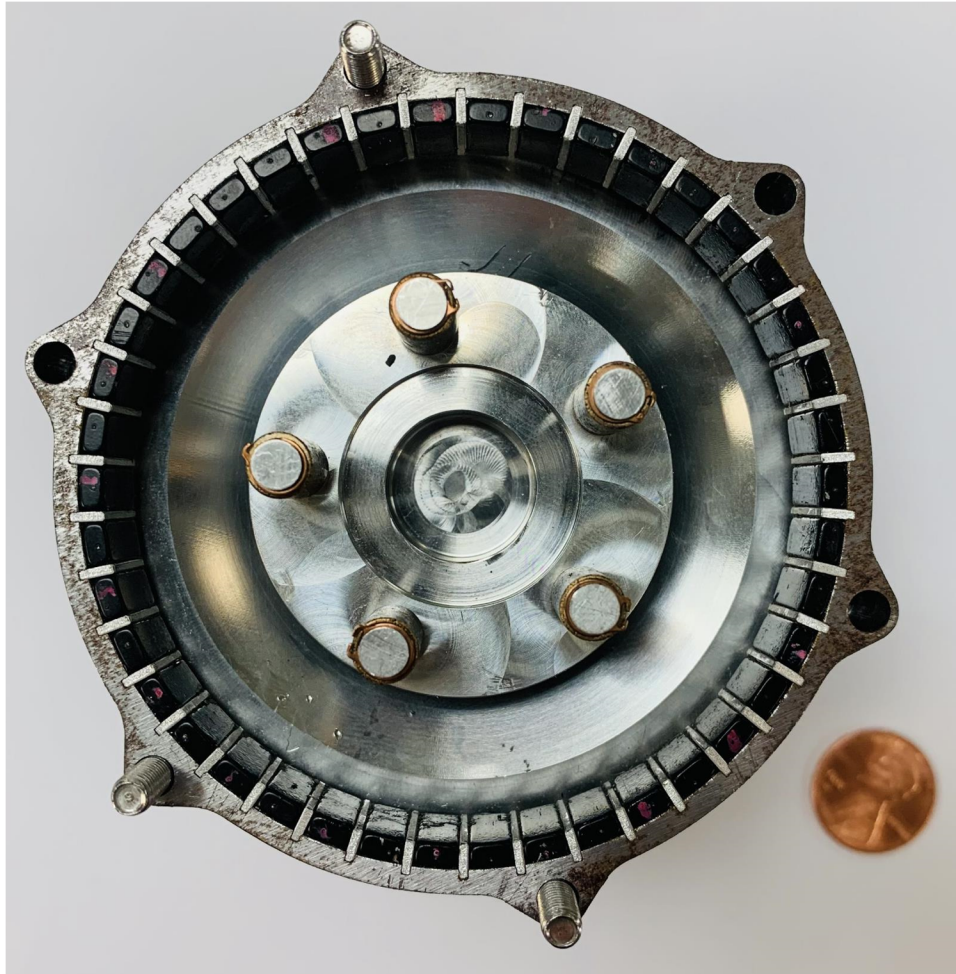
(b)

Figure 7.2: The (a) PMs and (b) back iron of the inner rotor in the CP CyMG prototype.



(a)

Figure 7.3

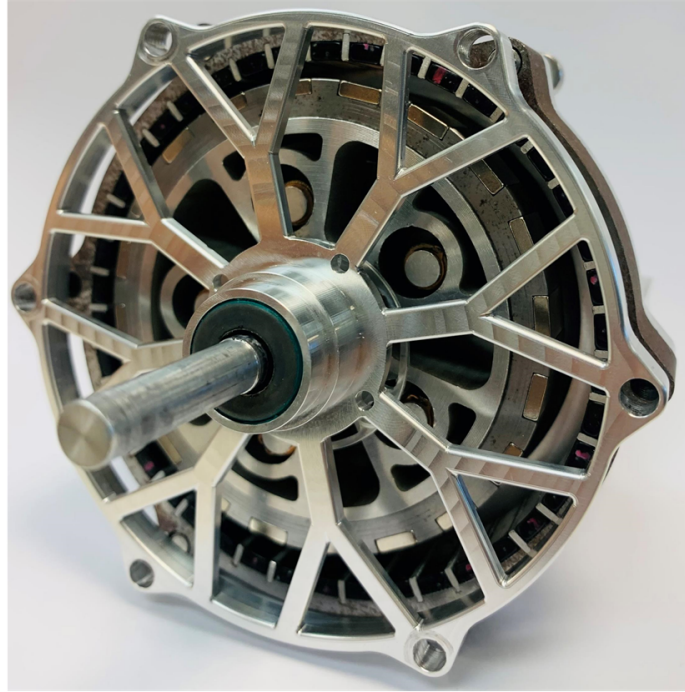


(b)

Figure 7.3: The (a) inner rotor and (b) outer rotor of the CP CyMG prototype with a penny provided for a size reference.

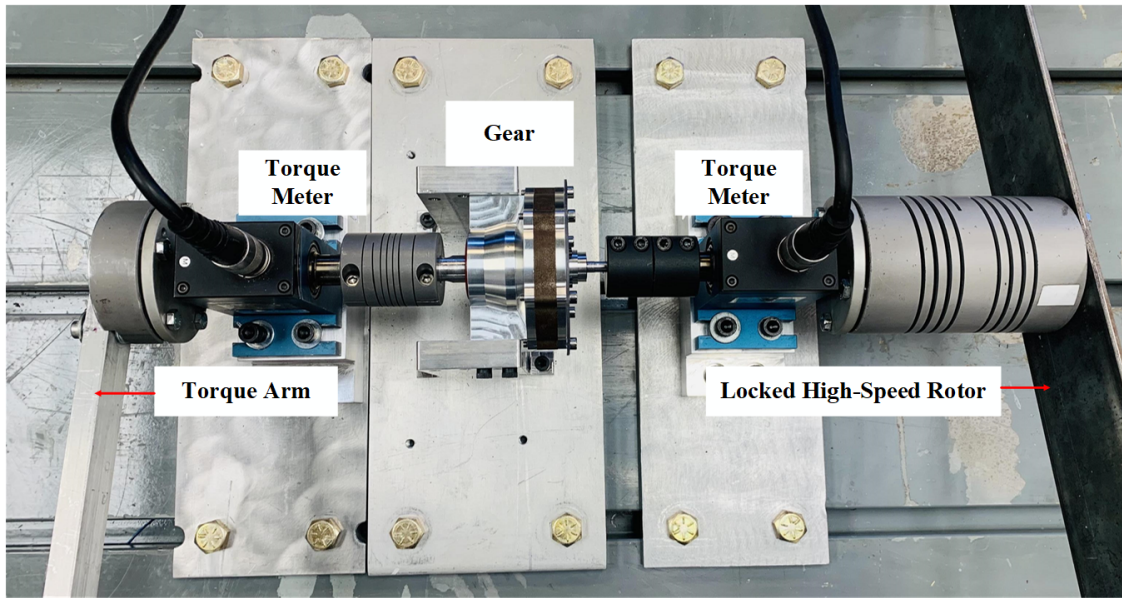
Figure 7.4a shows the assembled prototype. The inner rotor was placed inside the outer rotor with certain considerations. The test bed of the CP CyMG prototype is shown in Figure 7.4b, where two torque meters are used to measure the torque on the shafts. Also, a handle was used to fix the high-speed rotor for the slip torque measurement. Figure 7.4b shows a handle on the left side of gear that was used as the torque arm to ease the

experiment procedure. The low-speed rotor was turned to measure the stall torque.



(a)

Figure 7.4



(b)

Figure 7.4: (a) The assembled structure, and (b) test bed of the CP CyMG prototype with gear ratio 20:1.

Table 7.2 presents the experimental torque measurements of the SPM CyMG and the CP CyMG. Table 7.2 demonstrates a good agreement between the simulated and the measured slip torques of the CP CyMG.

Table 7.2: EXPERIMENTALLY MEASURED SLIP TORQUE.

Measurement	SPM CyMG		CP CyMG	
	3D FEA	Experiment	3D FEA	Experiment
Slip Torque	5.36 Nm	5.10 Nm	3.548 Nm	3.365 Nm
Specific Torque		9.75 (Nm/kg)		6.45 (Nm/kg)

## 8. CONCLUSION

This work has compared several different topologies of magnetic gears with different permanent magnet arrangements for high-speed applications and evaluated them in different metrics. Two new topologies have been introduced and their operating principles have been provided, reluctance cycloidal magnetic gear (Rel CyMG) and consequent pole cycloidal magnetic gear (CP CyMG). Additionally, the design and fabrication of a CP CyMG have been described and its experimental test results provided.

High-speed applications have electromagnetic and mechanical challenges such as higher eddy current losses at higher speed rotations and permanent magnet (PM) retention challenges like an increased effective air gap that results in torque reduction, respectively. Coaxial reluctance magnetic gears (Coaxial RMGs) are alternative solutions, which eliminate the PMs on the high-speed rotor. This research proposes utilizing a reluctance rotor in the cycloidal magnetic gears (CyMGs). Also, rotors with consequent pole PMs reduce the magnet reduction and can potentially address some mechanical challenges; therefore, they have been introduced as the inner rotor of the CyMGs as well.

First, an independent optimization on the coaxial RMG and the coaxial surface permanent magnet gear (SPMG) topologies has been provided for comparing the performance of these topologies in several different metrics such as volumetric torque density (VTD), specific torque (ST), PM specific torque (PM ST). There were significant differences between the achieved torque densities of coaxial RMGs and coaxial SPMGs. Coaxial SPMGs uti-



lize more PMs and they have higher torque densities. Although coaxial RMGs eliminate PMs on the inner rotor, comparing PM STs for these topologies illustrate a better PM utilization in coaxial SPMGs. Also, the coaxial RMGs have lower efficiencies than the coaxial SPMGs in multiple speeds considered for the simulations. The simulation results were contrary to the results of nonoptimized comparisons in previous papers. Also, the operating principles of coaxial RMGs were established in a correct format as the existing literature didn't derive correct equations.

Second, ST and PM ST comparison between the optimized Rel CyMGs, SPM CyMGs, and SPM CoMGs shows the better performance of SPM CyMGs at higher gear ratios and SPM CoMGs at lower gear ratios. However, the PM count in the Rel CyMG is about half of the PM count in SPM CyMGs. Therefore, the wider PMs make the manufacturing process easier. Also, the impact of Halbach arrays in SPM CyMGs and Rel CyMGs was evaluated, which verified higher achievable torque densities in both topologies.

Third, introduces a new variation of the CyMG which uses a CP inner rotor. This topology facilitates the use of fewer and wider PMs on the inner rotor, which may help with manufacturing considerations for this rotor. A CP rotor also may provide inherent PM retention, which can eliminate the need for a PM retention sleeve and enable a smaller effective air gap. A GA and 2D FEA were used to parametrically optimize CP and SPM CyMGs by independently maximizing their PM ST and VTD. The results reveal that CP designs with positive PM grips and smaller air gaps (due to the inherent PM retention) can achieve higher PM STs at the higher gear ratios in the study. However, the results

also indicate that optimum CP designs generally achieve lower VTD values than optimum SPM designs. The studies on eccentric forces show that CP CyMGs have higher magnetic forces than SPM CyMGs at no load and full load. Also, the 3D end effects in SPM CyMGs were lower than different CP rotor combinations in CyMGs.

Finally, a CP CyMG prototype was design, fabricated, and tested to validate the models and explore the challenges. The prototype was optimized for cost and time rather than torque density. Therefore, the structure and outer rotor of an SPM CyMG were used in addition to off-the-shelf PMs. The prototype showed good agreement with the simulation results regarding its slip torque, which was measured to be 3.365 Nm in the experiment and 3.548 Nm in 3D FEA simulations.

## REFERENCES

- [1] N. Frank and H. Toliyat, "Gearing ratios of a magnetic gear for wind turbines," in *Proc. IEEE Int. Elect. Mach. Drives Conf.*, 2009, pp. 1224–1230.
- [2] K. Uppalapati, J. Z. Bird, D. Jia, J. Garner, and A. Zhou, "Performance of a magnetic gear using ferrite magnets for low speed ocean power generation," in *Proc. IEEE Energy Convers. Congr. Expo.*, 2012, pp. 3348–3355.
- [3] T. Frandsen, L. Mathe, R. H. N. Berg, T. Matzen, P. Rasmussen, and K. Jensen, "Motor integrated permanent magnet gear in a battery electrical vehicle," *IEEE Trans. Ind. Appl.*, vol. 51, no. 2, pp. 1516–1525, March-April 2015.
- [4] T. F. Tallerico, Z. A. Cameron, J. J. Scheidler, and H. Haseeb, "Outer stator magnetically-g geared motors for electrified urban air mobility vehicles," in *Proc. AIAA/IEEE Elect. Aircraft Technol. Symp.*, 2020, pp. 1–25.
- [5] L. MacNeil, B. Claus, and R. Bachmayer, "Design and evaluation of a magnetically-g geared underwater propulsion system for autonomous underwater and surface craft," in *Proc. Int. Conf. IEEE Oceans*, 2014, pp. 1–8.
- [6] B. Praslicka and et al., "Practical analysis and design of a 50:1 cycloidal magnetic gear with balanced off-axis moments and a high specific torque for lunar robots," in *Proc. IEEE Int. Elect. Mach. Drives Conf.*, 2021, pp. 1–8.

- [7] K. Atallah and D. Howe, "A novel high-performance magnetic gear," *IEEE Trans. Magn.*, vol. 34, no. 4, pp. 2844–2846, July 2001.
- [8] P. O. Rasmussen, T. O. Anderson, F. T. Jorgensen, and O. Nielsen, "Development of a high performance magnetic gear," *IEEE Trans. Ind. Appl.*, vol. 41, no. 3, pp. 764–770, May-June 2005.
- [9] M. C. Gardner, M. Johnson, and H. A. Toliyat, "Analysis of high gear ratio capabilities for single-stage, series multistage, and compound differential coaxial magnetic gears," *IEEE Trans. Energy Convers.*, vol. 34, no. 2, pp. 665–672, June 2019.
- [10] M. Johnson, A. Shapoury, P. Boghrat, M. Post, and H. A. Toliyat, "Analysis and development of an axial flux magnetic gear," in *Proc. IEEE Energy Convers. Congr. Expo.*, 2014, pp. 5893–5900.
- [11] S. Gerber and R. J. Wang, "Torque capability comparison of two magnetically geared pm machine topologies," in *Proc. Int. Conf. Ind. Technol.*, 2013, pp. 1915–1920.
- [12] M. C. Gardner, M. Johnson, and H. A. Toliyat, "Comparison of surface permanent magnet coaxial and cycloidal radial flux magnetic gears," in *Proc. IEEE Energy Convers. Congr. Expo.*, 2018, pp. 5005–5012.
- [13] J. Rens, K. Atallah, S. D. Calverley, and D. Howe, "A novel magnetic harmonic gear," *IEEE Trans. Ind. Appl.*, vol. 46, no. 1, pp. 206–212, January-February 2010.
- [14] F. T. Jorgensen, T. O. Andersen, and P. O. Rasmussen, "The cycloid permanent magnetic gear," *IEEE Trans. Ind. Appl.*, vol. 44, no. 6, pp. 1659–1665, November-

December 2008.

- [15] K. Davey, T. Hutson, L. McDonald, and G. Hutson, "The design and construction of cycloidal magnetic gears," in *Proc. IEEE Int. Elect. Mach. And Drives Conf.*, 2017, pp. 1–6.
- [16] C. Liu, J. Yu, and C. H. T. Lee, "A new electric magnetic-gear machine for electric unmanned aerial vehicles," *IEEE Trans. Magn.*, vol. 53, no. 11, pp. 1–6, November 2017.
- [17] Y. Wang, J. Ma, C. Liu, G. Lei, Y. Guo, and J. Zhu, "Reduction of magnet eddy current loss in pmsm by using partial magnet segment method," *IEEE Trans. Magn.*, vol. 55, no. 7, pp. 1–5, July 2019.
- [18] L. Li, W. Li, D. Li, X. Zhang, and Y. Fan, "Influence of sleeve thickness and various structures on eddy current losses of rotor parts and temperature field in surface mounted permanent-magnet synchronous motor," *IET Elec. Power Appl.*, vol. 12, no. 8, pp. 1183–1191, September 2018.
- [19] F. Chai, Y. Li, P. Liang, and Y. Pei, "Calculation of the maximum mechanical stress on the rotor of interior permanent-magnet synchronous motors," *IEEE Trans. Ind. Electron.*, vol. 63, no. 6, pp. 3420–3432, June 2016.
- [20] K. Aiso, K. Akatsu, and Y. Aoyama, "A novel reluctance magnetic gear for high-speed motor," *IEEE Trans. Ind. Appl.*, vol. 55, no. 3, pp. 2690–2699, May-June 2019.

- [21] K. Li, Z. Zhu, and P. Wu, "A reluctance magnetic gear for high speed and vibration motor systems," pp. 1–5, 2018.
- [22] A. F. Shevchenko, A. G. Pristup, G. B. Vyalcev, D. M. Toporkov, and K. T. Alieva, "Electromagnetic torque of reluctance magnetic gear," pp. 402–405, 2018.
- [23] K. Aiso, K. Akatsu, and Y. Aoyama, "A novel magnetic gear for high speed motor system," in *Proc. IEEE Int. Elect. Mach. Drives Conf.*, 2017, pp. 1–7.
- [24] M. S. Arani and S. A. Afsari, "Design of rotor structure for reluctance magnetic gear to improve torque characteristic," in *Proc. Power Electron. Drives Syst. Technol. Conf.*, 2020, pp. 1–5.
- [25] S. Hasanpour, M. C. Gardner, M. Johnson, and H. A. Toliyat, "Comparison of reluctance and surface permanent magnet coaxial magnetic gears," in *Proc. IEEE Energy Convers. Congr. Expo.*, 2020, pp. 307–314.
- [26] M. Johnson, S. Hasanpour, M. C. Gardner, and H. A. Toliyat, "Analysis and benchmarking of radial flux cycloidal magnetic gears with reduced permanent magnet piece count using consequent poles," in *Proc. IEEE Int. Elect. and Mach. Drives Conf.*, 2021, pp. 4334–4341.
- [27] K. Aiso, K. Akatsu, and Y. Aoyama, "A novel reluctance magnetic gear for high-speed motor," *IEEE Trans. Ind. Appl.*, vol. 55, no. 3, pp. 2690–2699, May-June 2019.
- [28] K. Li, Z. Zhu, and P. Wu, "A reluctance magnetic gear for high speed and vibration motor systems," in *Proc. Int. Conf. Mechatronics Mach. Vision Pract.*, 2018, pp. 1–5.

- [29] A. F. Shevchenko, A. G. Pristup, G. B. Vyalcev, D. M. Toporkov, and K. T. Alieva, “Electromagnetic torque of reluctance magnetic gear,” in *Proc. Int. Sci. Tech. Conf. Actual Problems Electron. Instrument Eng.*, 2018, pp. 402–405.
- [30] J. A. Tapia, F. Leonardi, and T. A. Lipo, “Consequent-pole permanent-magnet machine with extended field-weakening capability,” *IEEE Trans. Ind. Appl.*, vol. 39, no. 6, pp. 1704–1709, November-December 2003.
- [31] S. Chung, J. Kim, Y. Chun, B. Woo, and D. Hong, “Fractional slot concentrated winding pmsm with consequent pole rotor for a low-speed direct drive: reduction of rare earth permanent magnet,” *IEEE Trans. Energy Conv.*, vol. 30, no. 1, pp. 103–109, March 2015.
- [32] Y. Ueda, H. Takahashi, T. Akiba, and M. Yoshida, “Fundamental design of a consequent-pole transverse-flux motor for direct-drive systems,” *IEEE Trans. Magn.*, vol. 49, no. 7, pp. 4096–4099, July 2013.
- [33] H. Huang, L. Jing, R. Qu, and D. Li, “The demagnetizing protection of halbach consequent pole in a magnetic-gear machine,” in *Proc. Int. Conf. Elect. Mach. and Sys.*, 2018, pp. 365–370.
- [34] H. Huang, D. Li, W. Kong, and R. Qu, “Torque performance of pseudo direct-drive machine with halbach consequent pole,” in *Proc. IEEE Energy Convers. Congr. Expo.*, 2018, pp. 3286–3293.
- [35] H. H. J. Shen, H. Li and M. Jin, “A coaxial magnetic gear with consequent-pole

- rotors,” *IEEE Trans. Energy Conv.*, vol. 32, no. 1, pp. 267–275, March 2017.
- [36] H. Y. Wong, J. Z. Bird, S. Modaresahmadi, and W. Williams, “Comparative analysis of a coaxial magnetic gear with a flux concentration rotor and consequent pole rotor typology,” *IEEE Trans. Magn.*, vol. 54, no. 11, pp. 1–5, November 2018.
- [37] S. Peng, W. N. Fu, and S. L. Ho, “A novel high torque-density triple-permanent-magnet-excited magnetic gear,” *IEEE Trans. Magn.*, vol. 50, no. 11, pp. 1–4, November 2014.
- [38] W. N. Fu and L. Li, “Optimal design of magnetic gears with a general pattern of permanent magnet arrangement,” *IEEE Trans. Appl. Supercond.*, vol. 26, no. 7, pp. 1–5, October 2016.
- [39] Y. Chen, W. N. Fu, and W. Li, “Performance analysis of a novel triple-permanent-magnet-excited magnetic gear and its design method,” *IEEE Trans. Magn.*, vol. 52, no. 7, pp. 1–4, July 2016.
- [40] M. Johnson, M. C. Gardner, and H. A. Toliyat, “Design comparison of ndfeb and ferrite radial flux surface permanent magnet coaxial magnetic gears,” *IEEE Trans. Ind. Appl.*, vol. 54, no. 2, p. 1254–1263, March-April 2018.
- [41] M. Johnson, M. C. Gardner, H. A. Toliyat, S. Englebretson, W. Ouyang, and C. Tschida, “Design, construction, and analysis of a large-scale inner stator radial flux magnetically geared generator for wave energy conversion,” *IEEE Trans. Ind. Appl.*, vol. 54, no. 4, p. 3305–3314, July-August 2018.



- [42] M. C. Gardner, B. E. Jack, M. Johnson, and H. A. Toliyat, "Comparison of surface mounted permanent magnet coaxial radial flux magnetic gears independently optimized for volume, cost, and mass," *IEEE Trans. Ind. Appl.*, vol. 54, no. 3, pp. 2237–2245, May-June 2018.
- [43] K. Aiso, K. Akatsu, and Y. Aoyama, "Reluctance magnetic gear and flux switching magnetic gear for high speed motor system," in *Proc. IEEE Energy Convers. Congr. Expo.*, 2017, pp. 2445–2452.
- [44] S. Gerber and R.-J. Wang, "Analysis of the end-effects in magnetic gears and magnetically geared machines," in *Proc. IEEE Int. Conf. Elect. Mach.*, 2014, pp. 396–402.
- [45] B. Praslicka, M. C. Gardner, M. Johnson, and H. A. Toliyat, "Review and analysis of coaxial magnetic gear pole pair count selection effects," *IEEE J. Emerg. Sel. Topics Power Electron.*, pp. 1–1, 2021.
- [46] L. Jian and K. T. Chau, "A coaxial magnetic gear with halbach permanent-magnet arrays," *IEEE Trans. Energy Conv.*, vol. 25, no. 2, pp. 319–328, June 2010.
- [47] L. Jian, K. T. Chau, Y. Gong, J. Z. Jiang, C. Yu, and W. Li, "Comparison of coaxial magnetic gears with different topologies," *IEEE Trans. Magn.*, vol. 45, no. 10, pp. 4526–4529, October 2009.
- [48] A. Rahideh, A. A. Vahaj, M. Mardaneh, and T. Lubin, "Two-dimensional analytical investigation of the parameters and the effects of magnetisation patterns on the

- performance of coaxial magnetic gears,” *IET Elec. Syst. Transp.*, vol. 7, no. 3, pp. 230–245, August 2017.
- [49] M. Johnson, M. C. Gardner, and H. A. Toliyat, “Analysis of axial field magnetic gears with halbach arrays,” in *Proc. IEEE Int. Elect. Mach. and Drives Conf.*, 2015, pp. 108–114.
- [50] H. Huang, R. Qu, and J. Bird, “Performance of halbach cycloidal magnetic gears with respect to torque density and gear ratio,” in *Proc. IEEE Int. Elect. and Mach. Drives Conf.*, 2019, pp. 1977–1984.
- [51] Y. Huang, J. Z. Bird, A. L. Vera, and R. Qu, “An axial cycloidal magnetic gear that minimizes the unbalanced radial force,” *IEEE Trans. Magn.*, vol. 56, no. 7, pp. 1–10, July 2020.
- [52] K. Davey, L. McDonald, and T. Hutson, “Axial flux cycloidal magnetic gears,” *IEEE Trans. Magn.*, vol. 50, no. 4, pp. 1–7, April 2014.
- [53] K. Li, J. Bird, J. Kadel, and W. Williamsn, “A flux-focusing cycloidal magnetic gearbox,” *IEEE Trans. Magn.*, vol. 51, no. 11, pp. 1–4, November 2015.
- [54] S. Gerber and R.-J. Wang, “Analysis of the end-effects in magnetic gears and magnetically geared machines,” in *Proc. Int. Conf. Elect. Mach.*, 2014, pp. 396–402.
- [55] M. C. Gardner, M. Johnson, and H. A. Toliyat, “Comparison of surface permanent magnet coaxial and cycloidal radial flux magnetic gears,” pp. 5005–5012, 2018.